Analysis and Design of Offshore Aquaculture Installations

Tomás Maria Fonseca Martins Alves Bernardo

Thesis to obtain the Master of Science Degree in

Naval Architecture and Ocean Engineering

Supervisor: Prof. Carlos Guedes Soares

Examination Committee

Chairperson: Prof. Yordan Garbatov

Supervisor: Prof. Carlos Guedes Soares

Members of the Committee Prof. Shan Wang

September 2020

Acknowledgements

This initially daunting task was made possible by the support and companionship of a group of people. Hence, I will begin by thanking them.

Firstly, a kind thank you to my family. For the endless hours hearing my complaints and frustrations, but also for sharing the joys of each small step overcame. Next to them I owe to all my friends and colleagues that shared the study space “sala de naval” with me during this year and a half. For they provided me with a lot of help and companionship, as well as feedback and problem-solving suggestions. They were with me almost every step of this journey.

A big thank you is reserved to Professor Roberto Vettor. For all his help and unconditional availability to help me in some problems that rose during the elaboration of this work., when he had non-obligation to do so. Also of great help was PhD student Zhongchi Liu. Who provided me with a tireless support during my validation process with his data, despite being fully occupied with his research work. A lot of information and insights were given to me by Dr. Carlos Andrade, of the Madeira government, so I must thank him for his always cooperative help.

At last, a thank you is reserved to my supervisor, Professor Carlos Guedes Soares for letting me pursue the thematic of aquaculture, and to the software support team at DNV-GL for the patient support in my long learning process with their software.

Abstract

This work rose from the interest in broadening the knowledge of the aquaculture sector. Its opportunities and challenges and in more detail the engineering behind the different approaches. The aim of this work will be then to specify the considerations for the initial design phase, and propose a numeric tool to aid in the process.

The works starts by reviewing the current procedures for analysing net structures, more specifically the computation of loads on them, and then proceeds to a review of the most prominent solutions available in the industry to face the challenge of offshore aquaculture developments, going also through the design considerations of this particular problem.

The feasibility of a commercially available numerical tool, SIMA, is assessed. Through a thorough validation process, where increasingly complex models are tested and the results compared. After the achievement of a satisfactory level of feasibility, the software was used to analyse an already built system, located in the Madeira archipelago. This analysis confronted the results obtained in SIMA with the solutions deployed in the field. By assessing the mooring system behaviour, it was found that it performed substantially well under the class society rules. Therefore, confirming that the numerical tool could be used as an evaluation tool in the design process. The last step of this work was to combine the knowledge obtained throughout the elaboration of this thesis and propose a possible concept to be deployed in an offshore location. A hydrodynamics analysis of the concept is performed using the numerical tool SIMA.

Index

List of figures

List of tables

Nomenclature

PEAP	Plano Estratégico para a Aquicultura Portuguesa
POEM	Plano de Ordenamento do Espaço Marítimo
SSS	Sea Surface Salinity
FAO	Food and Agriculture Organization of the United nations
DNV-GL	Det Norsk Veritas – Germanischer Lloyd
SPM	Single-Point Mooring
CFD	Computational Fluid Dynamics
DPS	Dynamic Position System
Rn	Reynolds Number
RAO	Response Amplitude Operator
Sn	Solidity Ratio
MBL	Mean Breaking Load
LRFD	Load and Resistance Factor Design
WSD	Working Stress Design
HMPE	High Modulus Polyethylene
SIMA	Simulation Workbench for Marine Applications
ABS	American Bureau of Shipping
MBL	Mean Breaking Load
ULS	Ultimate Limit State
CENTEC	Centro de Engenharia e Tecnologia Naval e Oceânica

1. Introduction

1.1 National Overview

Portugal, along with other countries, as seen an increase need of supplying the market of sea products with aquaculture productions. Due to the decline of fisheries stocks and the continuously demand for sea products. This need is well expressed in the "Estratégia Nacional para o Mar 2013-2020" (Portugal 2013) , where it is considered one of the five most important domains to develop. Having this on sight, a plan was proposed for the Portuguese aquaculture sector: the "Plano Estratégico para a Aquicultura Portuguesa" (PEAP)(DGRM 2014).

The PEAP offers and overview of the national natural conditions, preferred sites and active production units. According to it, the sea states during winter months of the continental western coast and north coast of the Atlantic islands can be very challenging. Driving a need to develop systems that could endure the harsh conditions (DGRM 2014). Albeit, the continental south coast (Algarve) and Madeira's south coast have more favourable conditions, with some facilities already producing in the area (DGRM 2014). These sites, as well as some other of interest, are advanced in the "Plano de Ordenamento do Espaço Marítimo" (POEM)(DGRM 2018).

In the POEM, at December of 2018, no offshore sites for the farming of fishes are stated. Only for fattening of wild caught bluefin tuna (*Thunnus thynnus*) and bivalve production (DGRM 2018). However, the implementations of 2 pilot projects are in progress in the main continent. One for the production of Gilt-head bream (Sparus aurata) and European Seabass (Dicentrarchus labrax) at the "Área Piloto de Produção Aquícola da Armona" (APPA), located at 2 nautical miles from the coast. Another for the study of the growth of Atlantic Salmon (Salmo Salar) in national waters, located 11 nautical miles off the coast of Aveiro. No information was found regarding offshore developments in the insular areas of Azores and Madeira.

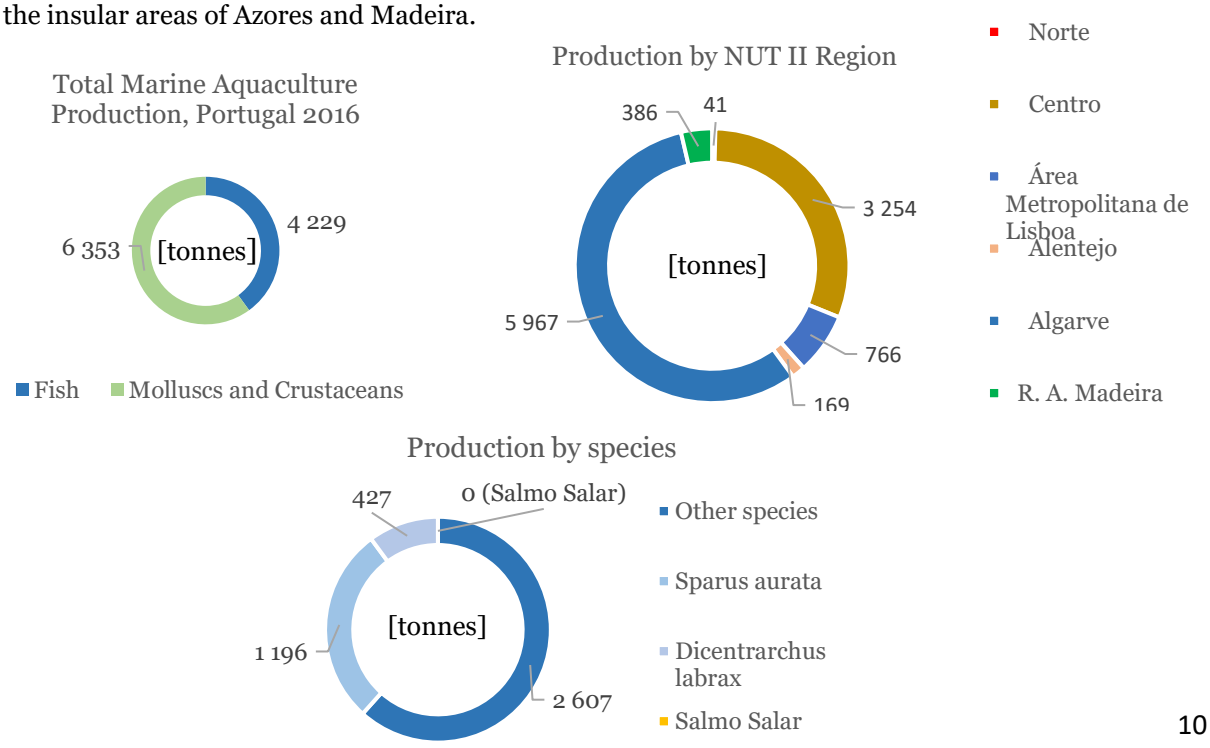

Figure 1 - Portuguese Marine Aquaculture Production in 2016. (INE and DGRM 2017)

According to the latest available statistics produced by the *Instituto National de Estatística* (INE)(INE and DGRM 2017), referring to the year of 2016, the majority of the national aquaculture production was molluscs and crustaceans (Figure 1). The production numbers by location and by species are available, although the discretized amount of each species in each location is not directly available.

1.2 Species Assessment

One of the key parameters for the design of an aquaculture system is the fish demands, with each species having its own requirements regarding temperature, oxygen levels, salinity, among others (Shainee et al. 2013). Although the perfect levels of this requirements might not be known for the farmed species, adequate levels have been found through experience and studies (Pillay 1992). This section will focus on the demands of the three species that are farmed in Portugal at the moment, namely Gilt-head bream (*Sparus aurata*), European Seabass (*Dicentrarchus labrax*) and Atlantic Salmon (*Salmo Salar*).

The Gilt-head bream (*Sparus aurata*) is a species that occurs naturally on the Portuguese waters (Colloca and Cerasi 2005). It has a water temperature survival range between 6°-32°, with optimal temperatures around 20°-30° (CNEXO 1983). Albeit, (Ibarz et al. 2003; Remen et al. 2015) found that 12° should be the lowest limit for the rearing of this species and below this temperature the animals refuse to intake any feed.

The European Seabass (*Dicentrarchus labrax*) also occurs naturally on the Portuguese waters (Bagni 2005). According to (Person-Le Ruyet et al. 2004) the optimal growth range is 19°-25°. Little knowledge exists about the survival range of water temperature for this species, but is known to tolerate a broad range of 5°-28° (Yılmaz et al. 2011).

A substantial amount of information exits regarding the Atlantic Salmon (*Salmo Salar*), primarily as a result of the large-scale farming and economic interest around this species. The preferred water temperature is 13°-17°, with better results around 13° (Thyholdt 2014). The minimum temperature is -0.5°, with death occurring due to ice crystals formation below this value (Lorentzen 2008). (Elliott and Elliott 2010) states that 30°-33° is the upper limit temperature of survival.

Regarding salinity each species has its own requirements, but since the scope of this work is offshore sea systems and the Sea Surface Salinity (SSS) will be considered uniform in the sites studied, no information will be seek respecting this parameter.

1.3 Concepts

In their publication “The State of the World Fisheries and Aquaculture” (FAO 2018), the Food and Agriculture Organization of the United Nations (FAO) states that in 2016 the global fish production surpassed the global fisheries capture. The demand for food and feed is increasing, and the expansion of aquaculture production presents itself as one good solution. However, the growth of land and near coast aquaculture has several setbacks. Due to environmental, spatial and social restraints. Thus, the expansion of aquaculture to offshore waters is globally understood as a viable solution (Lovatelli, Aguilar-Manjarrez, and Soto 2013).

As DNV-GL mentioned on its article (Flagstad and Tvedt 2018) big expectations are placed on the aquaculture production and this will require an advance in knowledge, in order to fully take advantage of the offshore waters capabilities. The overall impression of my research is well expressed in the report written by (CEA 2018) where it is said that Norway and China are leading the development of the offshore aquaculture production. With big investments being made in the field and a lot of research as well. The report also points an interesting view, it says that these pioneer projects will be the foundation and lead the trend for the next decades.

By focusing on these two countries, Norway and China, a brief summary of the systems or concepts in development will be made. These two countries follow different approaches regarding the development of the offshore aquaculture sector. Norway uses a system of "development licenses", that awards exploitation licenses to companies that present an innovative project to outcome territorial, environmental and technological barriers (Moe 2017). China set a goal to have 178 pilot farms by 2025 in a national demonstration zone. These farms and projects are, in some cases, backed by the government to a certain extent (Kiernan 2018). The Chinese government aims to be at the forefront of the aquaculture fish products supply to meet its growing demand worldwide.

The concepts and designs developed are sourcing a lot of knowledge from the offshore oil and gas industry. Reason why a certain resemblance is visible between rigs and some of the emerging design solutions. Nonetheless, some interesting solutions are being pursued such as vessel shaped farms and closed cage systems.

- **Closed Cage**

In a closed system, a better control over the fish environment exists, with a better management of the water flow and quality. In addition, an improved handling of the fish waste is possible. Therefore, reducing the environmental pollution. Being a close structure exposed to sea loads and having a free surface, this system will have sloshing inside. The structure can be flexible or rigid. If flexible, then the deformation due to loads will affect the hydrodynamic behaviour of the structure. This calls for a hydro-elastic analyses (Strand 2018).

- **Vessel Shape**

The two known designs of a vessel shaped cage differ from each other, but on its essence, they are a vessel shaped floater divided in multiple cages and making use of a single-point mooring (SPM) solution, as well described in (Li et al 2017). This choice of mooring aims to allow the farm to position itself in a favourable position when facing waves and currents. As a benefit, it enlarges the area of waste spreading. Although, some complications due to insufficient water flow might arise from such mooring. When the farm is orientated in such way that the front cages reduce the water exchange of the downstream cages (Li et al. 2018).

- **Rig Type**

As mentioned before, one of the strategies to tackle the offshore environment challenges is by seeking knowledge and solutions from the offshore oil and gas industry and adapting it to the aquaculture needs (Bore and Fossan 2015). These designs are made of a series of joint beams,

sometimes forming a truss like structure. (Bore and Fossan 2015) also states that one of the advantages of these designs is the low natural frequencies, as a result of the small water plane area.

(a) *(b)* *(c)*

Figure 2 - (a) Closed concept by Marine Harvest. (b) Vessel Shaped concept HavFarm by Nordlaks. (c) Rig-type concept ocean Farm by Salmar

Table 1 shows some of the ongoing, and planned, pilot projects. By location and concept type. The concepts Aquapod™ and SeaStation™, are two already commercially available and used products. They differ somewhat from the above mention types and resemble more like traditional gravity net cages. The Aquapod™ is a rigid geodesic sphere and SeaStation™ is a self-tensioned net cage, with a single spar on its centre (Decew et al. 2006; Pérez et al 2003).

Table 1 - Ongoing and planned offshore aquaculture projects. Data from (CEA 2018; Harkell 2018)

Offshore Aquaculture		
Norway	Closed	4
	Rig Type	5
	Vessel Shape	1
	Semi Closed	1
	Open Cage	2
China	Rig Type	5
	Vessel Shape	1
USA	SeaStation™	3
	Aquapod™	1
Mexico	Aquapod™	1
Panama	SeaStation™	1
Japan	Rig Type (mixed with open cage)	1

2. Literature Review

The above-mentioned need to move further offshore the production of sea products brings with it some challenges. Offshore structures are subjected to larger and harsher loads from the environment than coastal closed structures.

These loads are caused by their exposure to waves, wind and current. Therefore, the goal to move aquaculture systems further offshore introduces the need to study and understand how these structures behave under the imposed loads and conditions. In this chapter a short description of the work and efforts done to model the loads on the main components of a typical aquaculture system will be done.

Aquaculture systems are on their essence made by three components. A rigid, or somewhat flexible, construction that provides the structural support to the system and its solidity. A flexible, or in some closed cage designs rigid, structure that provides a mean to imprison the fishes. Commonly through the use of a net or fabric, in a bag like fashion, structure. And a mooring system to maintain the farm in a particular location. The loads on the structure and the net are crucial to the design of the mooring system. The forces on the net vary with its shape, which brings the issue of maintaining a minimum volume for the fish welfare (Shainee et al. 2013).

2.1 Loads on Nets

Some work has been developed on permeable structures, with an increase of research in recent years. As Kristiansen and Faltinsen (2012) commented, computational fluid dynamics (CFD) are impractical to assess the hydrodynamic forces, due to the large (in the order of millions) number of twines of a net. The same authors also say that two types of hydrodynamic force models are used: screen models and models based on the Morison equation.

Løland (1991) proposes a wake model and a method to compute the forces on the net through the use of the drag and lift coefficients and by the division of the net in a set of panels.

$$C_D = C_D(Sn, \theta);\ C_L = C_L(Sn, \theta) \tag{1}$$

Kristiansen and Faltinsen (2012), present a screen model, where the forces are dependent of the Reynolds number (Rn).

$$C_D = C_D(Sn, Rn, \theta);\ C_L = C_L(Sn, Rn, \theta) \tag{2}$$

This is important when validating model tests. This screen approach discretizes the net in a series of surface elements, whose properties reflect the twine and knot geometry of the actual net. In this screen model approach the drag and lift coefficients depend on the solidity ratio (Sn), angle of attack (θ) and the Reynolds number (Rn).

The Morison based approach implies the subdivision of the net in a smaller number of twines, in the form of cylinders, in such a way that the projected area is kept the same. A model where the drag and lift coefficients depend on the Reynolds number (Rn) is used by Le Bris and Marichal (1999) on their work on the behaviour of submerged nets, and by Moe et al (2010) and by Tsukrov et al. (2002).

A super-element model was proposed by Lader et al (2001), where the net is divided in small patches of four-sided super elements. The forces are computed through the Morison equation and the drag and lift coefficients are dependent on the Solidity ration (Sn) and angle of attack (θ), the Reynolds number (Rn) is not explicitly accounted for. This dependency of Sn and θ is also the base of the work of (Aarsnes et al 1990), later refined in the model of (Løland 1991)

Le Bris and Marichal (1999) pointed out that the hydrodynamic interactions between mesh sides are not taken into account. This is also referred by Kristiansen and Faltinsen (2012) as one of the objections to the Morison based approach. The objections are namely: each twine does not influence the adjacent ones, meaning that "shading effect" and velocity changes due to decrease in projected area for each twine are not accounted for; for inflow angles larger than 45°, the drag force computed is exaggerated.

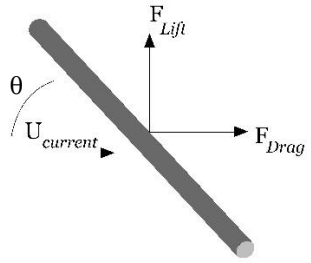

Figure 3 - Lift and drag forces on a twine in a uniform current

- **Empirical Loads on Nets**

From the towing tests of Rudi et al (1988), Aarsnes et al (1990) derived an empirical formulation for the hydrodynamic forces on stiff net panels under uniform flow. This method, that could be used for a preliminary assessment of loads, is limited for the range of solidity ratios (Sn) and Reynolds number (Rn) of the towing experiments, where the Reynolds number is based on the twine diameter. As a result, the empirical formulas proposed do not account for the drag and lift coefficient Reynolds number's dependency (Lader and Fredheim 2006).

Lader and Enerhaug (2005), compared the hydrodynamic forces computed with the empirical formulas of (Aarsnes et al 1990), eq. (3) and (4), and measurements of a model test.

$$F_D = \frac{1}{2}\rho C_D A U^2 \qquad (3)$$

$$F_L = \frac{1}{2}\rho C_L A U^2$$

$$C_D = 0.04 + (-0.04 + 0.33S + 6.54S^2 - 4.88S^3)\cos\alpha \quad (4)$$
$$C_L = (-0.05S + 2.3S^2 - 1.76S^3)sin2\alpha$$

Three cases were computed, to account for the change in the exposed area and the velocity reduction on the rear part of the net, called shadow effect.

- No change in the exposed area due to net deformation and no shadow effect.
- The exposed area changes and no shadow effect
- The exposed area changes and there is shadow effect.

The results of the authors are shown on Figure 4:

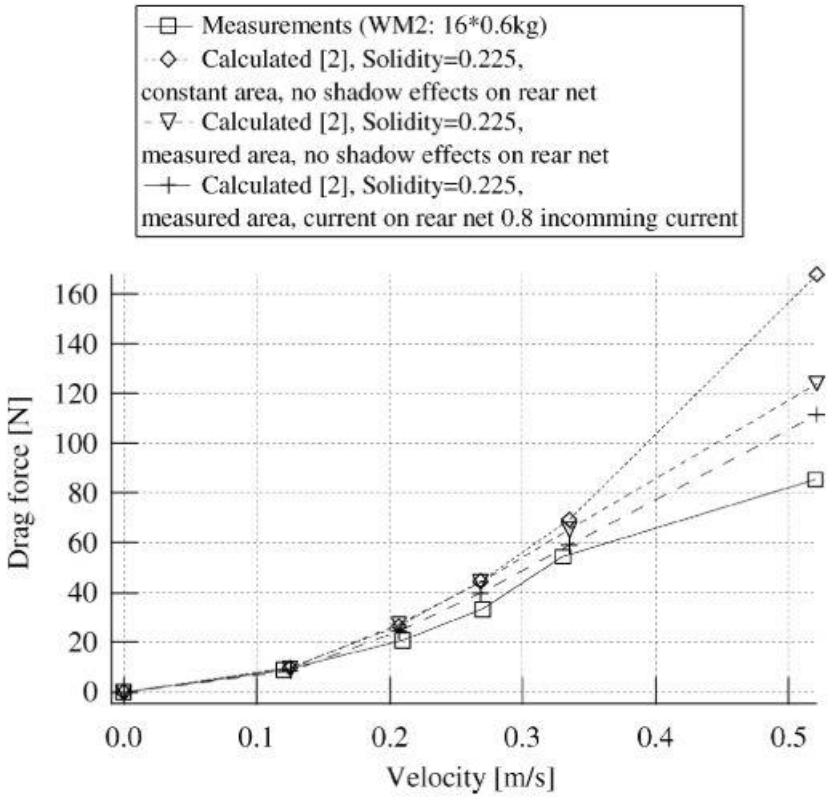

Figure 4 - Drag force computed with eq. (3) and (4), and obtained from experimental measurements. Reproduction of the results from Lader and Enerhaug (2005)

From Figure 4 it is clear that a deviation exists between the computed values and the values obtained experimentally. This was also observed by Kristiansen and Faltinsen (2012). According to the authors of the paper, the use of direct formulas for computing the global hydrodynamic forces on net cages overestimates the forces (the lift force is not shown, but a similar phenomenon occurs). Mainly because these empirical formulas do not take into account the net deformation and change of geometry.

The presence of the attack angle on the net in the formulas of the drag and lift coefficient implies a high dependency between the drag and lift force on the net and its geometry.

2.2 Loads on Structure

The majority of the work done in the analysis of fish farm behaviour under loads was performed for floating collar structures. Since those have been the standard in the industry for a long time. As referred in Li et al (2017) the responses of these structures is usually done by means of a strip theory analysis, and the drag force included via Morison equation. However, it is remarked that 3D frequency-dependent interactions and hydroelasticity effects are not accounted for in a 2D analysis. Since this effects are of major importance, the same authors proposed a beam model to compute the motions of the floating collar Such an approach was also previously done by Li and Faltinsen (2012).

As seen before, the emerging designs for offshore locations differ from the traditional floating plastic collar and become more similar to floating rigs and vessels. Therefore, the same procedures used for these structures can be applied, with the added complication to include the forces caused by the net cage. As clearly stated in Chakrabarti (2005) the method to compute loads on floating structures depend on their size relative to the wavelength. For slender structures normally the Morison equation is used to computed wave and current's loads. For larger structures a diffraction and radiation linear analysis is used.

2.3 Loads on Mooring

Mooring systems are used to maintain the structure in the desired place against waves, current and wind, by reducing its horizontal offset. Two systems are traditionally used, taut and catenary configurations. More on this on section 4.6. From the findings it was discerned that the modelling of the mooring lines varies a lot and is mainly dictated by the chosen software tool. Shen et al. (2018) used elastic trusses, with adequate weight and stiffness, to model the mooring lines, the forces are computed by Morison equation. Other approaches have been adopted, (Bore and Fossan 2015) using tubular beam elements to model the mooring lines due to limitations of the software employed.

Two approaches are taken regarding mooring analysis: uncoupled and coupled. The uncoupled analysis is recognized to be simpler and faster, and the coupled to be more accurate, although more time consuming.

The uncoupled analysis consists in computing the floating body motions and then, in a second analysis, imposing these motions as conditions at the end of the mooring system. The drawbacks of this analysis are the failure to incorporate the damping effect (on the low frequencies motions of the body) and current loads of the mooring system, and not accounting with the influence of the mooring system in the body wave frequency motion. These drawbacks gain more importance as the depth of the system increases. In a coupled approach, the motions and loads of both the floating body and the mooring system are solved for each time step. Therefore, the interaction between the two is considered. For a

coupled analysis regularly a non-linear time domain method is used, aiming for equilibrium at each time step (Jo et al. 2013).

3. Theoretical Background

The loads mentioned in the last chapter will be assessed numerically with a commercial software. This commercial software, used to perform a wave-structure interaction analysis of the structure(s), relies on 3D potential theory.

Hence, a brief summary of the theory supporting it will be done, going through the key equations and concepts. The theory regarding other aspects of the analysis performed will be done as well, namely mooring and the software's procedure.

Firstly, the potential flow problem formulation will be presented. Within the linear theory the wave induced loads and motions can be evaluated, this will be done in the second section of this chapter. In addition, the irregular wave case will also be dealt with. Although, non-linear effects such as drift forces and sum/difference frequency effects are sometimes relevant for the analysis. The last sections are devoted to a review of catenary mooring analysis and to the load formulation employed by the commercial software.

3.1. Potential Flow

Since linear potential theory will be used, it will be relevant to start by the specifications of the free-surface potential flow problem definition. The following summary is based on the approach presented by (Faltinsen 1990).

When dealing with a potential flow, the velocity vector can be represented through a velocity potential.

$$\boldsymbol{V} = (u, v, w) = \nabla\phi = \frac{\partial\phi}{\partial x}\boldsymbol{i} + \frac{\partial\phi}{\partial y}\boldsymbol{j} + \frac{\partial\phi}{\partial z}\boldsymbol{k} \tag{5}$$

The fluid is considered to be incompressible, inviscid and irrotational, meaning that both the rotational and the divergent of the velocity are zero.

$$\nabla \times \boldsymbol{V} = 0 \tag{6}$$
$$\nabla . \boldsymbol{V} = 0$$

With a zero divergent of the velocity, the Laplace equation of the velocity potential has to be zero. Commonly it is said that the velocity potential has to satisfy the Laplace equation. Finding the velocity potential is, therefore, solving the Laplace equation with pertinent boundary conditions.

$$\nabla^2\phi = \frac{\partial^2\phi}{\partial x^2} + \frac{\partial^2\phi}{\partial y^2} + \frac{\partial^2\phi}{\partial z^2} = 0 \quad (7)$$

The problem of a three-dimensional body interacting with a fluid is a boundary value problem. Thus, it is required to have relevant constraints, the boundary conditions.
Such conditions are:

- **Body Boundary Condition**: states that the normal component of the fluid velocity is equal to the normal component of the body -surface motion, meaning that there is no fluid crossing through the body surface.

$\frac{\partial\phi}{\partial n} = 0$, if the body has no motion (8)
$\frac{\partial\phi}{\partial n} = \boldsymbol{U}.\boldsymbol{n}$, if the body is in motion, $\boldsymbol{U}$ is the body's velocity

- **Seabed Boundary Condition**: states that the normal component of the fluid velocity at the bottom is equal to zero.

$$\left.\frac{\partial\phi}{\partial z}\right|_{z=-h} = 0 \quad (9)$$

- **Kinematic Free-Surface Boundary Condition**: states that a particle that is on the free-surface, will remain on the free-surface.

$\left.\frac{\partial\phi}{\partial z}\right|_{z=\eta} = \frac{\partial\eta}{\partial t} + u\frac{\partial\eta}{\partial x} + v\frac{\partial\eta}{\partial y} + w\frac{\partial\eta}{\partial z} = \frac{\partial\eta}{\partial t} + \frac{\partial\phi}{\partial x}\frac{\partial\eta}{\partial x} + \frac{\partial\phi}{\partial y}\frac{\partial\eta}{\partial y} + \frac{\partial\phi}{\partial z}\frac{\partial\eta}{\partial z}$, where η is the free surface (10)
elevation

- **Dynamic Free-Surface Boundary Condition**: states that the fluid pressure at the free-surface is always equal to the atmospheric pressure.

$$\left.\frac{\partial\phi}{\partial t}\right|_{z=\eta} + \frac{1}{2}\left[\left(\frac{\partial\phi}{\partial x}\right)^2 + \left(\frac{\partial\phi}{\partial y}\right)^2 + \left(\frac{\partial\phi}{\partial z}\right)^2\right] + g\eta + \frac{P_\eta}{\rho} = C(t) \quad (11)$$

Since linear theory is considered, by preserving the linear terms in eq.(10) and (11) it is possible to have the free-surface boundary conditions for the linear hypothesis.

3.2. Motions and loads

As said previously, wave induced loads and motions can be evaluated within the linear hypothesis. These responses can be divided in responses in regular in irregular sea. First the regular sea case is approached.

3.2.1. Regular Waves

The problem of finding the motions and loads on a floating structure under the action of regular waves can be divided in two problems.

- Diffraction Problem
- Radiation Problem

As a result of being in the linear hypothesis, the loads from both problems can be summed up to give the total forces on the structure.

Diffraction Problem

The diffraction problem is the case when the structure is fixed, under the action of incident waves. The structure becomes then expose to two excitation loads: Froude-Kriloff loads and diffraction loads. The Froude-Kriloff force is caused by the pressure field of the undisturbed incoming waves, which are assumed to have a long wavelength in comparison with the structure, so the long wave approximation is used.

The Froude-Kriloff force is given by:

$$F_i^{FK} = -\rho \iint \frac{\partial \phi_I}{\partial t} n_i dS, \text{ where } \phi_I \text{ is the incident velocity potential} \quad (12)$$

The diffraction loads come by the changes on the pressure field caused by the structure. If the only force acting on the body surface was the Froude-Kriloff force, then a fluid transport would occur across the body surface. To achieve this counteraction the structure must create a pressure field. (Faltinsen 1990) proposes that this force, caused by the oscillation of the structure with a velocity equal in magnitude and opposite in direction of the fluid velocity, is given by:

$$F_i^{DF} = A_i 1 a_1 + A_i 2 a_2 + A_i 3 a_3 \quad (13)$$

Where A_{ii} are added mass terms and a_i are acceleration components. The total force on the structure in the radiation problem is therefore:

$$\mathrm{F} = \boldsymbol{F} = F_1 \boldsymbol{i} + F_2 \boldsymbol{j} + F_3 \boldsymbol{k} \quad (14)$$

$$F_i^{DF} = F_i = F_i^{FK} + F_i^{DF} = -\rho \iint \frac{\partial \phi_I}{\partial t} n_i dS + A_i 1 a_1 + A_i 2 a_2 + A_i 3 a_3$$

Radiation Problem

The radiation problem is the case when the structure is compelled to oscillate, in any degree of freedom, at the same frequency as the waves. The loads on the structure are, as identified by Faltinsen (1990): added mass, damping and restoring forces and moments.

Added mass should be seen as an additional force, induced by the changes on fluid pressure due to the structure oscillation. Added mass terms have different dimensions, such as mass, mass times length, moment of inertia, among others. The damping term is composed by the potential and the viscous damping. On this section only the potential damping coefficient will be dealt with. The viscous damping is explored on a further section.

The radiation force caused by the motion on the degree of freedom *j* is:

$$F_i^{RF} = -a_{ij}\frac{d^2\eta_j}{dt^2} - b_{ij}\frac{d\eta_j}{dt} \tag{15}$$

Where a_{ij} and b_{ij} are the added mass and damping coefficient. These terms, by definition, are given as:

$$a_{ij} = -\frac{\rho}{\omega}Re\left\{i\int_{c_0}\phi_j^R N_i ds\right\} \tag{16}$$
$$b_{ij} = \rho Im\left\{i\int_{c_0}\phi_j^R N_i ds\right\}$$

Where the radiated potential is needed for their computation. The normal procedure to follow when computing these terms is through strip theory. The added mass and damping coefficients are tabulated for a set of 2D shapes, such as cylinder, square and wedges. The submerged part of the structure is divided in several 2D cross-section (strips) and the added mass and damping coefficients computed for each cross-section. Then, these coefficients are integrated over the length of the ship to obtain the final value of the structure added mass and damping coefficient term.

The restoring forces and moments can be related with a spring constant. They are caused by the hydrostatic force acting on a point of the wetted surface due to its motion, and the structure weight. The restoring coefficient is characterized as:

$$F_i^{Rst} = -C_{ij}\eta_j, \qquad \text{with } i,j = 3{,}4{,}5 \tag{17}$$

A restoring coefficient due to the mooring is also of a certain importance to take into account when dealing with moored floating structures. More on this on the mooring section, further on.

The equations of motions for the floating structure are achieved by:

$$Radiation\ Forces + Restoring\ Forces + Exciting\ Forces\ =\ Inertial\ Forces$$

This then becomes:

$F_i^{RF} + F_i^{Rst} + F_i^{DF} + F_i^{FK} = F_i^M$, where $F_i^M = M_{ij}\frac{d^2\eta_j}{dt^2}$ and M_{ij} is the structure mass component (18)

By substitution and reordering of the above terms, the equation of motion formulation is obtained as:

$$-a_{ij}\frac{d^2\eta_j}{dt^2} - b_{ij}\frac{d\eta_j}{dt} - C_{ij}\eta_j + A_i1a_1 + A_i2a_2 + A_i3a_3 - \rho\iint \frac{\partial\phi_I}{\partial t}n_i dS = M_{ij}\frac{d^2\eta_j}{dt^2} \tag{19}$$

$$A_i1a_1 + A_i2a_2 + A_i3a_3 - \rho\iint \frac{\partial\phi_I}{\partial t}n_i dS = (M_{ij} + a_{ij})\frac{d^2\eta_j}{dt^2} + b_{ij}\frac{d\eta_j}{dt} + C_{ij}\eta_j$$

$$(M_{ij} + a_{ij})\frac{d^2\eta_j}{dt^2} + b_{ij}\frac{d\eta_j}{dt} + C_{ij}\eta_j = A_i1a_1 + A_i2a_2 + A_i3a_3 - \rho\iint \frac{\partial\phi_I}{\partial t}n_i dS = F_i^{ext}$$

Which in the matrix form becomes the known formulation:

$$[M + a]\left\{\ddot{\eta}\right\} + [b]\left\{\dot{\eta}\right\} + [C]\{\eta\} = [F^{ext}] \tag{20}$$

3.2.2. Irregular Waves

The use of linear theory is used to analyse the motions and loads under de action of irregular waves. It is used to treat the waves statistically, and the long-crested irregular sea is obtained as a sum of several different wave harmonic components., as shown on eq.(21).

$$\zeta = \sum_{j=1}^{N} \overline{\zeta_j}\sin(\omega_j t - k_j x + \varepsilon_j) \tag{21}$$

In this statistical treatment the wave amplitude is described by a wave spectrum. This variance density spectrum describes the distribution of the wave elevation (a time series) over its different frequencies. The spectrum can be computed from wave measurement or one of the formulations available can be used, where the input will be some parameters such as significant wave height (H_s) and peak period (T_p). Examples of such formulations are:

- JONSWAP spectrum
- Pierson-Moskowitz spectrum
- ISSC spectrum (a parameterized for of the Pierson-Moskowitz)
- ITTC spectrum (a form of the Pierson-Moskowitz)

Spectral Analysis

From the variance density spectrum, $S(\omega) = [m^2/Hz]$, some parameters of interest can be computed.

$$\sigma^2 = \int_0^\infty S(\omega)d\omega = m_0, \text{ variance spectrum} \tag{22}$$

The variance can be understood as the spectral moment of zero order (n=0). Being the spectral moment given by:

$$m_n = \int_0^\infty \omega^n S(\omega) d\omega \tag{23}$$

With the spectral moment definition, other parameters can be computed.

$H_s = 4\sqrt{m_0}$, significant wave height (average of the 1/3 largest waves) (24)

$T_m = 2\pi \left(\frac{m_0}{m_1}\right)$, mean wave period (25)

$T_z = 2\pi \sqrt{\frac{m_0}{m_2}}$, period between zero upcrossings (26)

$T_c = 2\pi \sqrt{\frac{m_2}{m_4}}$, mean period between crests (27)

It is assumed that the wave elevation is a Gaussian, stationary process with zero mean. Therefore, the probability distribution of a certain value ξ can be estimated from a Rayleigh distribution. This is also used to compute the maxima and minima.

$$p(\xi) = \frac{\xi}{E} exp\left(-\frac{\xi^2}{2\sigma^2}\right) \tag{28}$$

Due to the random distribution of phase angle, the amplitudes in each simulation are slightly different. It is found that over a large number of simulations, the extreme values obey to their own probability distribution. Therefore, Goda (2000), suggests that the most probable value for ζ_{max} (maxima of elevation) is:

$\zeta_{max} = \sqrt{2m_o \ln\left(\frac{t}{T_z}\right)}$, where t is the time duration (29)

To produce the wave elevation model time history, as mentioned before, the summation of independent harmonic components is used.

$$\zeta(t) = \sum_i \overline{\zeta_i} \cos(\omega_i t - \varepsilon_i) \tag{30}$$

The phase angle, ε_i, is randomly attributed and the mean amplitude of a component, $\overline{\zeta_i}$, is given by:

$$\overline{\zeta_i} = \sqrt{2S(\omega_i)\delta\omega} \tag{31}$$

Response Analysis

By considering that waves statistics change slowly, a stationary process can be assumed. Therefore, the response spectrum can be computed from the response amplitude operator (RAO) and the wave variance density spectrum.

$$S_j(\omega,\beta) = |RAO|^2 . S_\zeta(\omega), \quad \text{where } RAO(\omega,\beta) = \left|\frac{x_j(\omega,\beta)}{\zeta_a}\right| \tag{32}$$

The RAO are a useful and commonly used engineering concept. The RAO gives, as a function of frequency, the amplitude of the response per unit of wave amplitude. Complementary, for each wave direction a different RAO must be computed.

3.3. Mooring Systems

Position and motion control of the farms, against waves, current and wind loads, is accomplished by a mooring system. There are two main mooring systems philosophies used on floating structures. Systems made up of cables and the dynamic position systems (DPS), or a combination of both, as suggested by (Høiland 2017). On this work the dynamic position systems will not be discussed, in consideration of the research performed, no such systems were yet used for offshore aquaculture solutions.

Systems made up of cables can be of two types, taut and catenary. In taut systems the mooring line leaves the seabed with an angle, meaning that the anchor is under both horizontal and vertical loads. While on the catenary configuration the mooring lines terminate horizontally with the seabed, leading to horizontal forces on the anchor. The restoring forces on a taut system are provided by the cable axial stiffness. By opposition, on a catenary system the restoring forces are due to the cable weight. This force changes according to the cable configuration, introducing a geometric stiffness component. Next section describes how to perform a static analysis of a cable line.

3.3.1. Static Analysis of a Catenary Line

The following review is a description of the inelastic cable line (catenary) theory presented by Faltinsen (1990). Since it is an important part of this work, a more detail review will be made on this section.

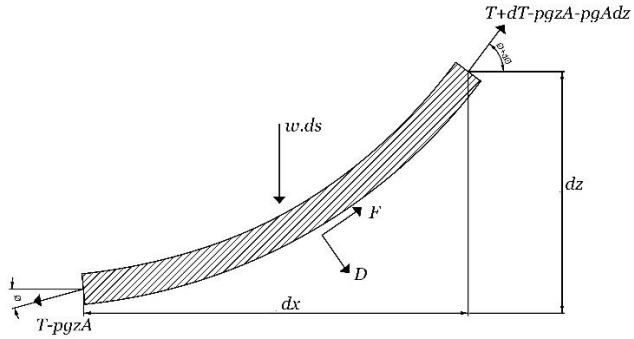

Figure 5 - Element of a mooring line. Image reproduced from Faltinsen (1990)

It will be assumed that the line is in a vertical x-z plane, no account of dynamic effects and the bending stiffness is neglected. With this in mind, the mean hydrodynamic forces on an element of the line are given by:

$$\begin{aligned} dT - \rho g A dz &= \left[w\sin\phi - F\left(1 + \frac{T}{AE}\right)\right] ds \\ Td\phi - \rho g A z d\phi &= [w\cos\phi + D(1 + \frac{T}{AE})]ds \end{aligned} \tag{33}$$

This set of equations are non-linear and an exact solution is hard to find. So, the author of the book proposes the neglection of the current forces *F* and *D*. The equations then become:

$$dT - \rho g A dz = w\sin\phi ds \tag{34}$$

$$Td\phi - \rho g A z d\phi = w\cos\phi ds \tag{35}$$

By introducing the notation $T' = T - \rho g z A$ and through integration, the following relations can be obtained:

$$s - s_0 = \frac{T_0'\cos\phi_0}{w}[\tan\phi - \tan\phi_0] \tag{36}$$

$$x - x_0 = \frac{T_0'\cos\phi_0}{w}\left(\log\left(\frac{1}{\cos\phi} + \tan\phi\right) - \log\left(\frac{1}{\cos\phi_0} + \tan\phi_0\right)\right) \tag{37}$$

$$z - z_0 = \frac{T_0'\cos\phi_0}{w}\left[\frac{1}{\cos\phi} - \frac{1}{\cos\phi_0}\right] \tag{38}$$

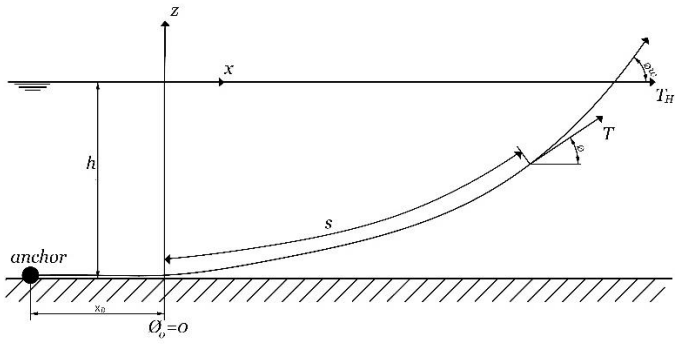

Figure 6 - Coordinates of a catenary system. Image reproduced from Faltinsen (1990)

By establishing that $\phi_0 = 0$, $x_0 = 0$, $s_0 = 0$ and $z_0 = -h$, eq. (37) becomes:

$$\frac{xw}{T_0'} = \log\left(\frac{1+\sin\phi}{\cos\phi}\right) \tag{39}$$

From the hyperbolic definitions of $senh = \frac{e^x - e^{-x}}{2}$ and $cosh = \frac{e^x + e^{-x}}{2}$ it is possible to rewrite eqs. (36) and (38):

$$s = \frac{T_0'}{w}\sinh\left(\frac{w}{T_0'}x\right) \tag{40}$$

$$z + h = \frac{T_0'}{w}\left[\cosh\left(\frac{w}{T_0'}x\right) - 1\right] \tag{41}$$

The quotient of eq. (34) with (35) gives:

$$T_0' = T'\cos\phi \tag{42}$$

The author states that the horizontal component at the water surface is:

$$T_H = T\cos\phi_w \tag{43}$$

and from the notation $T^{'} = T - \rho g z A$ and eq.(42) and (43), was derived the relation $T_0' = T_H$.
The tension on the line is then derived:

$$T^{'} = T - \rho g z A \rightarrow T - \rho g z A = \frac{T_0'}{\cos\phi} \rightarrow T = T_H + wh + (w + \rho g A) \tag{44}$$

The tension's vertical component is found by the integration of the axial tension:

$$dT'_Z = d(T'\sin\phi) = dT'\sin\phi + T'\cos\phi d\phi = w\sin^2\phi ds + w\cos^2\phi ds \rightarrow T'_Z = ws \quad (45)$$

At the point where the mooring line ends, at the water surface, this component becomes:

$$T_Z = ws \quad (46)$$

From eq.(44) the maximum tension on the line is:

$$T_{max} = T_H + wh \quad (47)$$

With the above equation and the discussion so far done, the author proposes the minimum line's length (l_{min}) and the horizontal distance (X) between the anchor and the line's end at the water surface:

$$l_{min} = h\left(2\frac{T_{max}}{wh} - 1\right)^{\frac{1}{2}} \quad (48)$$

$$X = l - l_s + x = l - h\left(1 + 2\frac{T_H}{hw}\right)^{\frac{1}{2}} + \frac{T_H}{w}\cosh^{-1}\left(1 + \frac{hw}{T_H}\right) \quad (49)$$

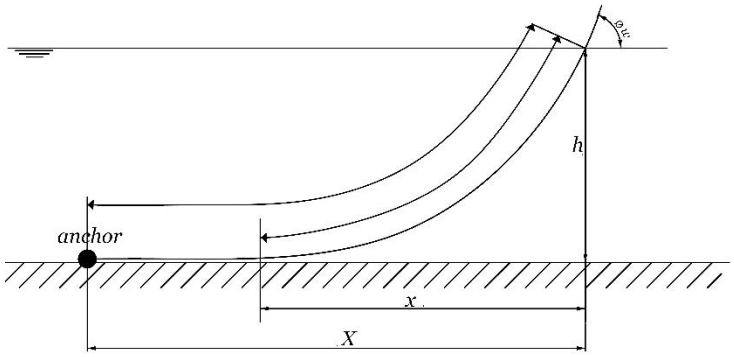

Figure 7 - Catenary line lengths. Image reproduced from Faltinsen (1990)

From the static analysis it is possible to obtain the mooring line restoring coefficient. Since the line can be compared with a stiff linear spring, the restoring coefficient is of great value to be used on a quasi-static/dynamic analysis of the system (Chakrabarti 2005).

With eq. (49) it is possible to plot a graph, shown on Figure 8. Aided by the graph and by knowing the average of the external forces (current, wave and wind) on the structure, it is possible to obtain the surge restoring coefficient C_{11} from:

$$T_H = T_{H_{avg}} + C_{11}\eta_1, \text{ where } \eta_1 \text{ is the horizontal motion of the structure} \quad (50)$$

An alternative method is by solving eq. (49) in order to T_H and then differentiating to X, as proposed by the author in (Faltinsen 1990).

$$C_{11} = \frac{dT_H}{dX} = w\left[\frac{-2}{\left(1 + 2\frac{T_{H_{avg}}}{wh}\right)^{\frac{1}{2}}} + \cosh^{-1}\left(1 + \frac{wh}{T_{H_{avg}}}\right)\right]^{-1} \tag{51}$$

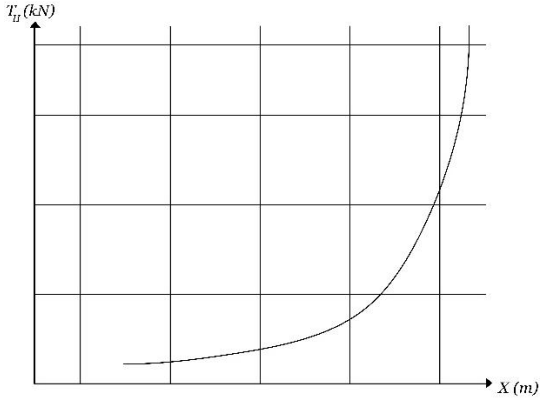

Figure 8 - Horizontal force from mooring line on a structure, as function of the horizontal distance between anchor and line's end. Image reproduced from Faltinsen (1990)

Elastic Cable

With the use of wire and synthetic cables, the line elasticity must be taken into account. By introducing the relation between stretched (dp) and unstretched (ds) length:

$$dp = ds\left(1 + \frac{T}{AE}\right) \tag{52}$$

The horizontal distance between the touchdown point and the fairlead, x, and the vertical distance, h, became:

$$x = \frac{T_H}{w}\cosh^{-1}\left(1 + \frac{hw}{T_H}\right) + \frac{T_Z . T_H}{w(AE)} \tag{53}$$

$$h = \frac{T_H}{w}\left[\frac{\sqrt{T_H^2 + (T_Z)^2}}{T_H} - 1\right] + \frac{T_Z^2}{2.AE.w} \tag{54}$$

It is important to point that wire cables have relatively linear elastic mechanical properties, whilst synthetic fibres cables have non-linear ones, such as the creep phenomenon(Wang et al. 2018). This should be taken into account in the design phase.

3.3.2. Dynamic Analysis of a Catenary Line

A dynamic analysis accounts for the additional loads on the mooring lines, the damping and inertial forces. As mentioned on section 2.3, the analysis can be coupled on uncoupled. Depending if the mooring line dynamics is influencing the floating structure motions or not (Chakrabarti 2005). On the same book, the author states that for deep-water mooring the coupled effects are important and should be analysed. The coupled effects are recognized to influence mainly low frequencies motions on floating structures such as FPSO's. In addition, on their publication about coupled mooring analysis of CALM buoys (Bunnik et al. 2002), the authors highlight that the dynamic behaviour of the mooring lines are relevant for first-order motions of floating structures such as buoys.

3.4. Software

3.4.1. FhSim

One of the softwares used in this work is the FhSim, developed at *SINTEF Fisheries and Aquaculture*. This software was conceived to work in a collaborative fashion, where new software components could be constantly added to improve its functionalities. This work will not contribute to its improvement, as the software will only be used from the user point of view, not a developer's one. Aquaculture systems are characterized by having several flexible components, like nets, cables and chains, represented by non-linear equations. Therefore, the software goal is to integrate these equations over a time period.

The modelling of the systems is broken up in several associated sub-models. Sub-models are made of SimObjects. Each SimObject is characterized by its mass, considered constant, and has a force as an input and its position and velocity as output. The outputs are obtained through the integration of the position and velocity derivatives. A detailed and more comprehensive description of the software can be found in (Reite et al. 2014). The net elements are modelled as an assemblage of triangular net elements, linked by it nodes, as proposed in (Priour 1999). Hydrodynamic forces are obtained by application of a Morison type expression, validated by (Birkevold et al. 2014), and external forces are applied in the nodes. Cable and chain elements are modelled as 6 DOF rigid bar elements. The imposition of axial and angular constraints makes it possible to achieve the desired structural properties, such as bending and axial stiffness.

3.4.2. SIMA

The analysis of the hydrodynamic loads and behaviour of the fish cage will be carried out with the software SIMA- *Simulation Workbench for Marine Applications (*SIMA*)* by DNV-GL, from the SESAM package.

The elements in the model will be subjected to weight, hydrostatic and hydrodynamic loads. The aerodynamics loads will not be considered in the analysis, for the sake of the analysis it will be

assumed that the majority of the structure is submerged, with the floating collar being partially submerge and only a reduce area is exposed to the wind.

A brief description of the load computation procedure employed by the software is given below.

3.4.2.1. Load Computation Procedure

- **Submerged Elements**

The software has two approaches to compute the loads on submerged elements through Morison equation or through MacCamy-Fuchs with quadratic drag. Since the farm system to be considered is composed mainly by slender structures, large diameter structures (compared with the wavelength) are non-existent, the Morison formulation will be used. Where the hydrodynamic force on each element of length dx is decomposed on its three components and given by eq.(55), eq.(56) and eq.(57). This formulation has the option of including a liner-drag term, C_{DL}, but the validation procedure carried out on chapter 0 showed that this term should not be taken into consideration, since it was not producing accurate results.

$$F_x = dx\left[(\rho A + m_a)\dot{u} - m_a\ddot{x} + C_D\left|U_c + u - \dot{x}\right|\left(U_c + u - \dot{x}\right) + C_{DL}\left(U_c + u - \dot{x}\right)\right] \quad (55)$$

$$F_y = dx\left[(\rho A + m_a)\dot{v} - m_a\ddot{y} + C_D\left|U_c + v - \dot{y}\right|\left(U_c + v - \dot{y}\right) + C_{DL}\left(U_c + v - \dot{y}\right)\right] \quad (56)$$

$$F_z = dx\left[(\rho A + m_a)\dot{w} - m_a\ddot{z} + C_D\left|U_c + w - \dot{z}\right|\left(U_c + w - \dot{z}\right) + C_{DL}\left(U_c + w - \dot{z}\right)\right] \quad (57)$$

- **Partially Submerged Elements**

For the partially submerged sections, each element is divided in sub elements and a 2D strip theory approach is used. The hydrodynamic force on each sub-element is given by eq.(58), where the contributors are the Froude-Krylov, diffraction, radiation and viscous drag forces. The added mass and damping coefficients are computed with the Frank close fit method (Frank 1967) and for the sake of simplification they are assumed to be constant, independent of depth. The viscous loads are computed via the Morison equation.

$$F_H = F_{FK} + F_S + F_R + F_D \quad (58)$$

Where the Froude-Krylov force is given by:

$$F_{FK\,y} = \left(\rho g A_S u_y + \rho A_S \dot{u}_y\right) dx \quad (59)$$

$$F_{FK\,z} = \left(\rho g A_S u_z + \rho A_S \dot{u}_z\right) dx$$, A_S is the submerged cross-section area of the sub-element

The diffraction force by:

$$F_{S\,y} = \left(A_{22}^{(2D)}\dot{u}_y + B_{22}^{(2D)}u_y\right)dx$$
$$F_{S\,z} = \left(A_{33}^{(2D)}\dot{u}_z + B_{33}^{(2D)}u_z\right)dx \quad (60)$$

Where u_y and u_z are the velocity of the water particles on the sub-elements.

The radiation forces:

$$F_{R\,y} = (A_{22}^{(2D)}\ddot{y} + B_{22}^{(2D)}\dot{y})dx$$
$$F_{R\,z} = (A_{33}^{(2D)}\ddot{z} + B_{33}^{(2D)}\dot{z})dx \quad (61)$$

The software employs a simplification by using constant added mass coefficients, in a way that eq.(60) and eq.(61) became:

$$F_{S\,y} = \rho A_S C_{my}\dot{u}_y dx$$
$$F_{S\,z} = \rho A_S C_{mz}\dot{u}_z dx$$
$$F_{R\,y} = -\rho A_S C_{my}\ddot{y}dx$$
$$F_{R\,z} = -\rho A_S C_{mz}\ddot{z}dx \quad (62)$$

The viscous drag forces, divided in longitudinal and transverse, depend on the relative fluid velocity, given by:

$$u_r = u_{current} + u_{wave} - u_{subelement} \quad (63)$$

The longitudinal force for a slender element is given by:

$F_{D\,x} = \frac{1}{2}\rho C_{Dx}L_w|u_{rx}|u_{rx}dx$, where is the wetted cross section circumference (64)

And the transverse forces, dependent of the sub-element width (b) and height (h), are:

$$F_{D\,y} = \frac{1}{2}\rho C_{Dy}h_{rel}|\boldsymbol{u}_\mathbf{r}|u_{ry}dx$$
$$F_{D\,z} = \frac{1}{2}\rho C_{Dz}b_{rel}|\boldsymbol{u}_\mathbf{r}|u_{rz}dx \text{ , where } \boldsymbol{u}_\mathbf{r} = u_{ry} + u_{rz} \text{ and } h_{rel} = \frac{A_S}{A}h \text{ , } b_{rel} = \frac{A_S}{A}b \quad (65)$$

- **Net Elements**

The loads on the net elements are computed through the method of empirical expressions presented by Aarsnes et al. (1990)and mentioned in section 2.1, where the lift and drag force are dependent of the solidity ratio and the drag and lift coefficients, by equation (3). The drag and lift coefficients are not an input, they are rather computed with the solidity ratio and element's angle with

the current, as shown on equation (4). Therefore, they only depend of the solidity ratio and angle of attack. In the software, contrary to the authors method, the velocity reduction factor is not computed empiricaly but it is defined by the user.

The software does not explicitly asks for the twine geometry, its diameter and halflenght, but they are accounted for with the solidity ratio. The software uses a square net mesh, whose solidity ratio is given by:

$$S_n = \frac{2d}{\lambda} - \left(\frac{d}{\lambda}\right)^2 \tag{66}$$

The net element is discretized in several sub elements and then, iteratively, the equilibrium position of each sub element is found taking into account the drag, lift, buoyancy and weight force. Starting at the bottom, where the conditions are known, and going all the way up to the last sub element on the floating collar (Løland 1991). In this way the loads and shape of the net element are found.

- **Time integration methods**

The method employed by the software to find the solution of the dynamic equations is the Newmark β family step-by-step integration method. Within the family, it is possible to choose between different techniques, depending of the value used for β and γ. For this work it was chosen the – constant average acceleration method, with $\beta = \frac{1}{4}$ and $\gamma = \frac{1}{2}$ - by virtue of its known unconditionally stability (Chang 2009). For a θ=1, the relation between displacements, velocities and accelerations is given by:

$$\begin{aligned} \dot{r}_{t+\Delta t} &= \dot{r}_t + (1-\gamma)\ddot{r}_t \Delta t + \gamma \ddot{r}_{t+\Delta t}\Delta t \\ r_{t+\Delta t} &= r_t + \dot{r}_t \Delta_t + \left(\frac{1}{2} - \beta\right)\ddot{r}_t(\Delta t)^2 + \beta \ddot{r}_{t+\Delta t}(\Delta t)^2 \end{aligned} \tag{67}$$

A full description of the implementation of the method is provided in (SINTEF 2019).

3.4.2.2. Model Building

The model building process in SIMA is similar to the other tools in the SESAM package. The initial step is to set up the environment of the analysis: the type of bottom, water depth and the set of environmental loads (wind, waves and current). The second step would be to model the geometry of the structure, this is done in two parts: first the nodal points and then the slender elements. The several nodal points that characterize the structure should be define, with their respective boundary conditions. To model the slender elements is necessary to first define the cross-section's properties of the element, the diameter, weight, axial stiffness, among others. Then, the line-type of the element is defined, where the length, number of elements and type of cross-sections (an element can be made of several cross-sections) are specified. The last step is to specify the nodal points where the ends of the element attach to.

4. Design of Fish Cages

4.1.Classification Societies Standards

From the research carried out for this thesis it can be said that the rules and standards for offshore aquaculture production systems are still on their beginnings. As said on Chapter 1.3, China is already producing fish with an offshore system, so it is reasonable to assume that the farm had to be approved by a classification society. However, no information was found regarding the approval of this Chinese structure. The majority of the information found was produced by DNV-GL, evidencing it as the leading class society on this field. The American Bureau of Shipping (ABS) produced a document in 2018, providing guidelines for the design and surveying of offshore fish farms, as an answer to a need that they saw in the market.

A Norwegian technical standard is already in place and used for aquaculture systems, the NS 9415. On 2017 DNV-GL came forward with a document stating the rules for classification of offshore fish farm units (DNVGL-RU-OU-0503). On the publication (Flagstad and Tvedt 2018), the authors draw attention to a diagram, based on a diagram from the EXPOSED Operations Centre, where they define the area of applicability of each standard. The authors stated that the NS 9415 standard is only suited for wind seas and a wave height of up to 3m. Whilst the DNVGL-RU-OU-0503 rules applies to locations of swell sea. A definition of wind and swell sea seems important to be made, as well as of "offshore".

On Dean and Dalrymple (1991), the distinction between wind and swell sea is:

- Wind Sea: steep waves generated by local winds; With wavelengths of 10/20 times the wave height, smaller than 130 meters, and a period of 1-10 s.
- Swell Sea: long waves generated by distant winds; With wavelengths of 30/500 times the wave height, in the order of hundreds of meters, and a period of 10-30 s.

The use of the above definitions as a criterion to distinct offshore from non-offshore operations is somewhat poor. It gives rise to a grey area, where both conditions might occur. In this rule (DNVGL-RU-OU-0503) there are no specifications regarding the distinction between both.

Froehlich et al. (2017) did a review of a large number of publications, to evaluate the defining characteristics of an offshore aquaculture site. The most common ones were water depth, current velocity and distance from shore. The conclusion was "there is no clear consensus describing what offshore aquaculture really means"(Froehlich et al. 2017). Thus, since there is still a lack of a more precise regulatory framework, the design of offshore aquaculture systems is still strongly dependent of the rules and standards of the offshore oil & gas/energy. The following section will discuss the current classification guidelines of DNV-GL and its relevant documents.

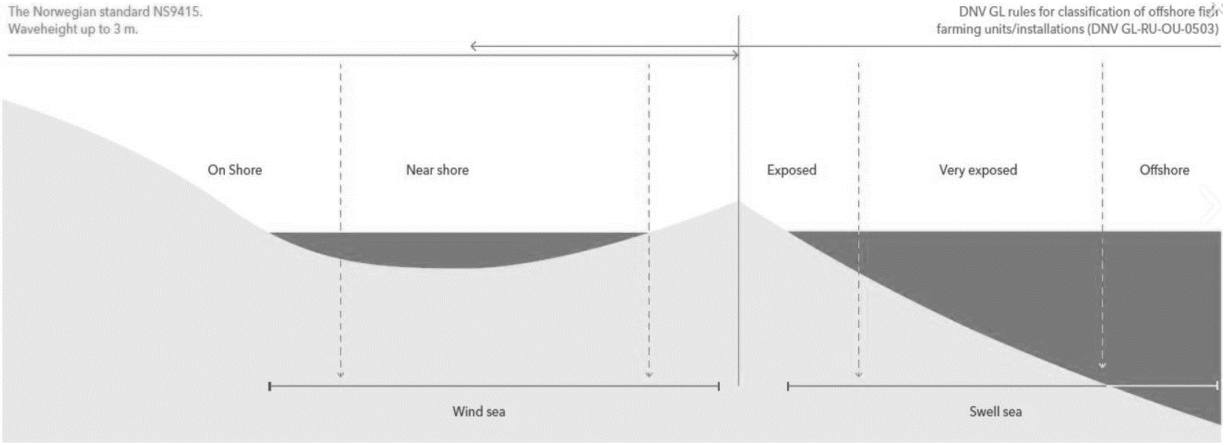

Figure 9 - Applicability of Classification Rules and Standards, redrawn by DNG-GL, from the original publication by SINTEF (SFI EXPOSED)

Another Norwegian standard exists to regulate the operational side of the farms. The *Technical requirements for fish farming installations – NYTEK*. It regulates and directs the establishment of a fish farm and acquisition of equipment. It also provides guidelines to the operation of the farms, with a strong emphasis on the prevention of fish escape.

4.1.1. Regulations Revision

The desired class notation for offshore fish farming installations is the **OI** notation. This notation applies for non-self-propelled fish farming installations, deployed at a given location for an extended period of time, in conformity with all the offshore standards of the classification society. An overview of the different standards and rules on force for offshore aquaculture systems is presented in Figure 10.

There are two paths to follow in the design method chosen, the Load and Resistance Factor Design (LRFD) and the Working Stress Design (WSD). As pointed in the review made by (Yu et al. 2016), the main difference between both is the fact that the LRFD method uses different factors for different loads categories, while the WSD method uses a factor that is non-dependent of the load type. In this work the WSD method was chosen.

According to the document that guides the design process, *OS-C201* (DNV-GL 2015b), the WSD method is characterized by: comparison of the calculated stress with maximum permissible stress, defined by the multiplication of the characteristic strength (or capacity) with a permissible usage factor.

The loads may be divided in: permanent and variable functional loads, such as structure mass, weight of equipment and storage; environmental loads, such as hydrodynamic, waves, current and wind; and accidental, deformation and fatigues loads. The functional loads should be assessed via regular static analysis. The environmental loads, together with environmental data acquisition and modelling, should be assessed with the guidance of *RP-C205* (DNV-GL 2017a). Accidental loads

analysis should follow the directives of *OS-A101* (DNV-GL 2015a). Fatigue analysis is to be carried out through the recommended practice *RP-C203* (DNV-GL 2016).

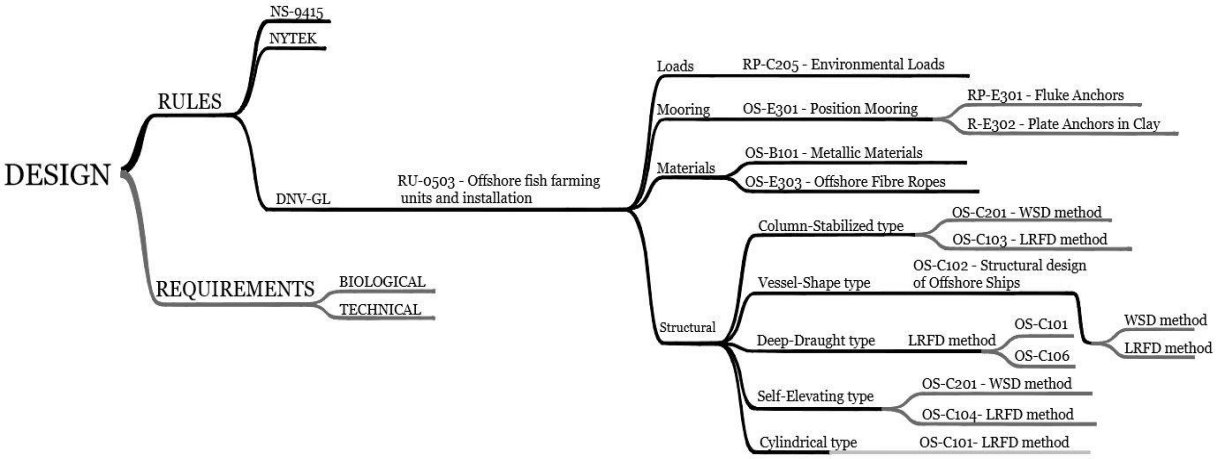

Figure 10 - Overview of the existing regulations and the important documents for the design phase

4.2. Design Principles

The design process can be a prosperous but complicated stage. Due to its emerging character, the offshore aquaculture has still not built up a design trend. Therefore, from this creative detachment can arise important innovative solutions. On the book (Pahl et al. 2015), the steps of the design process can be summarized as:

- Selection and identification of the task
- Identification of requirements and constraints
- Search for working principles, and therefore solutions
- Selection and evaluation of suitable candidates
- Finalize and detail design

In order to identify the task, it is important to identify the main stakeholders. (Shainee et al. 2013) identify the fish, fish farmer and the society as the three main stake holders. From them it is possible to proceed to the identification and the formulation of the task. The task proposed is the conception of a system, placed on an offshore location on Portuguese waters, that can produce fish. That at the same time is a source of wealth and employment for the surrounding community. To formulate the problem to be solved, the requirements or each stakeholder should be identified. According to (Shainee et al. 2013) the following requirements are of importance for the design of a aquaculture system.

For the fish, the parameters are mainly biological. Such as: salinity, temperature, pollution, stocking density, among others. The water motion and available cage volume are also important.

For the farmer, the system should provide good accessibility conditions and allowed tasks such as: feeding, harvesting, treatment, etc. to be performed. It should also provide good conditions for monitoring, whether through a clear water visibility or through installed monitoring technology, or both.

For the society, the production system should have a low environmental impact, with low pollution, escapes and small impact on the ecosystem. It should a good source of employment, income and provide good quality produce.

With the task and requirements settled, the following step is to proceed to the creative domain. Through the analyse of existing ideas and their working principles, on the aquaculture as well as other floating structures fields, and come up with a possible solution, to be evaluated on a further step.

4.3. Possible Solutions

In their work Shainee et al. (2013) make a very interesting review and categorization of different concepts. It is proposed two categories, based on the ability of the system to endure the external conditions. In each category a subdivision is done, with respect to the strategy employed. The categories are:

- Designed to withstand and dissipate the loads
  - Floating rigid
  - Gravity net cages
- Designed to avoid the loads
  - Submerged
  - Submersible
  - Single Point Mooring (SPM) self-submersible

Through the use of the stake holders' requirements, the authors did an analysis of the solutions and reached the conclusion that the SPM was the best solution. It highlights several advantages such as: lower benthic impact, lower energy input, lower mooring cost, among others. For a more detailed understanding (Shainee et al. 2013).

From the research performed, alongside the contributions of the above-mentioned papers, some constraints and requirements were gathered. The next section will go through them in further detail.

4.4. Constraints and Requirements

In this work the primary focus will be on the livestock requirements and structural soundness. No analysis regarding the farmer/worker requirements will be done. Therefore, the motions and accelerations will not be assessed from a seakeeping criterion perspective. From the society perspective no analyses will be done. Therefore, some assumptions were made:

- If livestock conditions are good, then the system is economic viable.
- The offshore location will guarantee an effective spread of the residues.

The constraints and requirements identified as being essential to a successful design are:

- Structural soundness
- Low water motion
- Ability to maintain cage volume

To achieve structural soundness two approaches can be used, as mentioned on section 4.3, avoid or withstand the loads. Here a combination of both strategies is proposed: a rigid structure, with the ability to submerged.

The structural rigid system was chosen mainly because of two factors. First, the ability to maintain the cage volume, suffering no relevant net deformation under strong operational conditions. Second, the possibility to adapt its construction, assumed to be primarily of steel, to existing shipyards. Helping the existent installed resources to adapt to a new emerging market, similar to the Chinese strategy (Harkell 2018).

Although the investigation lead by (Shainee et al. 2013) demonstrated that the SPM cage design might be the best solution for offshore locations, it was decided that for the scale of the cage design this work wants to propose, the SPM mooring solution might be too uncertain, because no utilization is known of a SPM system for such large floating structures. So, a more traditional mooring arrangement is proposed, as described in chapter 7.

4.5. Information Gathering

A good place to start idealizing a structural concept is by looking at what has already been done and learn from it, as mentioned in section 1.3. Figure 11 shows a gathering of pictures of the following relevant projects and concepts is shown:

- **Designed to avoid loads:** Refamed TLC; OCAT; SeaStation;FarmOcean; AquaPod
- **Designed to withstand loads:** Havmerd(OceanFarm); SeaCulture; Artic Offshore Farming; Smart Fish Farm

It is important to note that no Chinese project is shown above, since the visual content found regarding these projects was very scarce. As mentioned before, information on the offshore aquaculture development in China is very scarce.

For the above projects, an aggregation of the volumes and biomass production was done in table 2. For some the information was available while for others an estimation was done based on small pieces of information found in disperse news articles.

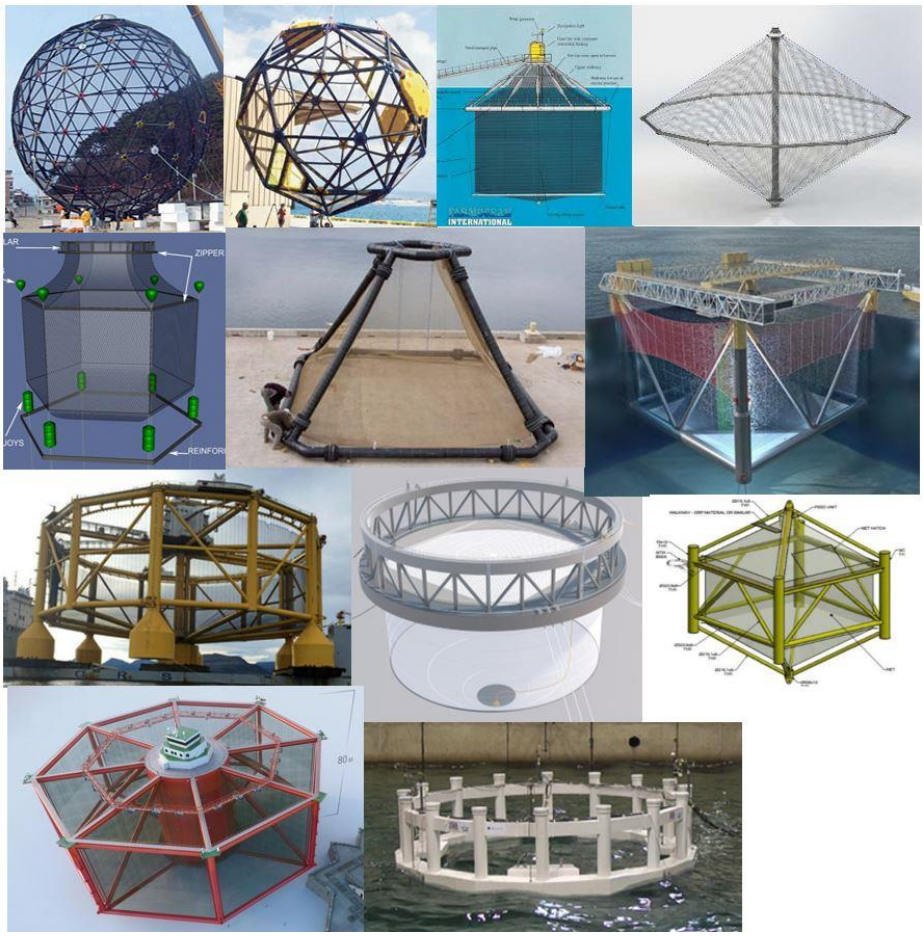

Figure 11-Gathering of projects and concepts. Reproduction of the designs of: InnovaSea Aquapod and SeaStation; Refamed TLC; OCAT cage; FarmOcean; Salmar SA; SeaCulture; NRS/Aker Solutions

*Table 2 - Properties of the concepts in focus. The values marked with * are estimates*

		Volume [m3]	Biomass [t]	Density [kg/m3]
Submersible	Refamed TLC	12,000	* 300	25
	OCAT	100	10	100
	SeaStation	600	* 12	20
	FarmOcean	6000	150	25
	Aquapod	450	10	22
Rigid	Havmerd (OceanFarm)	250,000	10,000	40
	SeaCulture	544	* 8	15
	Artic Offshore Farming	* 150,000	3,000	20
	Smart Fish Farm	510,000	20,000	39
			Avg. Density [kg/m3]	25

From Figure 11, it can be observed that the most common solution employed in rigid systems design is the used of reticulate structures with cylindrical elements. Although shapes are diverse, the majority of the designs employ a polygon shape that is “extruded” to the desired height. The bigger designs also try to implement some type of permanent equipment/facility, for farming support, on top of the structure. On the following section a design proposal is made, and the decision behind it are revealed.

4.6. Mooring design

As said earlier on section 3.3, the mooring system is necessary to keep the farm in place and to maintain operational condition. This means that it must withstand loads from the environment, under the action of waves, current and wind. The classification society DNV-GL, on its document (DNV-GL 2017b), states that the class notation POSMOOR is mandatory. The requirements for this notation are specified on (DNV-GL 2015c). This document specifies the modelling, analysis and equipment for a mooring system. This should be used as an aid during the design process, since no design guidelines are given by the classification society. On this work only a passive mooring system will be considered. The thruster assisted system will be left out, since it is not a common practice in aquaculture systems. Some proposals are appearing, mainly in the vessel shaped design proposed by Nordlaks AS(L. Li, Ong, and Jiang 2017), but they are considered out of the scope of this work.

4.6.1. Prevailing Practices

Currently the majority of the aquaculture installations at sea, using gravity cages or other system, use or a single point mooring (SPM) or some type of spread arrangement. The SPM system is employed, for example, in the pilot facility of *Seaculture SA*. in Portugal (Seaculture 2019). In this work, the focus will be on the spread arrangement.

Currently the spread mooring arrangements employed in aquaculture, for a single cage, consist of eight anchor points securing a rectangular shape grid. This grid is attached to buoys on each of its corners, to keep its buoyancy. The cage is attached to the square grid by bridle lines, this means that the cage is not directly connected to the anchors(Andresen 2017). The depth of the rectangular grid can be chosen to avoid the higher environmental loads that exist near the surface, as specified by (Decew et al. 2010). A representation of this conventional mooring arrangement is shown on *Figure 12*.

In some cases, it is desired to have a larger production capacity, thus a larger number of cages might be preferred over a larger cage. This is accomplished by a multiple cage grid arrangement. These arrangements normally take one of two possible geometries, grouped in a square or in an inline formation, shown on Figure 18. (Li et al. 2011) compared the hydrodynamic behaviour of these two configurations, a further look on this paper will be done in the next chapter. They found that not significant difference exists on the anchor lines tensions and cage volume of the two configurations. Although, they observed that in case of an anchor line failure, the peak loads on the remaining lines will be higher in the inline formation. It is also highlighted in this article that there are more aspects to consider in the choice of the mooring arrangement apart from the engineering ones.

Some particulars to consider in the design phase are wildlife safety and environmental concerns. Wildlife safety concern focus primarily in the seabed destruction caused by the mooring lines and the marine animals' entanglements. This is pointed out in (Decew et al. 2010), and as a solution to the entanglement, it is proposed a higher pretension on the lines and cables with larger diameters (Fredriksson et al. 2004). Regarding the environment, a significant concern is the dispersion of the waste and the flow circulation. The flow circulation might affect the oxygen supply to the farmed animals. As shown by (Løland 1991), the available oxygen can reduce drastically for a series of cages

placed after each other in the current direction (this depends on other factors as well, such as solidity and fish density). The farm's placing regarding the current also influences the dispersion of waste to the surrounding environment and to other facilities in the proximity.

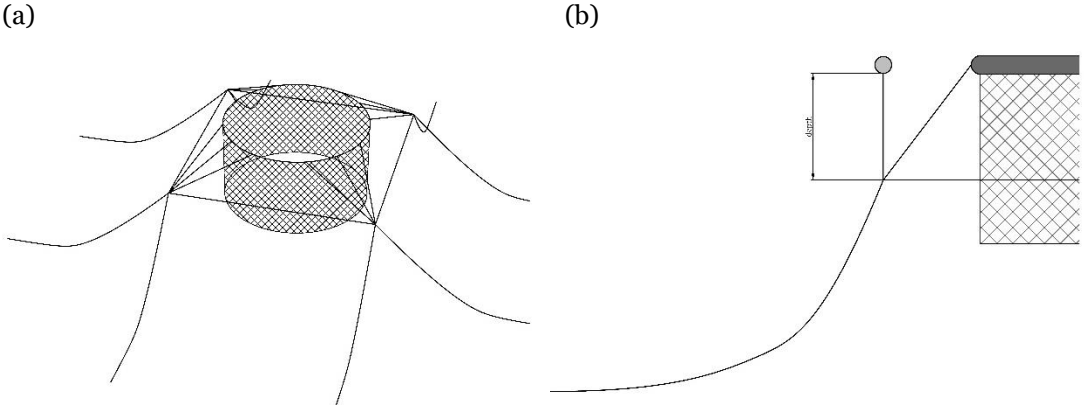

Figure 12 - Conventional mooring arrangement. (a) 3D View. (b) Cross section view

5. Software and modelling validation

The chosen software for the analysis of a fish farm was *SIMA- Simulation Workbench for Marine Applications* (*SIMA*) by DNV-GL. The software is a well-established and trusted commercially available tool. The proposition of this chapter is not to, at any extent, challenge the software, but rather to validate that the model building and testing is being well performed, to gain expertise and skill on its use, and to access this tool suitability for the desired analysis. In their memo at SINTEF (Aksnes 2106), the viability and consistency of results of this software for aquaculture structures was already access, with positive results.

This validation will be done in five stages. One with the analysis of (H. Moe, Fredheim, and Hopperstad 2010) a second with the numerical analysis of (Y.-C. Li et al. 2011), a third with the work of a fellow PhD researcher , the fourth will be a joint work with another fellow PhD researcher and the last with the results of the numerical software FhSim, provided by SINTEF. Some analysis uses more complex systems than others, the criteria for their choice was mainly due to their strength as good sources of results and the possibility of emulating their models in the SIMA platform.

5.1. Single cage numerical comparison

The first comparison analysis was done with the work of Moe et al. (2010), were the results of a numerical analysis are compared with a flume tank model test data from Lader and Enerhaug (2005) with a fairly good agreement. . This work was chosen because it accesses the net geometry as well as the drag forces upon the cage. It was also chosen by virtue of the solidity ratio used, 0.23, that is well within the rage of the most common used values, and it studies of the net behaviour with different weight configurations for several current velocities, which allow a broad comparison with the net behaviour in SIMA

5.1.1. The model

The model consists of a simple gravity net cage, with a stiff floating collar (just to assure a circular shape of the net's top) and suspended weights on its base, as shown on Figure 13. The weights are arranged in three different configurations. The cage is fully submerged, since no waves exist, only the effect of current is of interest.

Table 3 - Model properties and experimental set-up

Cage		
Diameter	1.41	[m]
Height	1.41	[m]
Net		
Sn	0.23	[-]
lw	17.6	[mm]
dw	2	[mm]
r, velocity reduction	0.8	[-]

Configuration	**Weight [kg]**	**nº of weights**	
Weight 1 – W1	0.4	16	
Weight 2 – W2	0.6	16	
Weight 3 – W3	0.8	16	
	Current Velocity Uc [m/s]		
W1	0.33	0.56	
W2	0.21	0.33	0.52
W3	0.34	0.5	

(a) (b)

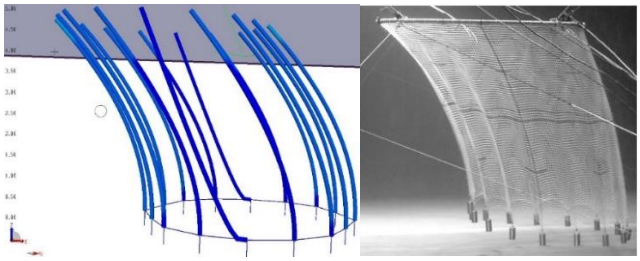

Figure 13 - Cage set-up (a) SIMA, (b) Moe et al.(2010)

5.1.2. Results

To compare the cage geometry between models the coordinates of several key points were measured. This allowed for a side view comparison between the numerical results of the source paper and the numerical results from SIMA.

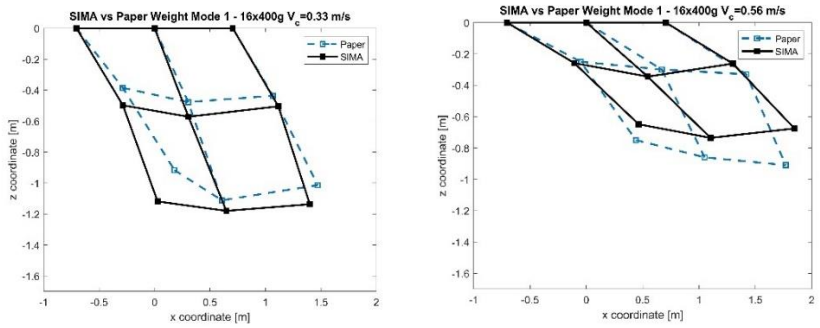

Figure 14 - Side view comparison, weight mode W1

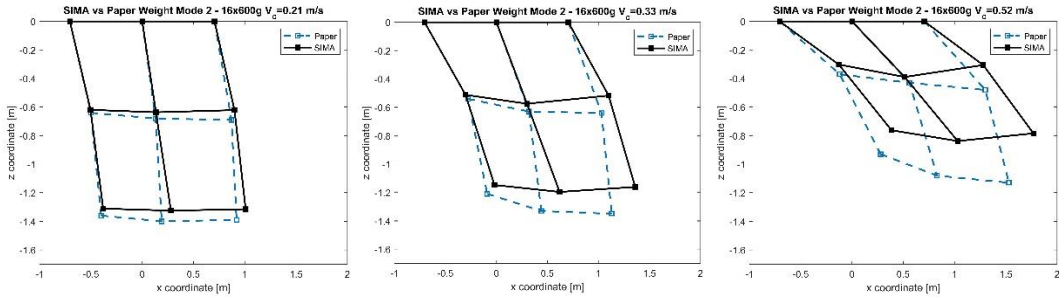

Figure 15 - Side view comparison, weight mode W2

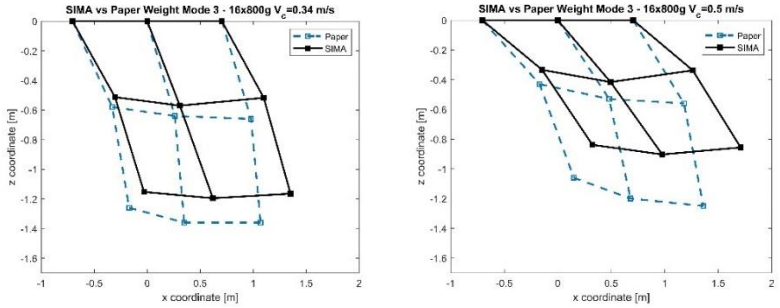

Figure 16 - Side view comparison, weight mode W3

In general, the displacements from SIMA are larger than the source paper. Somehow the load upon the net elements is larger. A good reason for this could be a modelling problem that rose.

In the source paper, the net was modelled as being buoyancy neutral. On SIMA this was not possible. For smaller current velocities the loads on the model were extremely higher than the source paper, and for the larger current velocities the static solution kept diverging and was unstable. (more on this stability on a later section of this chapter). The above results, and system stability, were achieved when the net had a volume of 0.2 $\left(\frac{m^3}{m}\right)$ and a weight of 0.5 $\left(\frac{\text{kg}}{m}\right)$.

This was somehow disappointing and not fully understood. Some tests were run with singular net elements with neutral buoyancy on SIMA, and static solutions were achieved successfully. So, it was not understood why it failed with the desired configuration for this comparison. It could be some limitation of the software, some modelling error or, less probable, some information missing on the source paper.

The drag forces were also compared, between the values from the source paper numerical analysis and the previously mentioned model test.

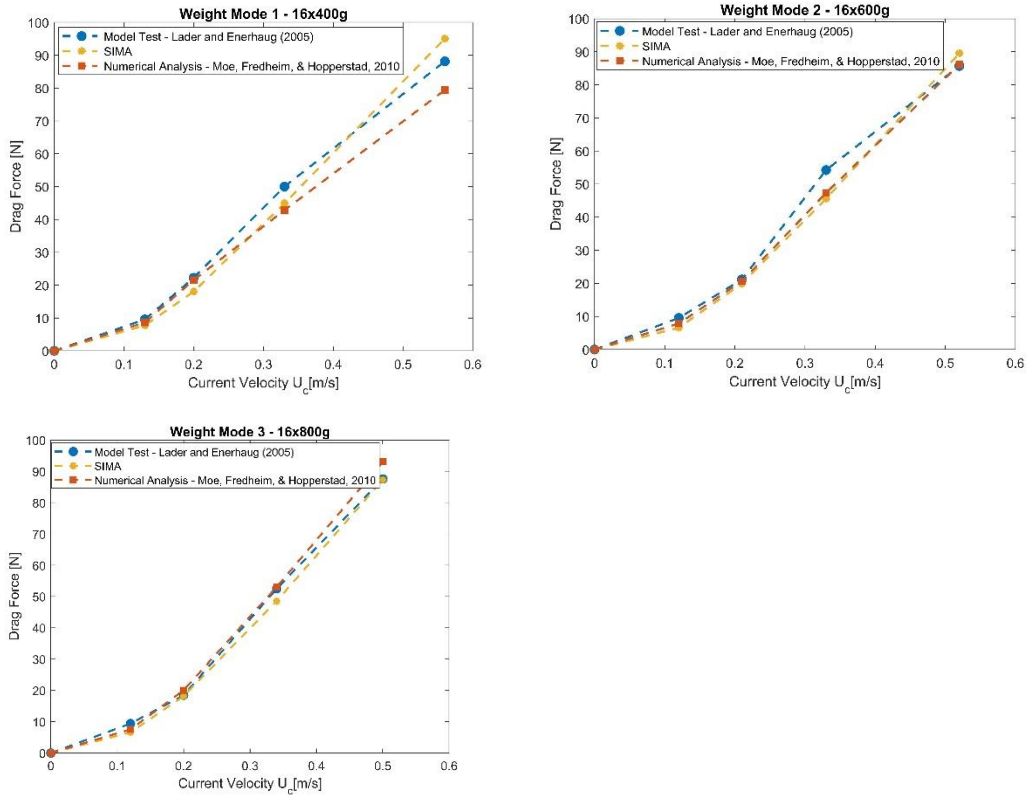

Figure 17 - Drag force upon the net cage

5.2. Numerical comparison of a grid system of cages

An attempt was done to analyse a more complex and realistic cage system, through the comparison of the mooring lines loads. Ideally with data from a fish farm in real sea conditions. The only real deployment data found was the experiments by (Fredriksson et al. 2007). This field experiment used a central spar fish cage, such as the *Ocean Spar* model, that was not possible to model in the *SIMA* software used on this work. So, an alternative had to be found. It was decided to use the results from a numerical analysis. The experiment and analysis of Li et al. (2011) was chosen, due to the clarity of the data expressed and to their comparison of two different arrangements of the fish farm, since it would be interesting to test the possibility of using *SIMA* to compare different cage arrangements.

5.2.1. The model

The model consists of four cages, arrange in two different layouts (L1 and L2), as shown on Figure 18. Each cage is a simple gravity net cage composed of a circular floating collar, a bottom weight ring and a flexible net. Some properties of the model used by (Li et al. 2011) were not made available in the agreement publication. So, some tuning of the model in this work had to be performed until an acceptable accordance was found.

Table 4 - Model properties

Floater		
Young Modulus	1000	[MPa]
Weight	1.2	[Kg/m]
Diameter	350	[mm]
Bottom Ring		
Young Modulus	10	[MPa]
Weight	35	[Kg/m]
Diameter	350	[mm]
Mooring Lines		
Young Modulus	20	[MPa]
Weight	3.5	[Kg/m]
Diameter	40	[mm]
Axial Stiffness (*EA*)	2.5e5	[N]
Grid Lines		
Young Modulus	20	[MPa]
Weight	1.43	[Kg/m]
Diameter	40	[mm]
Axial Stiffness (*EA*)	2.5e5	[N]
Net		
Sn	0.12	[-]
lw	11.7	[mm]
dw	0.72	[mm]

Nº elements	
Floater	48
Bottom Ring	48
Mooring	15
Grid	5
Bridle	7

Some unavailable data was taken from other works. Namely the net drag and added mass coefficients. The drag coefficient was computed according to eq.(4) and the added mass coefficient as proposed by (Chen and Christensen 2016) on their study on the resistance of porous nets.

$C_m = 0.34\frac{1-n}{n}$, where n is the net porosity (68)

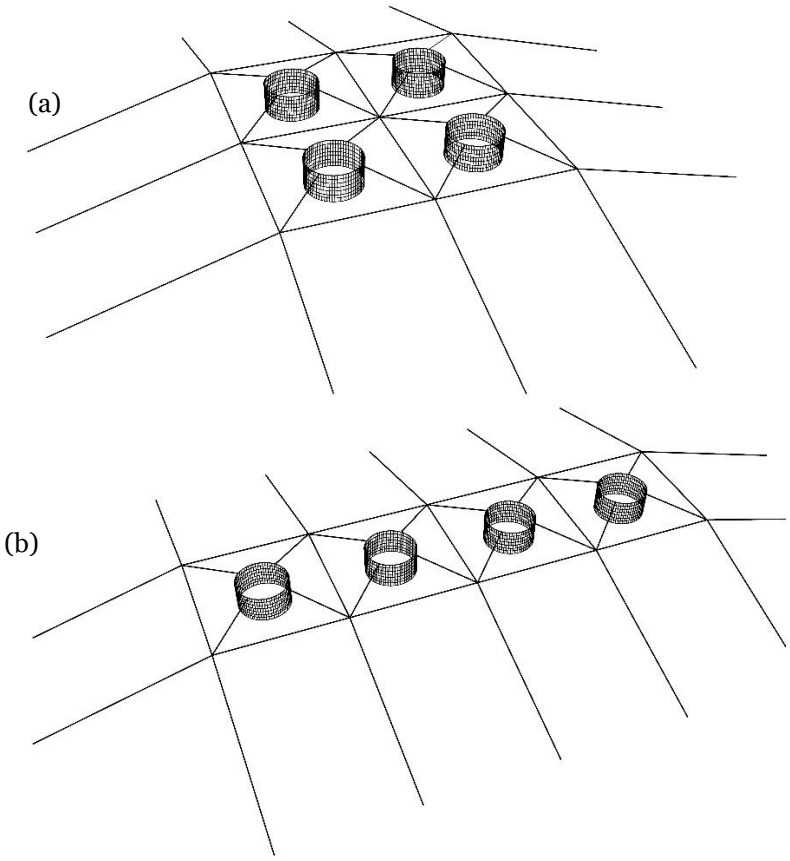

Figure 18 - (a) Layout 1;(b) Layout 2

The system was under the action of regular waves, with a height $H = 5.6\ m$ and a period of $T=8.8s$ with no current. The waves came from a direction of 0º with the system. Figure 19 shows the model implemented on *SIMA*.

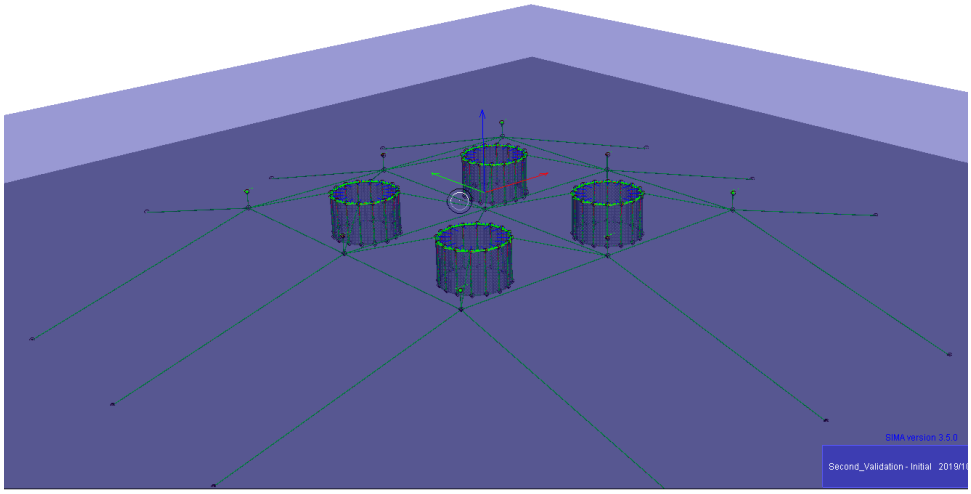

Figure 19 - SIMA model of layout 1, L1

5.2.2. Results

The axial tension on the mooring, grid and bridle cables of the system were assessed and compared with the numerical results of Li et al. (2011). Since some parameters were unknown, as mentioned in the previous section, some runs of the SIMA model were done to tune the model.

The final results for layout number 1 (L1) are shown graphically on Figure 20.

Although there was a certain degree of uncertainty in the construction of this model, due to the lack of some information on the system properties, there was a good agreement between the two analysis.

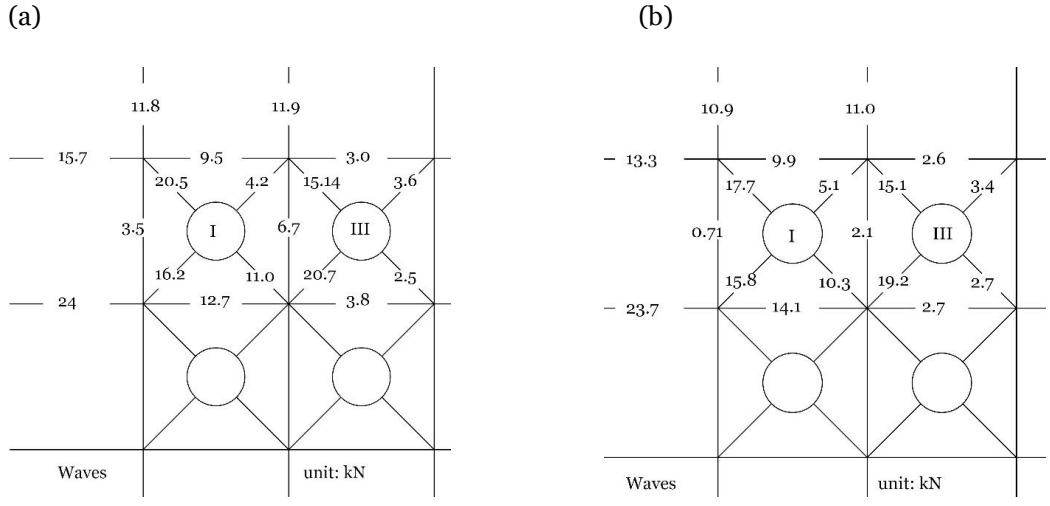

Figure 20 – Maximum axial tension on the mooring system. (a)paper results; (b) SIMA analysis results

The results for layout number 2 (L2) are presented on fig Figure 21.

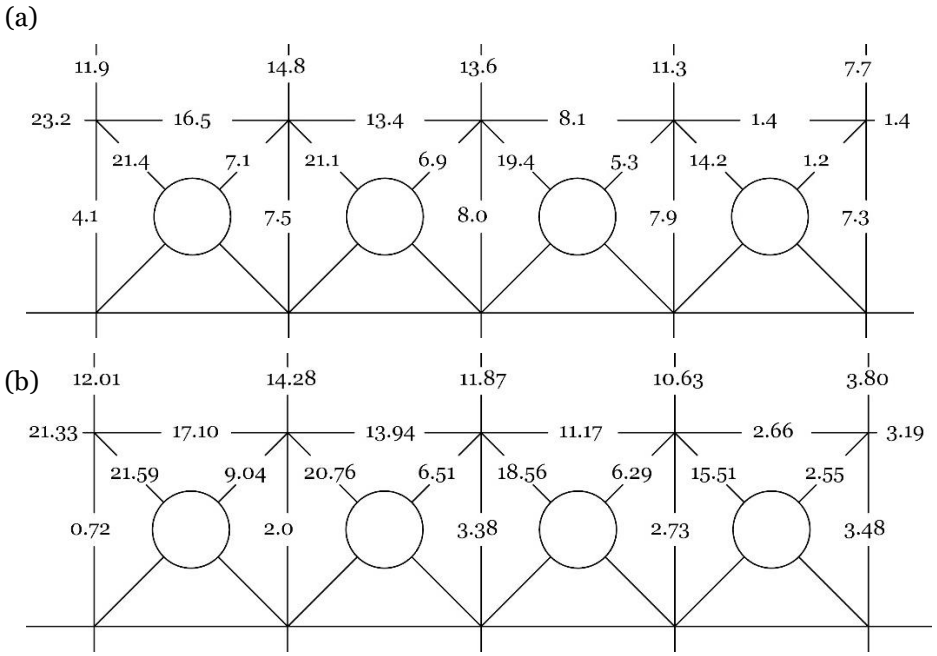

Figure 21 – Maximum axial tension on the mooring system. (a)paper results; (b) SIMA analysis results

In general, a good agreement exists between the two sets of values. As with the values from L1, the maximum value of tension for the perpendicular (with respect to the current's direction) grid lines (marked in red in Figure 22) are well below the values of obtained in the reference numerical analysis. These low values of tension on these mooring lines is due to the fact that they remain mostly slack during the analysis. This slack configuration is caused by the coming together of the grid points (as illustrated on Figure 22), due to movement of the cage in the direction of the waves, and the consequent force caused by the bridle lines on the grid points in question.

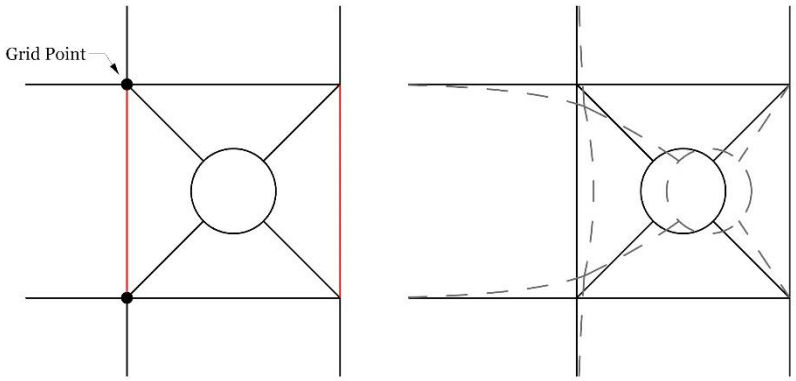

Figure 22 - Slackness of perpendicular grid lines

No significant reason was found as why this behaviour was expressed so strongly on the *SIMA* compared with the numerical analysis of the paper.

5.3. ABAQUS model numerical comparison

In order to reach the validation goal of this chapter, and simultaneously share knowledge and experiences, a comparison with the calculations of Zhongchi Liu at CENTEC was conducted. Together, a simple model of a moored gravity net cage was agreed upon. With this decision it was hoped that the influence of the different modelling parameters on the cage behaviour could be understood. In addition, this validation enables a comparison between two different numerical softwares, specifically of the modelling process, analysis procedures and results treatment.

5.3.1. The model

The third validation analysis will be done with the numerical results obtained by Zhongchi Liu on his research using ABAQUS. A simple system was modelled, represented on Figure 23. The values of the displacements on specific points as well as the mooring line axial forces were then compared. Both systems consist of a cylindrical cage, with a floating collar and a weight ring on its bottom, which was held in place by four horizontal mooring lines, on a 45° angle with the direction of the waves and current.

The modelling differences between the two systems are:

- The representation of the net
- The mooring line

The net is represented in different ways on both approaches. In the software *SIMA* the net is represented by a series of vertical bar elements, subdivided in smaller elements, with equivalent properties (more on chapter 3, section 3.4.2). In the work of Zhongchi Liu, the net is represented by an equivalent net, with less twines, but equivalent properties, as done by (Le Bris and Marichal 1999) and (Moe, Fredheim, and Hopperstad 2010). Each twine is modelled as a truss element, with no bending or compression stiffness. The properties and dimensions of the models are shown on Table 5.

In the work of Zhongchi Liu the mooring is modelled as a non-linear spring, uncapable of compression. Such representation is not available in the *SIMA* workbench element library. So, a cable/bar element with as equivalent as possible properties was used.

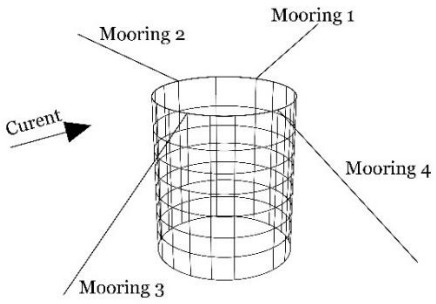

Figure 23 - Modelled system, with four mooring lines and a simple gravity net cage

Table 5 - Model properties

Cage		
Diameter	20	[m]
Height	20	[m]
Floater Ring		
Diameter of Tube	300	[mm]
E	950	[MPa]
Bending Stiffness	3.78e05	[N.m2]
Thickness	48	[mm]
Weight	16.78	[kg/m]
C_D transversal	1.2	[-]
C_M	2	[-]
Mooring		
Stiffness	6000	[N/m]
Axial Stiffness (*EA*)	1.91e05	[N]
Cd	0	[-]
Ca	0	[-]

Base Ring		
Diameter of Tube	100	[mm]
E	950	[MPa]
Bending Stiffness	4.6e03	[N.m2]
Thickness	0	[mm]
Weight	23.56	[kg/m]
C_D transversal	1.2	[-]
C_M	2	[-]
Net		
Sn	0.25	[-]
lw	15	[mm]
dw	2	[mm]
Environment	Height [m]	Period [s]
Regular waves	1	10
Current velocity	0.5	[m/s]

Nº elements	
Floater	60
Bottom Ring	60
Mooring	30

The models were run under a regular wave plus current situation.

5.3.2. Results

Similarly to the first validation, the selected points for the displacements measurements are shown on Figure 24. It was decided that the most interesting locations were the floating collar, mid-depth and at the base, again similar to the first validation. Since the displacements of this points would give a good overview of the cage behaviour in waves and the net deflection behaviour.

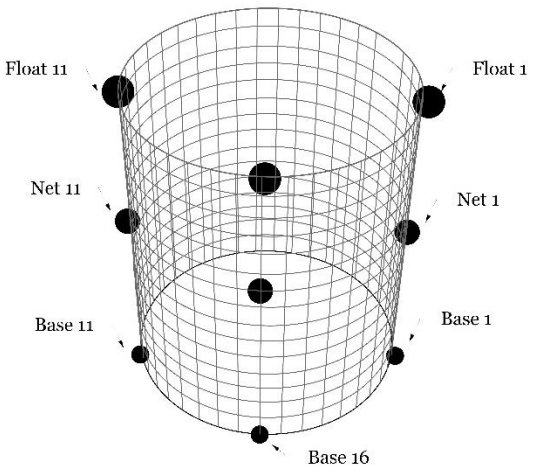

Figure 24 - Points of interest for measurements

Since there was no significant movement of the cage in the y direction, the displacements were compared for the x and z direction. Being the positive x direction aligned with the positive current direction. The comparison was divided between upstream and downstream points.

(a) *(b)*

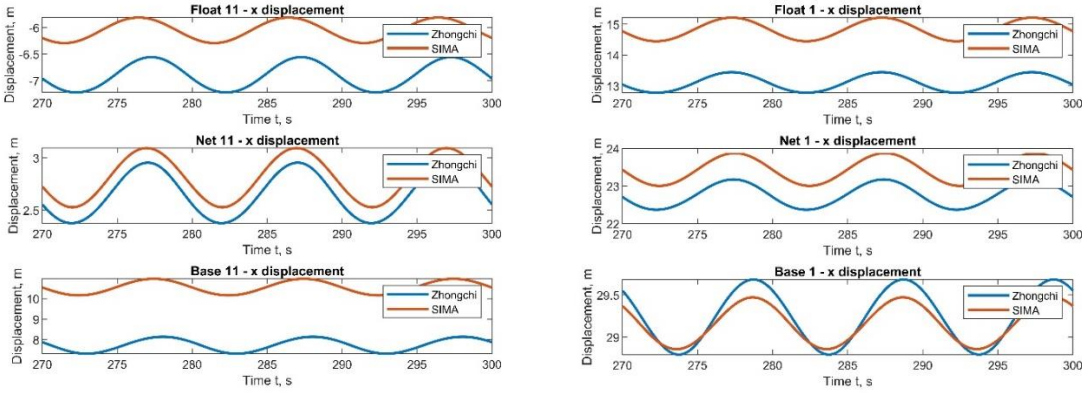

Figure 25 - (a) Upstream x displacements. (b) Downstream x displacements

(a) *(b)*

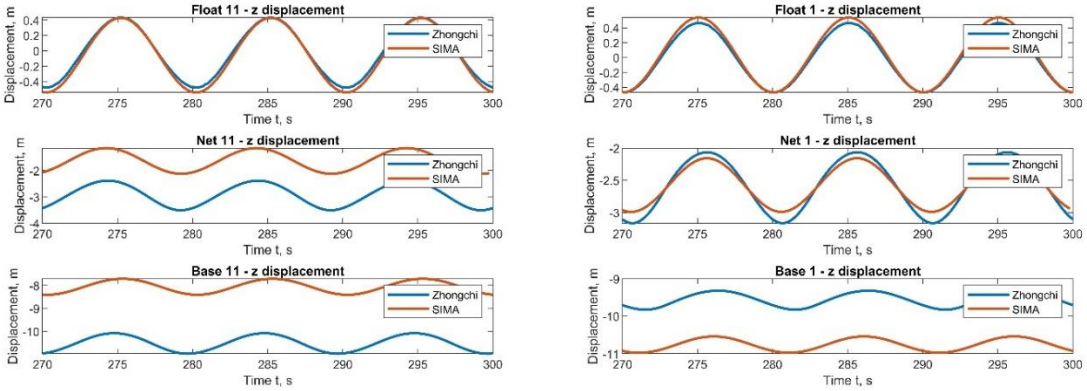

Figure 26 - (a) Upstream z displacements. (b) Downstream x displacements

From the above plots it can be seen that the behaviour of the two models is quite similar, regarding the amplitude and period of the response. Although, there are some differences to remark, as the difference in the overall x displacement of the two models and the z displacement of the net and base points.

This difference can be better visualized in Figure 27(a). The difference in the x displacement could be related with the above discussed modelling of the mooring lines. Although the main reason should be the computed forces on the cage, namely the drag and hydrodynamic forces on the net. SIMA could be computing larger forces or it could be taking into account more force components that are not being accounted for in the numerical analysis of Zhongchi Liu. This larger displacement of the SIMA model cage in turn means that a larger axial force on the mooring lines was computed, as shown on Figure 27(b).

(a) *(b)*

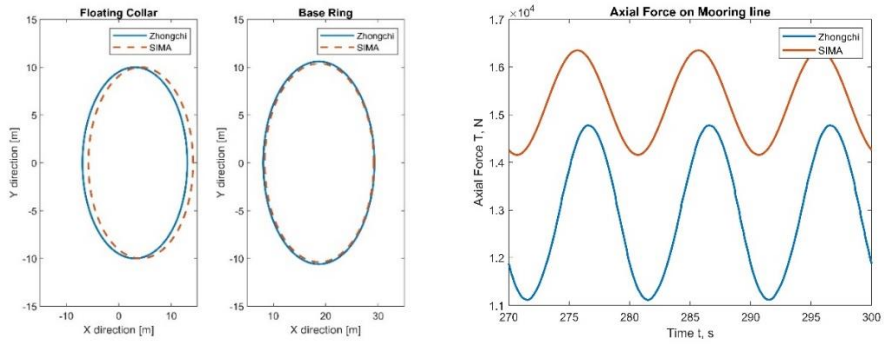

Figure 27 - (a) Top view of the model cage. (b) Upstream mooring line axial force

The difference in the z displacement of the base points, means that the behaviour of the net on the two models is different, that they have different shapes. This can be well observed by a side view of the net on the two models for the same time instant. It is clear that the shape developed by the two systems is quite different. This is mainly due to the deflection of the base ring. As seen on Figure 28, the base ring on the SIMA model has a much larger deflection than the other.

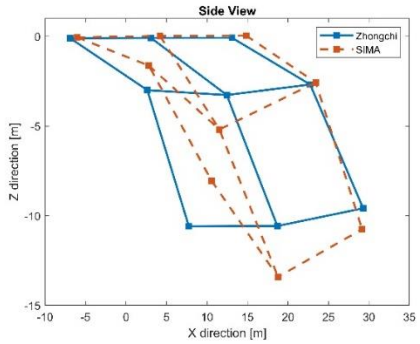

Figure 28 – Representation of the cage's side view, based on the points of interest

In order to study the influence of this parameter and to reach some accordance between models, a second simulation was run with a stiffer base weight ring.

Table 6 - Bending stiffness of the two analysed cases

Base Ring		
Case 1	4.6e03	[N.m2]
Case 2	4.6e05	[N.m2]

In this new model there was a better agreement between the displacements, both x and z, of the two systems. The displacements of the floating collar remain the same the between cases, but the displacements of the mid depth and base points got closer to the values of Zhongchi Liu. This improvement is related with the increased similarity between the two systems' net shape, as shown on Figure 31(a).

(a) *(b)*

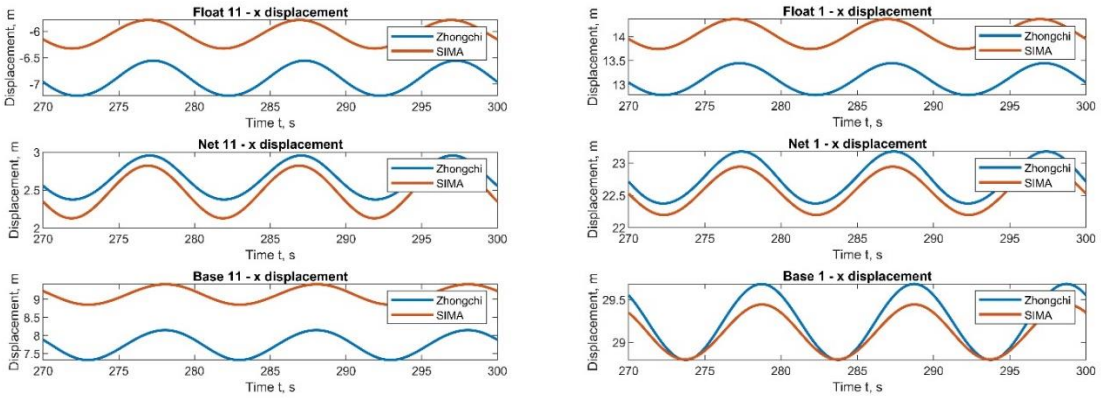

Figure 29 - (a) Case 2, upstream x displacement. (b) Case 2, downstream x displacement

(a) *(b)*

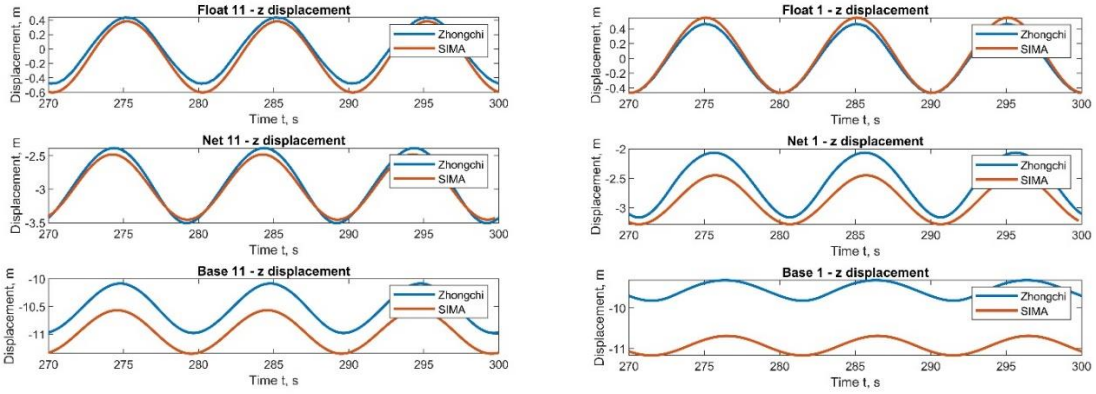

Figure 30 - (a) Case 2, upstream z displacement. (b) Case 2, downstream z displacement

(a) *(b)*

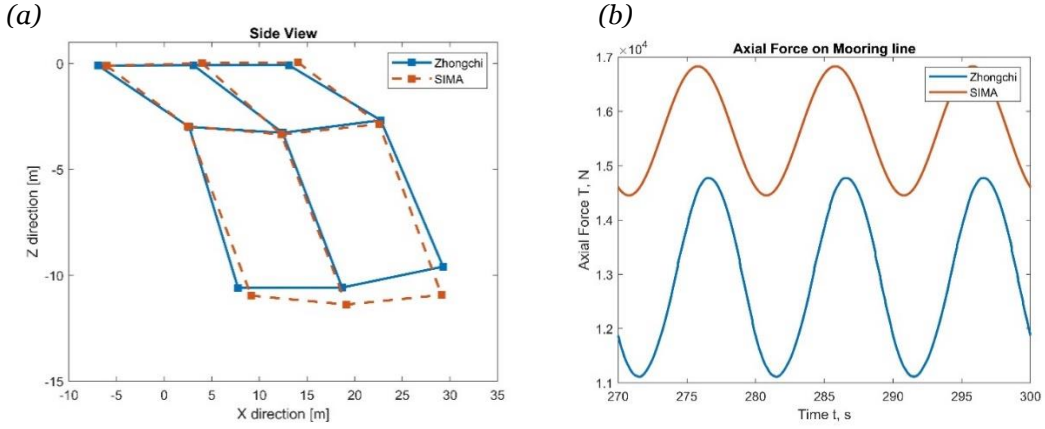

Figure 31 - (a) Case 2, representation of the cage's side view, based on the points of interest. (b) Case 2, mooring line axial force.

This new shape of the cage increased the axial force on the mooring lines, mainly because of larger forces on the net, due to fact that the projected area of the net elements located upstream increased with their more vertical position and therefore there was a smaller angle with the current.

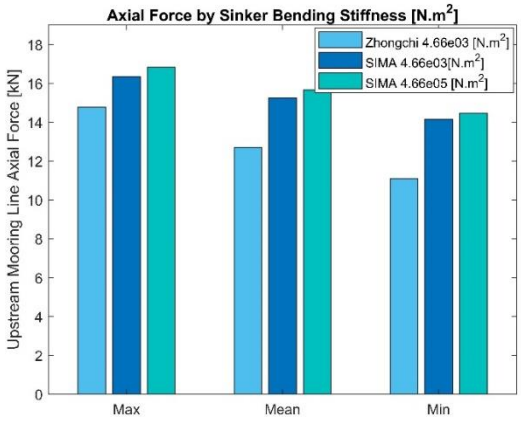

Figure 32 - Axial force variation with sinker bending stiffness

As in section 5.1, the simulation in SIMA produced higher values than the study it was compared with. As mentioned earlier on this section, the cause must be in the load's computation. A probable culprit could be that way the net elements are handled. On the Zhongchi work the net is discretized in less elements, with equivalent properties, and the load is computed for each element, both vertical and horizontal elements. On SIMA, the net is discretized in net panels, modelled by a bar an equivalent bar element, and the load is also computed for each sub-element. Due to the bar discretization, there are only vertical members in a SIMA's net element.

5.4. Comparison with an analytical analysis of a single cage

The fourth analysis resulted from a collaboration with Sarat Mohapatra at CENTEC, that will eventually culminate in the publication of a paper. A mathematical model for the wave-cage interactions was made, by Sarat Mohapatra, and the results compared with the numerical model implemented in SIMA. The following analysis will compare the displacements of both models.

5.4.1. The model

The model built was a flexible gravity net cage, with the particularity of having a fixing bottom. This configuration was chosen by the analytical model author. This configuration has the potential to be interesting from a study perspective, since it is different from the traditional gravity cage and the effects of different parameter's variations on the structure dynamics could be assess in a novel way.

The mathematical description of the analytical model will not be made in this work, since it was done by a different author, in this work only the numerical model is described since it was an important part of this thesis development. Since the bottom is fixed, there is no necessity for weight sinker ring. Also, the floating ring was modelled as rigidly as possible, since in the analytical model it had no flexibility. Table 7 presents the main parameters of the system.

The models were run under a regular wave scenario, with no current.

Table 7 – System main parameters

Cage		
Diameter	6	[m]
Height	7	[m]
Floater		
Diameter	500	[mm]
Axial stiffness	6.5e07	[N/m]
Net		
Weight	0	[kg/m]
Solidity ratio	0.25	[-]
V. reduction ration	1	[-]
Axial stiffness	100	[N/m]

Mooring		
Stiffness	10	[N/m]
Environment		
Depth	50	[m]
	Height [m]	Period [s]
Regular waves	1	10

Nº elements	
Floater	100
Bottom Ring	20
Mooring	20

5.4.2. Results

As mentioned above, a comparison between the displacements of the cage on both models was performed. The selected point for the measurements was as indicated in Figure 33.

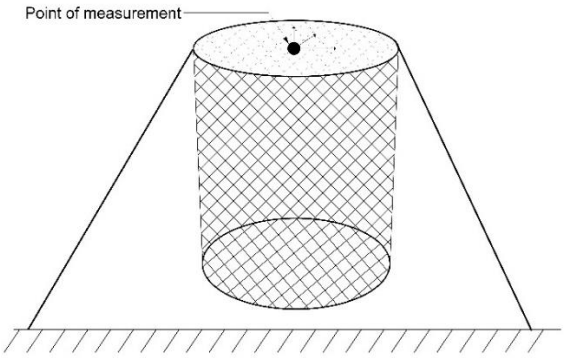

Figure 33 - Simplified cage model diagram

It is necessary to remark that this validation was the one that achieved the best agreement. The main reason being the fact that, contrary to the other validation processes where the source model and results were immutable and no conversation with the authors was possible, this model and analysis were built side-by-side. Therefore, a tuning process was possible and time was available to gain knowledge and adapt the analytical and numerical model.

Firstly, the two cages, analytical and numerical, were compared simply for their horizontal displacement under the action of regular waves. Following the effects of some parameters variations was studied.

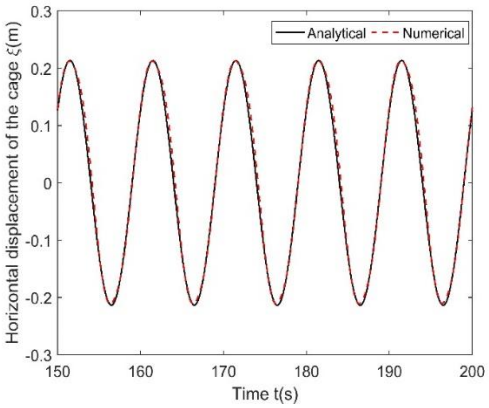

Figure 34 - Comparison of horizontal displacement between analytical and numerical model

(a) *(b)*

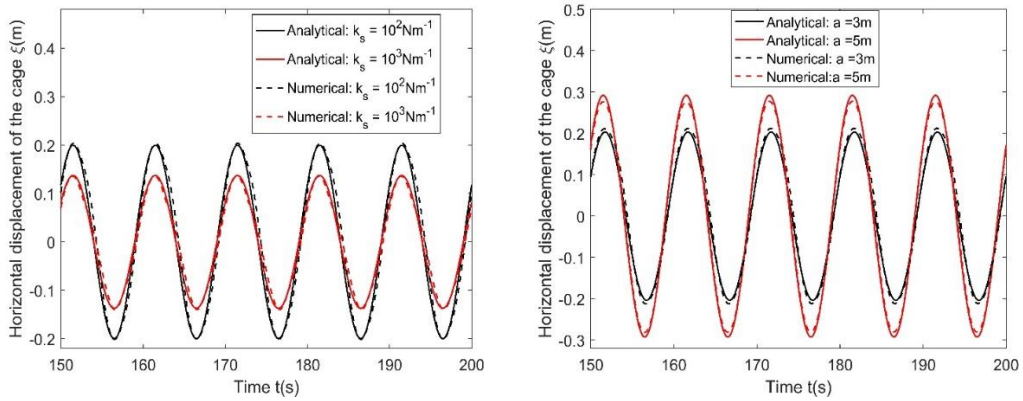

Figure 35 –(a) Comparison of horizontal displacement between analytical and numerical model, for different mooring stiffness. (b) Comparison of horizontal displacement between analytical and numerical model, for different cage radius.

(a) *(b)*

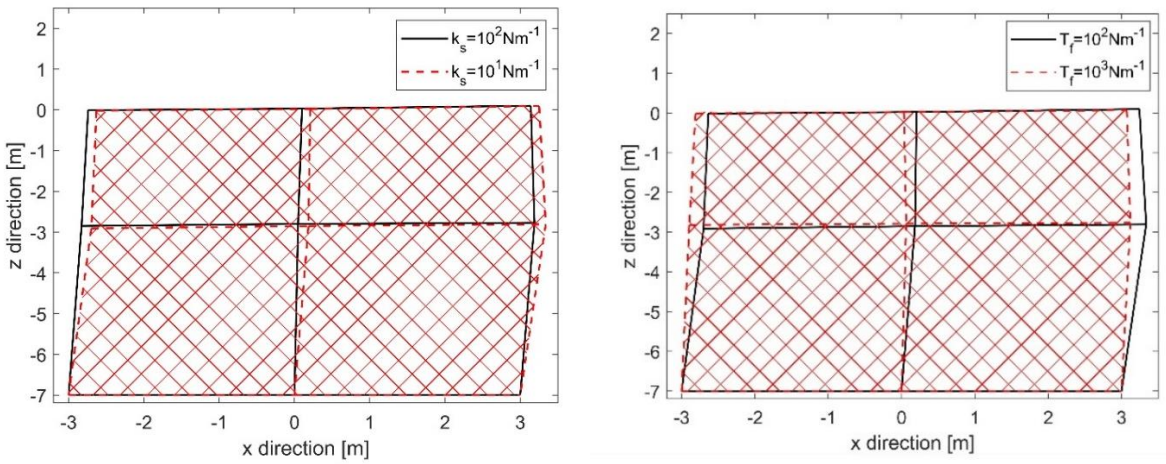

Figure 36 - (a) Comparison of horizontal displacement of the moored flexible cylindrical net cage, different mooring stiffness. (b) Comparison of horizontal displacement of the moored flexible cylindrical net cage, different membrane stiffness.

Although this fixed bottom set up is not common, nor will it exist in the industry, this analysis is useful to substantiate the usability of the numerical tool SIMA in the analysis of structures with flexible net elements. It is also useful to understand the impact of the variation of some parameters in the behaviour of a cage with a porous, flexible net membrane. Figure 36(a) sustains the premise that a stiffer mooring system reduces the dynamic response of the cage. Interesting is the finding that, a wider cage, in this set up and for the same height, leads to larger horizontal displacements. Mainly due to the increase in the net panels size, which in turn increases the are exposed to the wave loads.

As mentioned, the results have a good agreement. In the future, such good agreements are only possible, if possible, when there is a detailed modelling and analysis procedure between the parties involved in the different possible models (analytical, numerical or experimental)

5.5. Comparison with a well-established numerical tool

As mentioned earlier, this software was used as a validation tool due to its robustness and well proven capability.

A model cage was provided by SINTEF, and the same cage was modelled in SIMA. Then the results were compared to verify if the results from SIMA were reasonable and within the expected range of values.

5.5.1. The model

Some properties of the cage were not known nor could be apprehended from the input's files. So, several iterations of the model were done in SIMA until an acceptable match was found. The main properties of the system are shown on, where the unknown properties, with the respective assigned values, are highlighted in grey. The net properties were unknown. This has the potential to be a major source for errors and undermine the whole comparison, since the net plays a major role in the analysis and is the biggest contributor to the loads on the cage system. To minimize this, values normally used in nets for this size of cage were assigned, and then iteratively were tuned until the acceptable match, mentioned above was achieved, the final values are shown on Table 8.

From the unknown properties, the most critical were the net solidity ratio and net velocity reduction factor. Since the variation of these properties could have an impact on the final values. As opposed to the floating collar's drag coefficient and the net's mass and volume (the net was modelled as almost buoyancy neutral), which have a significantly low impact on the final result (Aksnes 2106). The drag coefficients of the bottom ring and lines were tuned around the most common values, taking into account their diameter.

Table 8 - Model Properties

Floater		
Diameter (cage)	50	[m]
Diameter	500	[mm]
Young Modulus	9	[GPa]
Weight	30	[Kg/m]
Cd	0.6	[-]
Bottom Ring		
Diameter	200	[mm]
Young Modulus	0.8	[GPa]
Weight	35	[Kg/m]
Cd	0.6	[-]
Mooring Lines		
Diameter	50	[mm]
Young Modulus	1	[GPa]
Weight	2.4	[Kg/m]
Cd	0.5	[-]

Nº elements	
Floater	5
Bottom Ring	3
Mooring	100
Grid	20
Bridle	10

Grid Lines		
Diameter	50	[mm]
Young Modulus	1	[GPa]
Weight	2.4	[Kg/m]
Cd	0.5	[-]
Bridle Lines		
Diameter	50	[mm]
Young Modulus	16	[GPa]
Weight	2.2	[Kg/m]
Cd	0.5	[-]
Net		
Sn	0.27	[-]
Mass	1	[Kg/m]
r	0.85	[-]

Firstly, the analysis was done for conditions of current only and then for a regular waves plus current condition. They are summarized in Table 9 . The current direction was 0°, i.e. the same direction as the positive x axis.

Table 9 - Environmental Conditions Simulated

Current	Uc [m/s]		
C1	0.1	[m/s]	
C2	0.25	[m/s]	
C3	0.5	[m/s]	
Waves and Current		Hwav [m]	T [s]
C1	0.5	1	10

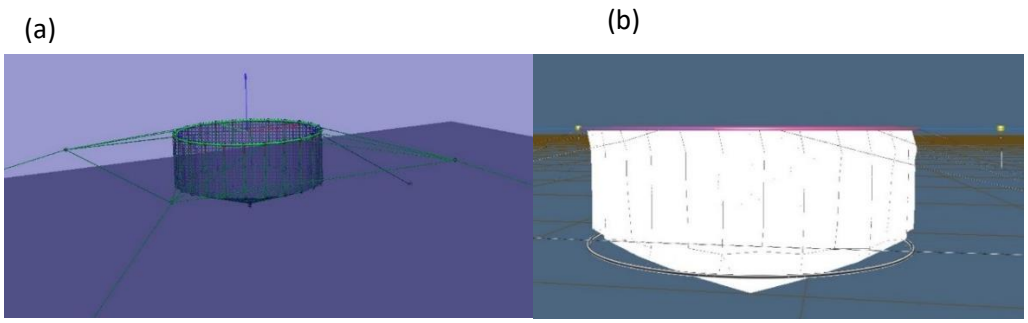

Figure 37 - Modelled cages systems. (a)SIMA (b) FhSim

As can been observed, the two models are not completely identical. There are some differences in their shape, as better illustrated in Figure 38 . More specifically the method used to connect the cage to the bottom ring. The model used in FhSim is the equal to the real-life systems used today in the aquaculture industry. Where the net is shaped like a bag, with its corners connected to the base ring by a cable. This configuration was more complex and troublesome to model in SIMA, although possible, and at the time of this model's construction my knowledges of the SIMA software were not enough to build this configuration. Later on, on a more advance phase of this work, the amount of time required to rebuild and analyse the new model was considered very high. With this in mind, it was decided that it was not worth the workload when considering the purpose and scale of this thesis.

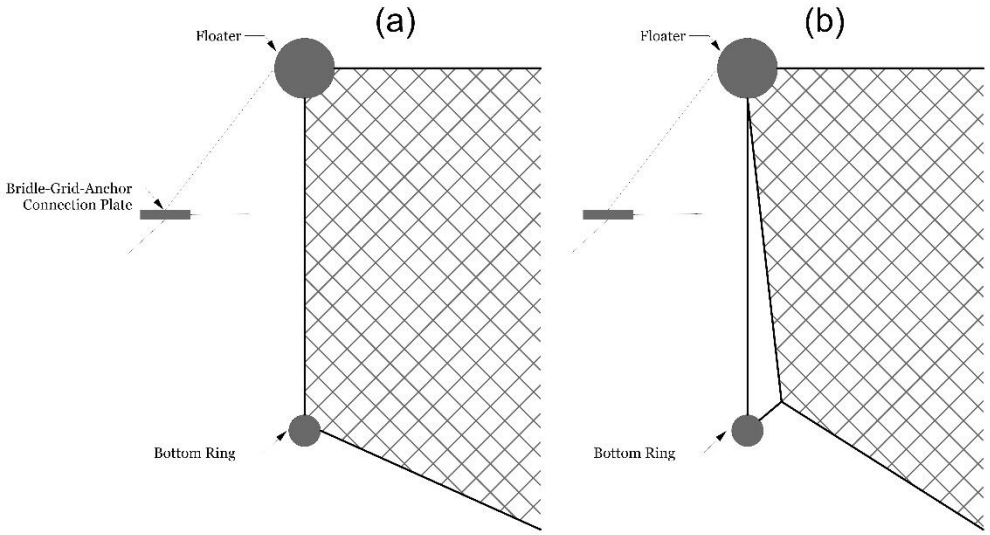

Figure 38 - Cross section view of modelled cages. (a) SIMA (b) FhSim

5.5.2. Results

A qualitative and quantitative analysis of the results was done. The qualitative analysis was done through graphical representation of the cage's lines and net. Values were taken from selected points and then a representation of the cages was done. Although it is not a perfect match of the cage's deformation and displacements, for the purpose of comparison it will fit quite reasonably.

- **Current Only**

The axial forces on the mooring lines were compared. Divided in upstream and downstream lines, due to the symmetry only one line from of type was evaluated. The values from each simulation are represented on Table 10 and on Figure 39.

Table 10 - Mooring lines axial force in [kN]

		Upstream		Downstream	
	Uc [m/s]	FhSim	SIMA	FhSim	SIMA
Condition 1	0.1	11	10.4	7.9	7.6
Condition 2	0.25	20.2	22.1	2.9	5.2
Condition 3	0.5	60.1	62.4	0.9	3.4

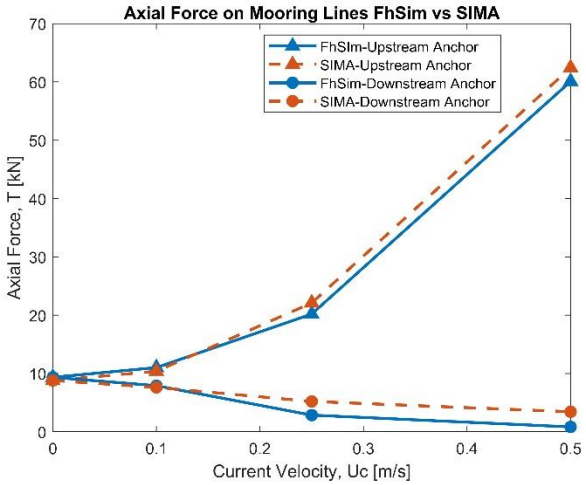

Figure 39 - Mooring Line Axial Force for static analysis

In general, it appears to exist a good agreement between the two simulations, although with SIMA values being consistently higher. For the mooring lines located downstream of the cage, the difference is quite significatively, in particular for higher current velocities. A possible explanation might be the modelling and computation of the contact between the mooring line and the seabed. As the cage moves in the direction of the current, the downstream mooring lines became slacker, the touchdown point moves away from the anchor and the length of the line that rests on the seabed increases. If this is not properly modelled, the length of the resting line could be different between the two simulations, and therefore the length of the suspended line is larger for the SIMA simulation. Which results in an increase of the axial force on the line.

As said above, the coordinates of selected points were compared. First the position of the floating collar and the base ring of the two simulations were compared, for the three conditions of current. Shown on the figure *Figure 40*.

The second graphical comparison was the top view from the whole cage system, *Figure 40*. Through this view it is possible to access the similarity, or not, of the mooring, grid and bridle lines of the two systems. Although, for clarity of the representation, only one of 4 of the 12 bridle lines are shown (the middle).

The third comparison was to access the cage's deformation. It is a simplistic view, since the registered points were only on the floating collar and base ring. It was assumed that the net remained straight between these two points. When it is known that in reality this does not happen, and the net

deflects like an arc. A complete deformation view was not possible, since there was not enough points, between the floater and the base, measured in the net to reproduce it. This comparison is shown for the three cases on

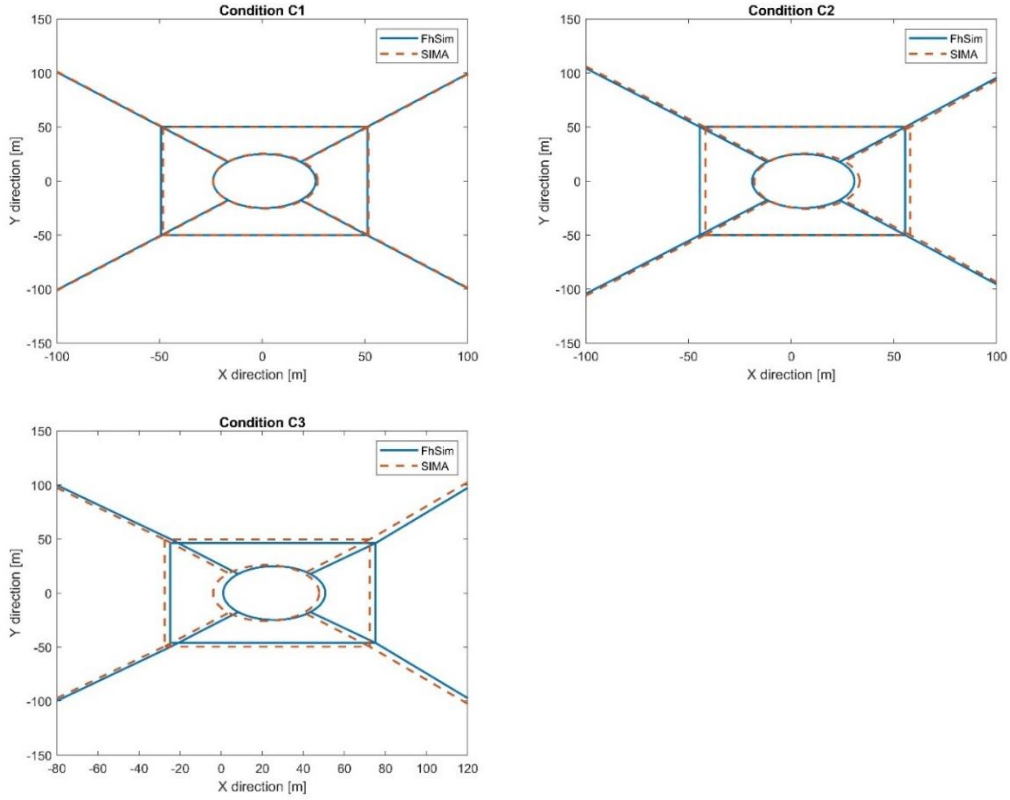

Figure 40 - Top view of the cage system layout the main lines, for condition C1, C2 and C3

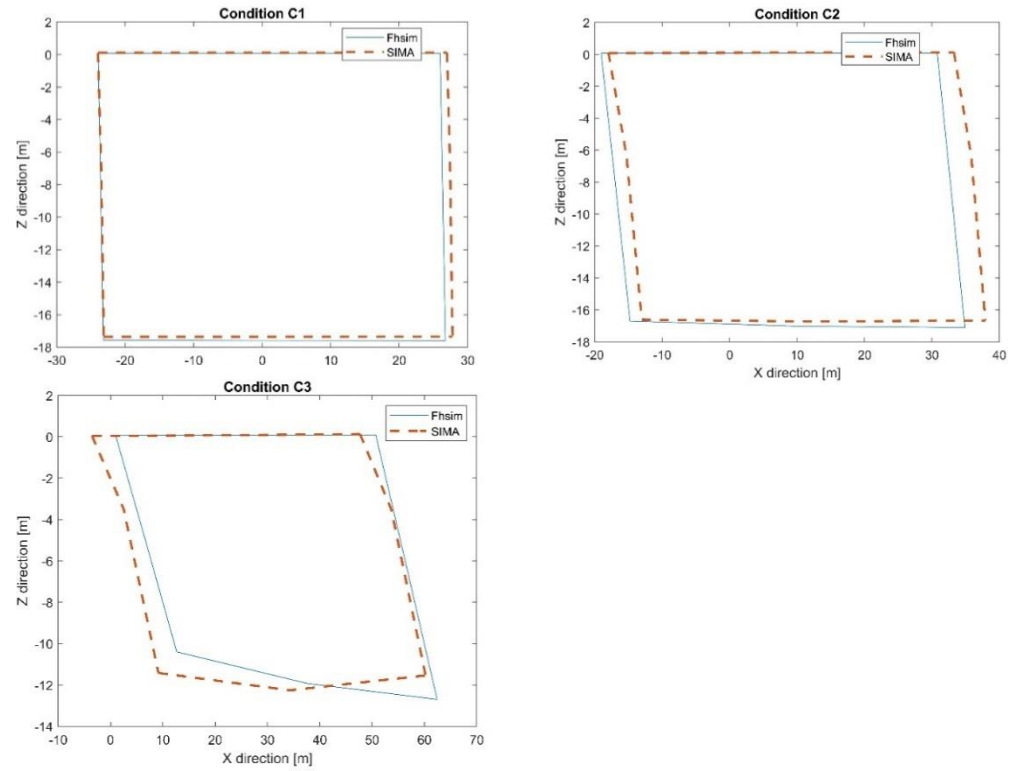

Figure 41 - Cage's side configuration, for condition C1, C2 and C3.

The coordinates of the selected points also allowed for a net's volume reduction comparison. Using the method presented on (Lader and Enerhaug 2005), through the computation of the volume reduction coefficient, the quotient between the deformed and the undeformed volume of the net.

$$C_{vr} = \frac{V_p}{V_{p0}} \tag{69}$$

The method used an approximate volume, by dividing the net in two triangular prisms, and computing its volumes through the coordinates of some key points.

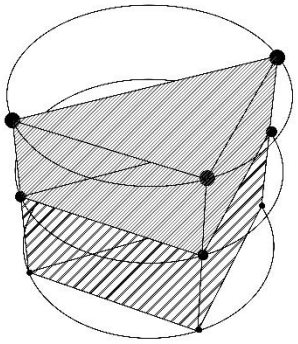

Figure 42 - Cage division in two prisms

The volume reduction coefficients for the three conditions are presented on Table 11:

Table 11 - Volume reduction coefficient of the cage

	Uc [m/s]	FhSim	SIMA
Condition 1	0.1	0.97	0.99
Condition 2	0.25	0.9	0.96
Condition 3	0.5	0.55	0.65

From the above values it is safe to state that the SIMA's model has less deformation than the FhSim model, since the volume reduction coefficient is directly linked to the cage shape. The lesser deformation could be related with the previously mentioned difference in the cage modelling. This also raises the believe that the cage in FhSim is more flexible and its behaviour more realistic and closer to the real-life situation. This is somewhat confirmed by a visualization of the final deformation of the two simulations, as shown on Figure 43.

(a)

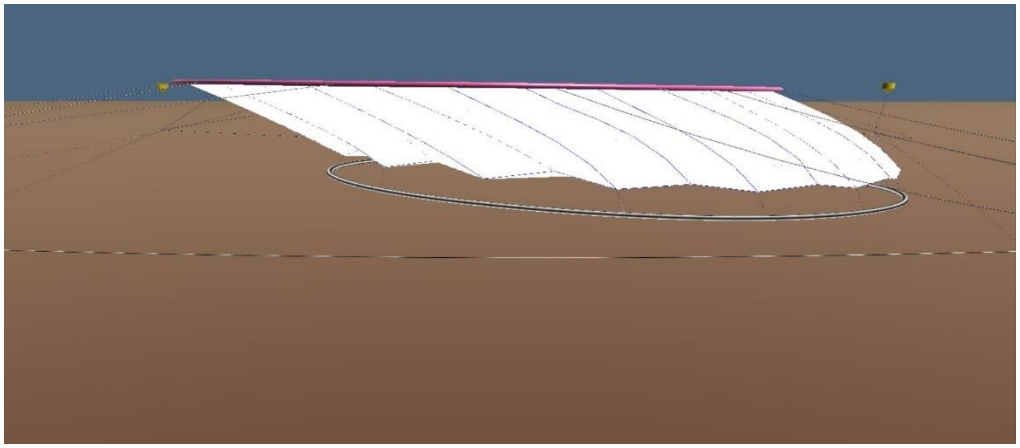

(b)

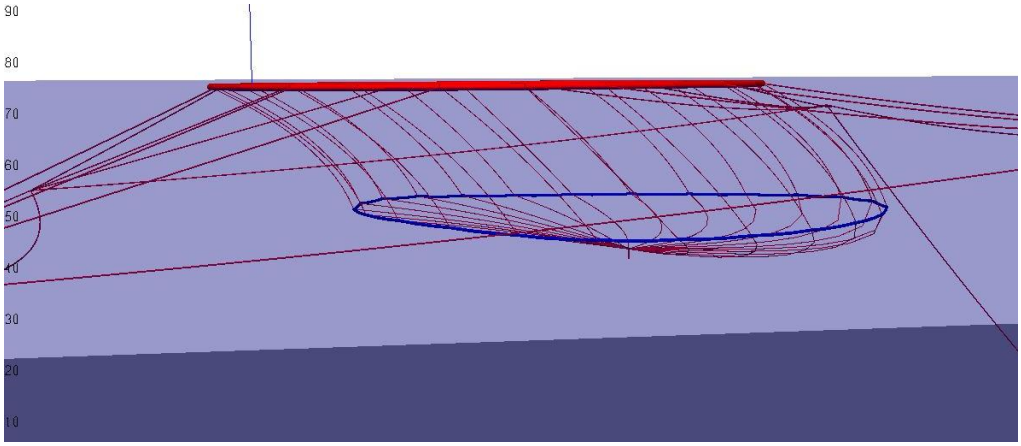

Figure 43 - Cage deformation during dynamic analysis. (a) FhSim model (b) SIMA model

- **Waves and Current**

For the dynamic analysis, with waves and current, one condition was analysed, as mentioned on Table 9. The displacements of certain key points, the same used in the other validation analysis of this work, were access and compared. The same was done for the axial force on the mooring lines, both upstream and downstream.

Firstly, a top view of the whole system, at the same time instant, was compared. Where it seems that the position of the two models is quite similar. Although, the scale is rather large, so a closer look does reveal that a difference of about one meter exists in the horizontal displacement of the two cages.

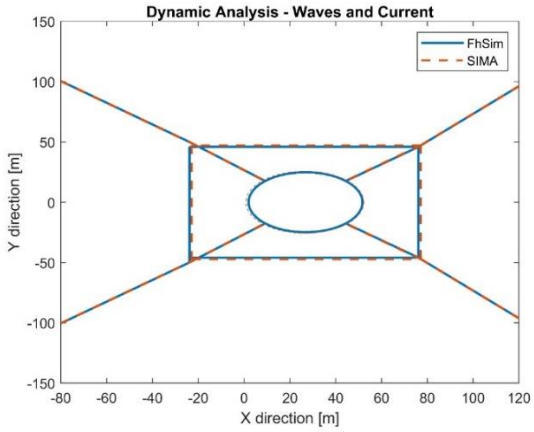

Figure 44 - Top view of the cage system layout the main lines, for dynamic condition C1

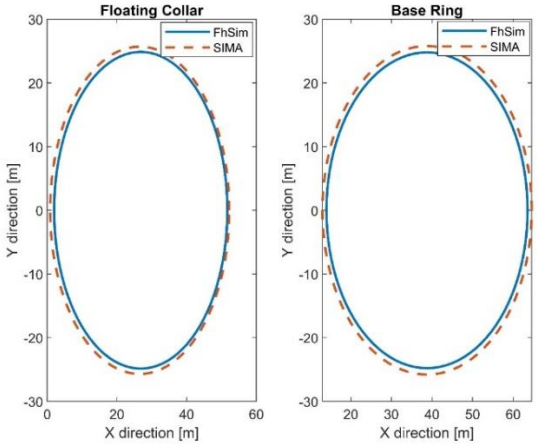

Figure 45 - Top view of the position of the floating collar and base ring of the two models

This difference means that the FhSim model, which has a larger displacement in the positive x direction, should have larger axial force in the mooring lines due to an increase of the suspended line length. In Figure 46 it is observed that the opposite happens, the axial force is larger for SIMA's model. Although the difference is quite small if we look at the order of magnitude of the results.

Both the differences in the x displacement of the cage and its upstream mooring line forces are quite acceptable and could be caused by differences in the solving method of both softwares or in the load's formulation and computation.

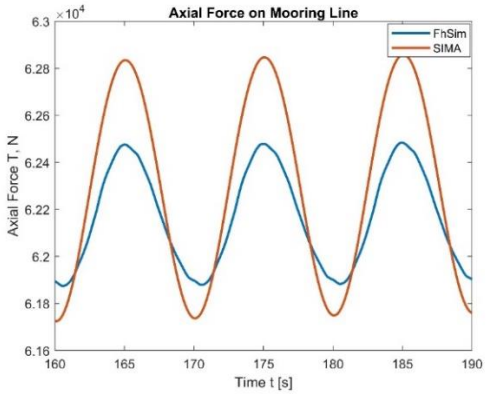

Figure 46 - Axial force on upstream mooring lines

The key points analysed were located in the floating collar, mid-depth of the net and at the base, both for upstream and downstream location. Through Figure 47 the above difference of the x displacement of the two models is confirmed, and it also reveals that the horizontal offset of SIMA's model is larger than the FhSim model. It could be cause by differences in the computed drag load on the net or in the mooring line axial stiffness.

(a) *(b)*

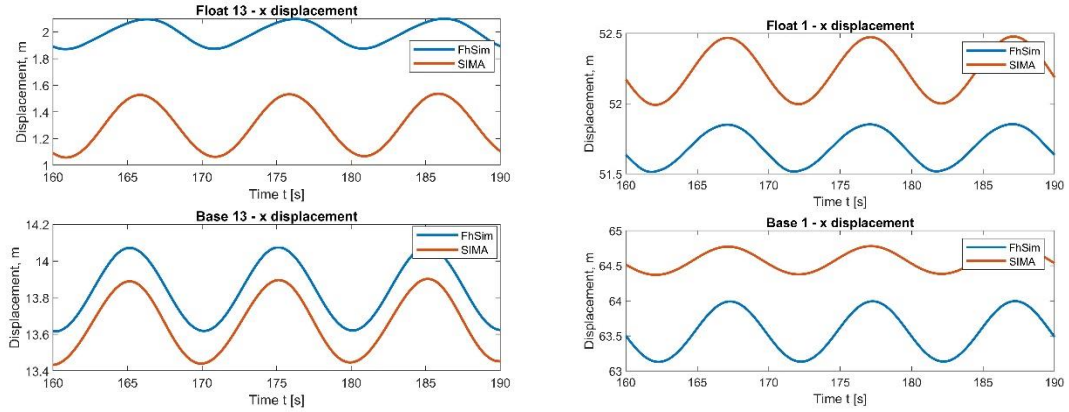

Figure 47 - (a) Dynamic case, upstream x displacement. (b) Dynamic case, downstream x displacement.

(a) *(b)*

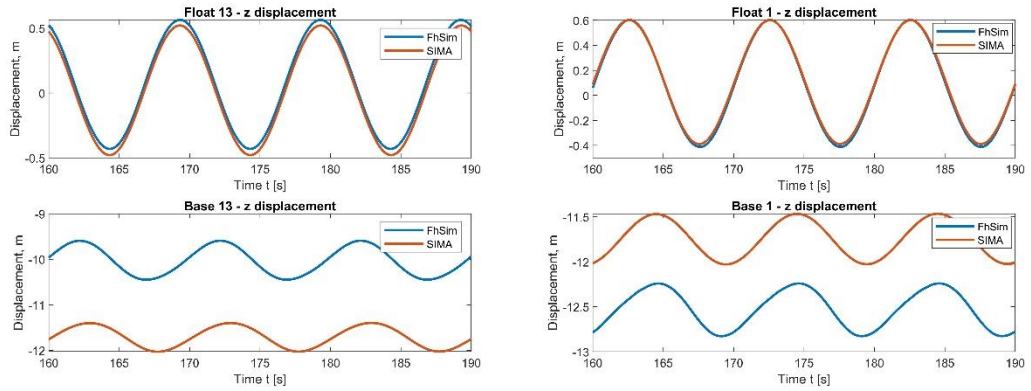

Figure 48 - (a) Dynamic case, upstream z displacement. (b) Dynamic case, downstream z displacement

Other interesting observation of the above plots is the difference of phase between the points in the floating collar and the base. For the x displacements, the phase difference between the displacement of the floating collar and the base is larger for the SIMA model, but the opposite happens for the z displacements, where the phase difference is larger for the FhSim model. Although is difficult to produce some conclusion from these observations, they do support the idea that the net behaves slightly different in the two software. Its undulatory movement due to the waves and current is different. The difference in the behaviour of the net can also be observed through a side view.

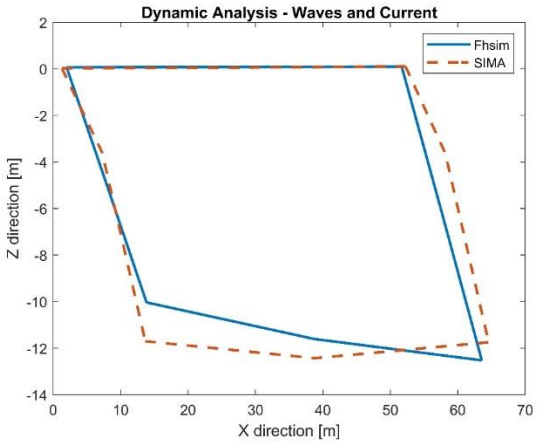

Figure 49 - Cage's side configuration, for dynamic condition C1.

To remark that this is a representation made with the coordinates of the previously mentioned key points. So, it is not a true reproduction of the cage shape, but its purpose its to give an idea of the shape assume by the cage through the comparison of the key points.

The shape assumed by the base of the net is the main difference between the models. This could be due to the fact that, as mentioned initially, the Young's Modulus of the base ring was unknown. So, it is correct to assume that the modelling of the base ring was not done correctly. A more flexible base ring in SIMA would eventually result in a more deformed cage, leading to a decrease in the load of the cage due to the increase in the angle between the net panels and the incoming flow and a decrease on the exposed area.

The results of this section somewhat are the culmination of this validation process and come in line with the results from the other sections. Where the loads on the cage and mooring lines are reasonably similar between models, but the cage's shape and behaviour have some divergences.

5.6. Conclusion

The results of these analysis were relevant to draw some important conclusions. It was concluded that this software is not the best tool to analyse the behaviour of a free hanging net. As can be seen by the results, there are some discrepancies between the experimental net behaviours and the ones predicted by the software. One major cause of these might be the way the software represents a net panel, through an equivalent single vertical cable/bar element. This of course does not take into account the physical linkage of the twines between each other. Several horizontal linking elements were tested in the models to try to bypass this lack of connectivity, but the results indicated some differences between simulated and experimental results, and the added complexity of this increased the computation effort in such a way that it was not worth the gains. Another important point is the influence of each twine in the flow of the others. The wake effect is not properly modelled in the SIMA software, which may lead to higher loads on the net elements located downstream and an overall increase of the cage load(Aksnes 2106). Although there is the possibility to set the velocity reduction

factor for each net element, it remains constant throughout the simulation. When ideally it should be adjusted with the changing position and angle of the elements.

Therefore, for more detailed analysis of the net geometry a numerical tool with a more complex description of the equivalent net element should be used, but this work is focused mainly on the forces caused by environment onto the net cage, and the suitability of this tool for this purpose was backed up by the results. Since there was a good agreement between the net displacements in some important locations, namely the floating collar and the bottom aft end, and the mooring lines axial forces. This lead us to affirm that the global forces on the net cage were being reasonably computed, to a certain extent.

Therefore, the results of these validation processes suggest that the chosen software *SIMA* is a good tool to perform an assessment of the loads on a fish farm system and its mooring systems. As long as, care is taken in the modelling process and as much properties as possible are gathered for the system to be simulate. Since the quality of the results are largely dependent of the proper similarity between the model and the object of study.

6. Case Analysis

On the south side of Madeira island there is already an aquaculture installation. With around 20 cages on a site approximately 0.5 nautical miles from the coast for the production of Gilt-head bream (*Sparus aurata*). On this chapter a review of the mooring system of this farm will be conducted. An analysis will be performed and a solution will be proposed. Then, this solution will be compared with the real one employed in the site.

The following sections will describe the system configuration and specifications, the weather regime of the location and an outline of the analysis procedure.

6.1.System Specifications

The farm consists of 20 net gravity cages, installed together on a mooring grid with an orientation from northwest to southeast, as shown on Figure 50. The site has water depths between 30 and 70 meters.

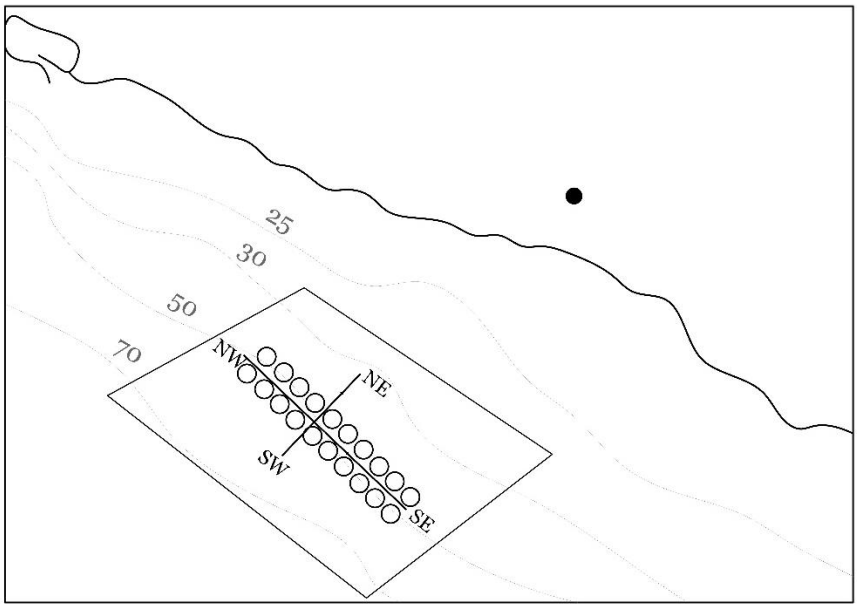

Figure 50 - Location and orientation of the farm site in Arco da Calheta

The cages used are of the plastic floating collar type, also called pens. They have two diameters, 12,7 and 25,5 meters. In total there are 14 pens with 25,5 m and 6 pens with 12,7 m. The mooring system has a catenary configuration and is made of synthetic rope and weight anchors. On Table 12 the main specifications of the pens are presented. The mooring specifications are described in the next section, section 6.2.

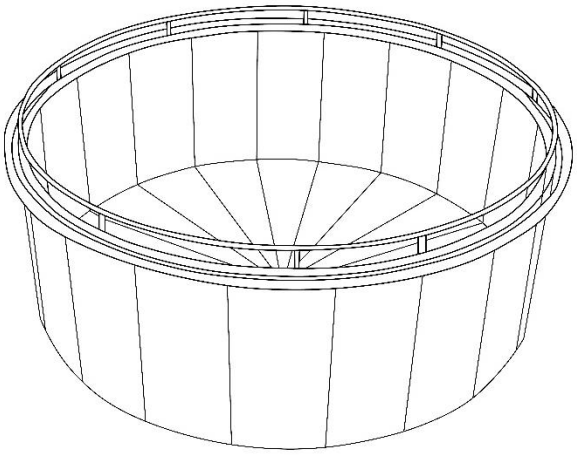

Figure 51 - Representation of a plastic collar type cage (pen) used in this system

Table 12 - System main specifications

	Pens		
	40 Cage	80 Cage	
Diameter	12.5	25	[m]
Circumference	40	80	[m]
Height	9	10	[m]
Floater			
Diameter	3 x Ø250	2 x Ø400	[mm]
Weight	36	57.5	[kg/m]
Sinker			
Diameter	Ø315	Ø315	[mm]
Weight	43	43	[kg/m]

The specifications of the nets used were supplied by the company, although some data was missing or not available to the company. This data is detailed in Table 13.

The axial stiffness of the nets was not available, therefore the average value found in Moe et al. (2007) was used, since it was the best estimation it was possible to find. The solidity ratio was computed as shown in Grue (2014), using the nets known half-length and a proposed a twine diameter, since this was an unknown value. The twine diameter was proposed in a way that the solidity ratio was in accordance with the average values used on the aquaculture industry (0.2~0.35). The same author proposes a velocity reduction factor of the nets, computed with the drag coefficient's relation of eq.(4).

The added mass of the net was also not available and it was not feasible to perform model tests to determine its value. The approach used for fishing nets in Chen and Christensen (2016) was adopted. Where the added mass coefficient is computed by an empirical formula, eq. (70).

$$C_a = 0.34\frac{1-n}{n} \tag{70}$$

The porosity n, as described by (Gjøsund and Enerhaug 2010), is a function of the twine length (m) and diameter (d).

$$n = \frac{m^2}{(d+m)^2} \tag{71}$$

Table 13 - Net specifications

Nets						
	40			80		
	Base	Bottom 4 m	Top 5 m	Side	Base	
Net type *	210/48	210/48	210/72	210/120	210/120	[-}
Density	360	360	345	340	340	[gr/m2]
Axial. Stiff	143	143	143	337	337	[N]
lw	10	10	15	20	20	[mm]
dw	1.5	1.5	1.5	2.3	2.3	[mm]
Sn	0.28	0.28	0.19	0.22	0.22	[-]
r	0.8	0.8	0.85	0.85	0.85	[-]
n	0.75	0.75	0.82	0.80	0.80	[-]
Cm	0.110	0.110	0.071	0.083	0.083	[-]
Mass	0.9	0.9	0.9	1.7	1.9	[Kg/m]

(*) – net type explanation can be found in (Cardia and Lovatelli 2015)

Some data used in the simulation differs slightly from the computed values, because some divergence problems rose with some of the data. Although all the changes are within commonly used values, the above table shows the values as inputted in the simulation.

The wave data for a period of 40 years was available in the form of an occurrence table,

Tp(s Hs(m)	**< 5**	**5-6**	**6-7**	**7-8**	**8-9**	**9-10**	**10-11**	**11-12**	**12-13**	**13-14**	**14-15**	**15-16**	**16-17**	**17-18**	**18-19**	**>19**
0.5	0.00	0.00	0.00	0.00	0.00	0.00	0.00	0.00	0.00	0.00	0.00	0.00	0.00	0.00	0.00	0.00
1	0.00	0.00	0.00	0.00	0.00	0.00	0.01	0.00	0.00	0.00	0.00	0.00	0.00	0.00	0.00	0.00
1.5	0.00	0.01	0.02	0.02	0.05	0.06	0.16	0.43	0.37	0.11	0.02	0.00	0.00	0.00	0.00	0.00
2	0.00	0.02	0.16	0.08	0.13	0.11	0.22	0.98	1.95	0.94	0.22	0.00	0.04	0.01	0.00	0.00
2.5	0.00	0.01	0.23	0.21	0.19	0.17	0.18	0.61	1.98	2.40	0.77	0.00	0.17	0.02	0.00	0.00
3	0.00	0.00	0.05	0.14	0.21	0.15	0.20	0.32	0.76	1.62	1.22	0.00	0.29	0.06	0.00	0.00
3.5	0.00	0.00	0.01	0.04	0.13	0.16	0.15	0.22	0.37	0.74	0.92	0.00	0.39	0.07	0.00	0.00
4	0.00	0.00	0.00	0.01	0.03	0.07	0.12	0.12	0.14	0.30	0.39	0.00	0.35	0.08	0.00	0.01
4.5	0.00	0.00	0.00	0.00	0.01	0.03	0.08	0.08	0.08	0.16	0.22	0.00	0.21	0.06	0.00	0.01
5	0.00	0.00	0.00	0.00	0.00	0.01	0.02	0.06	0.04	0.05	0.11	0.00	0.12	0.05	0.00	0.01
5.5	0.00	0.00	0.00	0.00	0.00	0.00	0.00	0.03	0.03	0.02	0.06	0.00	0.06	0.02	0.00	0.00
6	0.00	0.00	0.00	0.00	0.00	0.00	0.00	0.01	0.02	0.02	0.02	0.00	0.02	0.00	0.00	0.00
6.5	0.00	0.00	0.00	0.00	0.00	0.00	0.00	0.00	0.00	0.01	0.02	0.00	0.01	0.00	0.00	0.00
7	0.00	0.00	0.00	0.00	0.00	0.00	0.00	0.00	0.00	0.01	0.01	0.00	0.01	0.00	0.00	0.00
7.5	0.00	0.00	0.00	0.00	0.00	0.00	0.00	0.00	0.00	0.01	0.01	0.00	0.00	0.00	0.00	0.00
8	0.00	0.00	0.00	0.00	0.00	0.00	0.00	0.00	0.00	0.00	0.00	0.00	0.00	0.00	0.00	0.00
8.5	0.00	0.00	0.00	0.00	0.00	0.00	0.00	0.00	0.00	0.00	0.00	0.00	0.00	0.00	0.00	0.00

Table 14. Both a table for year-round and winter-time conditions were available. For this work only the winter-time table will be analysed since the focus is to show the applicability of the numerical tool and the higher loads of the winter conditions were thought to better serve this purpose. The available data, collected and sent by the company who owns the farm, had no directional information. First it was tried to use data from the ERA-Interim database, this had some obstacles due to the fact that the location is close to shore and the database had a relatively large resolution, 80km (Dee et al. 2011), which in turn resulted in values that were not similar to the ones provided by the company. Secondly, with the help of a researcher from the R&D group of Marine Environment, the higher resolution data of ERA5 was tried, but this was stalled before completion due to the general sanitary health situation. Hence, the procedure adopted was to use the same data, the provided one, for different directions. This is not the best procedure to undertake, but then again it is believed to fit the purpose of this work to a certain extent.

Table 14 - Occurrence table of wave by significant wave height and peak period

Tp(s Hs(m)	< 5	5-6	6-7	7-8	8-9	9-10	10-11	11-12	12-13	13-14	14-15	15-16	16-17	17-18	18-19	>19
0.5	0.00	0.00	0.00	0.00	0.00	0.00	0.00	0.00	0.00	0.00	0.00	0.00	0.00	0.00	0.00	0.00
1	0.00	0.00	0.00	0.00	0.00	0.00	0.01	0.00	0.00	0.00	0.00	0.00	0.00	0.00	0.00	0.00
1.5	0.00	0.01	0.02	0.02	0.05	0.06	0.16	0.43	0.37	0.11	0.02	0.00	0.00	0.00	0.00	0.00
2	0.00	0.02	0.16	0.08	0.13	0.11	0.22	0.98	1.95	0.94	0.22	0.00	0.04	0.01	0.00	0.00
2.5	0.00	0.01	0.23	0.21	0.19	0.17	0.18	0.61	1.98	2.40	0.77	0.00	0.17	0.02	0.00	0.00
3	0.00	0.00	0.05	0.14	0.21	0.15	0.20	0.32	0.76	1.62	1.22	0.00	0.29	0.06	0.00	0.00
3.5	0.00	0.00	0.01	0.04	0.13	0.16	0.15	0.22	0.37	0.74	0.92	0.00	0.39	0.07	0.00	0.00
4	0.00	0.00	0.00	0.01	0.03	0.07	0.12	0.12	0.14	0.30	0.39	0.00	0.35	0.08	0.00	0.01
4.5	0.00	0.00	0.00	0.00	0.01	0.03	0.08	0.08	0.08	0.16	0.22	0.00	0.21	0.06	0.00	0.01
5	0.00	0.00	0.00	0.00	0.00	0.01	0.02	0.06	0.04	0.05	0.11	0.00	0.12	0.05	0.00	0.01
5.5	0.00	0.00	0.00	0.00	0.00	0.00	0.00	0.03	0.03	0.02	0.06	0.00	0.06	0.02	0.00	0.00
6	0.00	0.00	0.00	0.00	0.00	0.00	0.00	0.01	0.02	0.02	0.02	0.00	0.02	0.00	0.00	0.00
6.5	0.00	0.00	0.00	0.00	0.00	0.00	0.00	0.00	0.00	0.01	0.02	0.00	0.01	0.00	0.00	0.00
7	0.00	0.00	0.00	0.00	0.00	0.00	0.00	0.00	0.00	0.01	0.01	0.00	0.01	0.00	0.00	0.00
7.5	0.00	0.00	0.00	0.00	0.00	0.00	0.00	0.00	0.00	0.01	0.01	0.00	0.00	0.00	0.00	0.00
8	0.00	0.00	0.00	0.00	0.00	0.00	0.00	0.00	0.00	0.00	0.00	0.00	0.00	0.00	0.00	0.00
8.5	0.00	0.00	0.00	0.00	0.00	0.00	0.00	0.00	0.00	0.00	0.00	0.00	0.00	0.00	0.00	0.00

The depth of the rectangular shape grid is not known. Therefore, based on the works (Decew et al. 2010; Grue 2014), a proposed depth of 7 meters is used for the analysis. The height of the base cone is also not known, and it was not possible to get this data from the manufacturer. So, a proposed height of 3 meters was used.

The next section shades some light in the modelling of this system.

6.2. System Model

With the above parameters and assumptions, a model was created in SIMA. In order to perform an analysis of the mooring system.

It was not possible to model the exact changing bathymetry of the site. Although a reasonable approximation was achieved. With the available chart, that originated Figure 50, a depth varying bottom was modelled, with parallel contour lines, as shown on Figure 52.

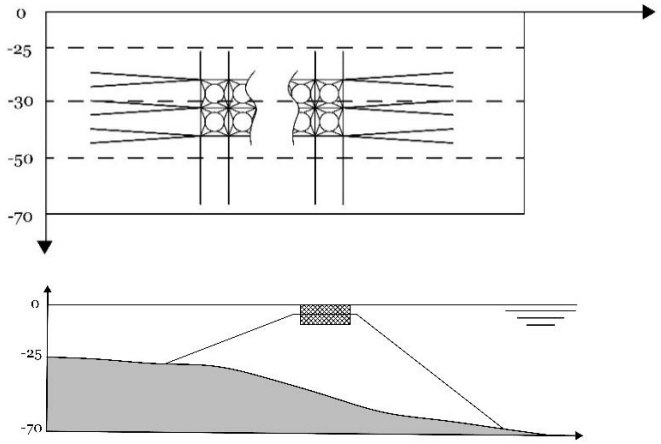

Figure 52 – Top and cross section of 3D bottom model (proportions exaggerated for visualization purposes)

The majority of the parameters of the mooring system were missed. The only information known was that it was made of one single type of synthetic fibre cable and its diameter. Therefore, some assumptions were done. It was decided to use the properties for polyester rope given in (Wang et al. 2018). The drag coefficients of the rope were computed as indicated by the rules (DNV-GL 2015c). The anchors used are drag anchors. The mooring system properties are summarized in Table 15.

Table 15 - Mooring system and model specifications

Mooring		
Diameter	40	[mm]
Axial Stiffness	8e06	[N]
MBL	400	[kN]
Weight	10.72	[kg/m]
Anchors Holding capacity		
Central Line	1.5	[tonne]
Cross lines	0.5	[tonne]
Nº of elements		
Floater	80	
Sinker	80	
Grid	10	
Bridle	15	
Mooring	30	

The pre-tensions of the system are shown graphically on Figure 53.

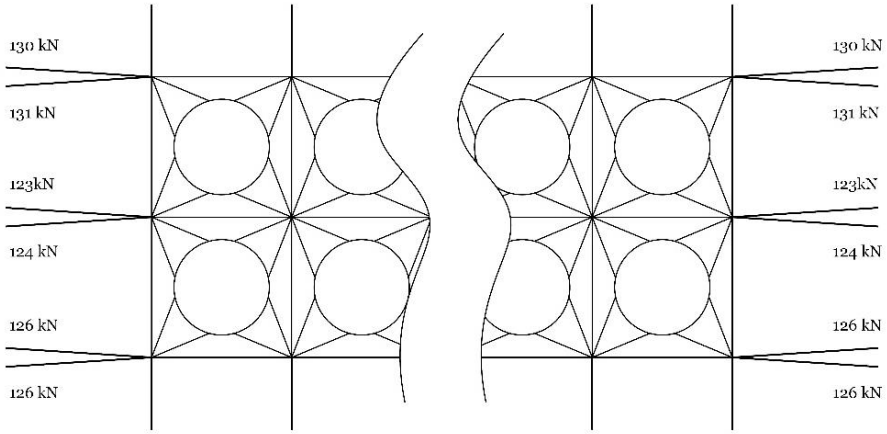

Figure 53 - Mooring lines pre-tension force

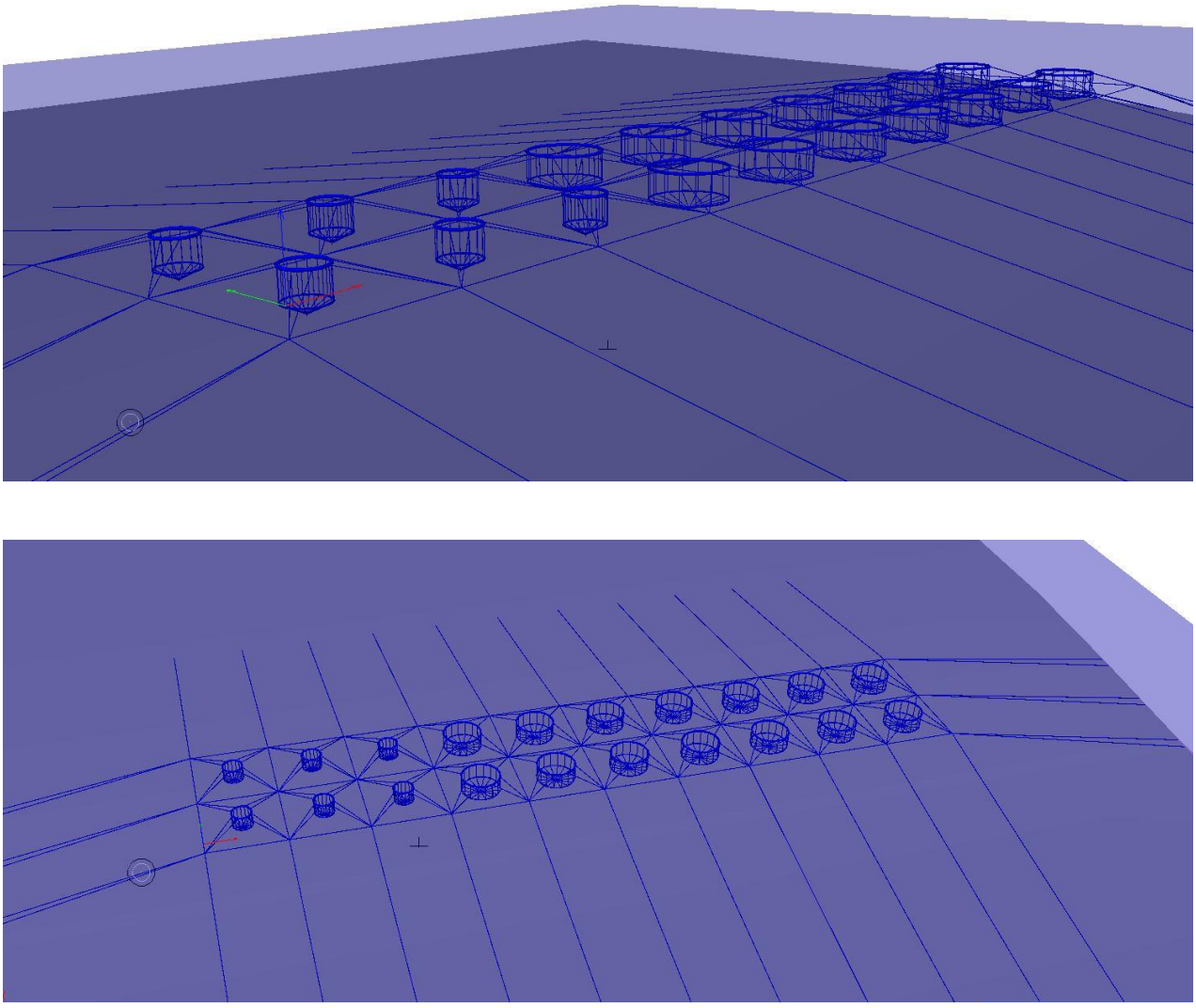

Figure 54 - 3D model built in SIMA

6.3. Analysis

With the data of the occurrence table, a collection of wave density spectrums based on the ITTC spectrum were computed and used as input for an irregular analysis. As explained in the previous chapter, performing irregular analysis with the software SIMA is not possible at the moment, therefore a similar procedure to the one used before is applied here. The RAO for the selected mooring lines were found and then the irregular responses were computed.

The angles analysed were as indicated in Figure 55. The analysis made to some directional data from *IPMA-Instituto Português do Mar e Atmosfera*, and the proximity to shore, made it clear that almost no wave loads would come from the directions between Southeast and Northwest(according to Figure 50). The numbering and labelling of the mooring lines are established in Figure 56.

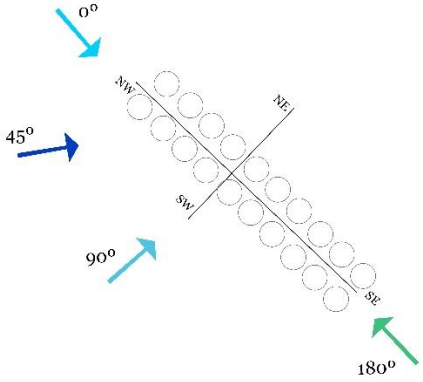

Figure 55 - Analysed angles

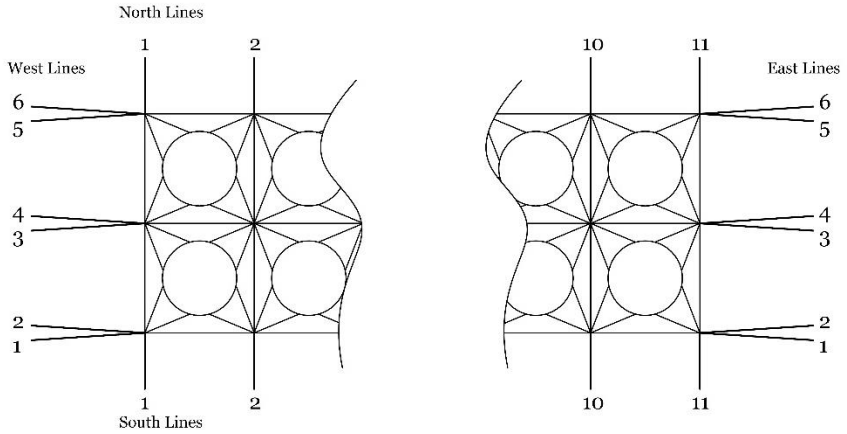

Figure 56 - Mooring lines labels and numbers

For the west and east side there are two lines clustered in each grid node. Since they display a similar behaviour, the RAO will only be shown for one in each pair. Hence Figure 57 shows the RAO for the axial force on west/east lines 2,4 and 6 are presented.

At first sight the RAO are a bit confusing. Although several runs and checks were made and it was concluded that the analysis was being well implemented. One possible reason for this behaviour is the complexity of the system, composed of several cable elements in different configurations, as well as

different cages with free hanging nets. Despite the apparent confusing look, some trends and observations can be made.

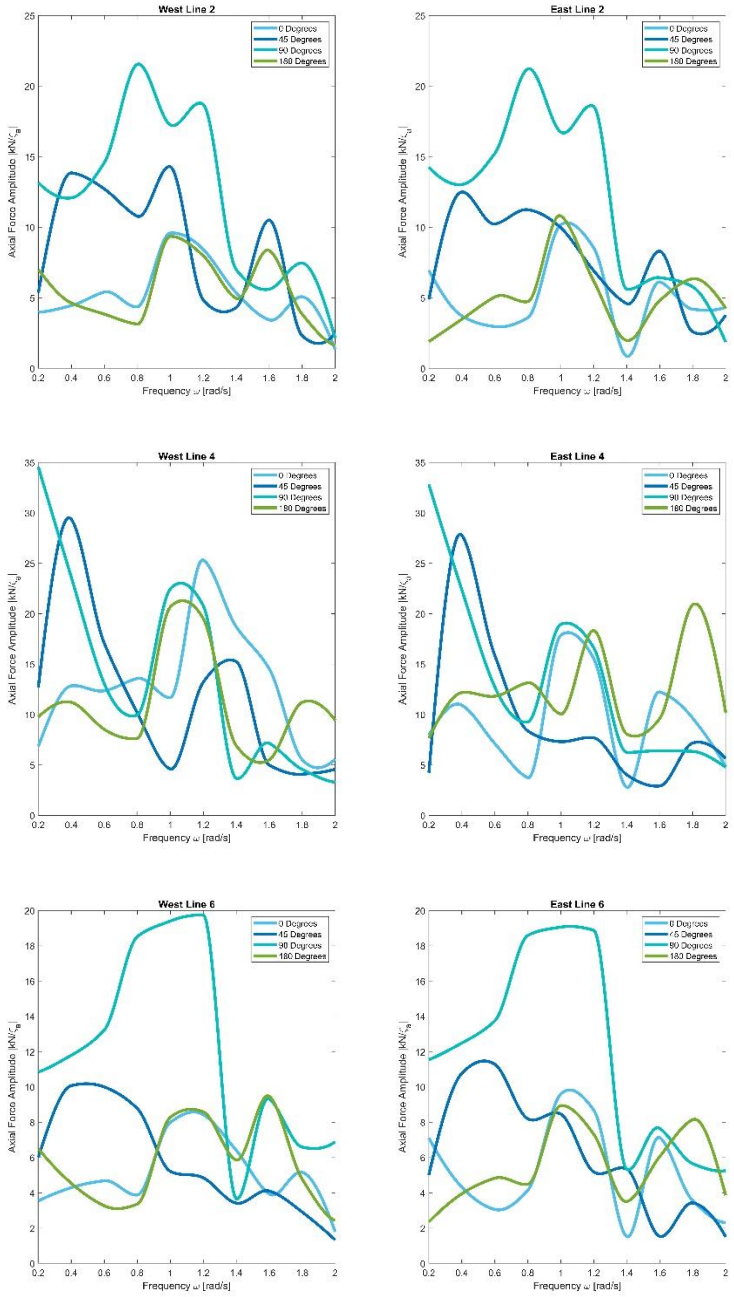

Figure 57 - RAO of axial force on mooring lines 2,4 and 6

From the results observation an asymmetry is highlighted, resulting in different responses between the mooring lines on the west and east side. This asymmetry must arise because of the fact that, although the moorings lines arrangements are equal between the two sides, the cages are different. The west side is dominated by the smaller 40m cages, while the east is dominated by the larger 80m models. The larger cages, due to their larger exposed area, are expected to have a larger response. Albeit,

their larger size also increases the shading effect, reducing the loads for the cages in their wake and consequently their response. Therefore, the balance between these two main phenomena will dictate the changes in response for the different sides and orientations of this system. This hypothesis can be observed in the larger responses of the west lines in a 0º wave orientation when compared with the response of the east lines in a 180º wave orientation. Aided by the larger responses of the west lines in a 180º wave orientation when compared with the east lines in a 0º wave orientation.

In addition to the above-mentioned observations, it is possible to verify that both for the 45º and 90º angles the responses are larger for lower frequencies, while in the 0º and 180 no clear distinction is observed between the lower and higher frequencies regions. Except of course for the response peaks that exist for each line.

A curious finding is that line 4, corresponding to the central line, is the one which bears the largest loads. Simultaneously it is also the line that presents the more fluctuations of the response. It was initially expected that the loads of line 2 would be higher than the loads of line 6, since line 2 would always be more exposed to the environment, but the findings contradict this and show that the loads of line 6 are in fact higher than then loads of line 2. Line 4 has a very large response for the low frequencies when the incidence angle is 90º. It is believed that the reason for such behaviour is the fact that for these small frequencies, large wavelength, waves the whole system (cages plus mooring grid) is moving almost as one identity. Therefore, when the system is in the crest of the wave cycle, this central mooring line is handling much of the load.

Taken together, these results suggest that the mooring forces are larger for the west lines.

The scatter diagram provided had a combination of 272 sea-states, for 16 different peak periods and 17 significant wave heights. With the RAO computed above it is possible to obtain the mooring line responses for each one of them. The resultant response's spectrums are subsequently used to compute the short-term response variance, R. The variance corresponds to the first spectral moment, as shown by eq.(23).

The short-term probability of exceedance, Q_S, can therefore be computed with a Rayleigh distribution.

$$Q_S(x|R) = exp\left(-\frac{x^2}{2R}\right) \tag{72}$$

$Q_L(x) = \int Q_S(x|R).f_R(r)$, where $f_R(r)$ is the joint probability of occurrence of the sea state (73)

Afterwards the long-term probability of exceedance is computed. On Figure 58 the probabilities for the axial force on the west and east mooring lines are shown.

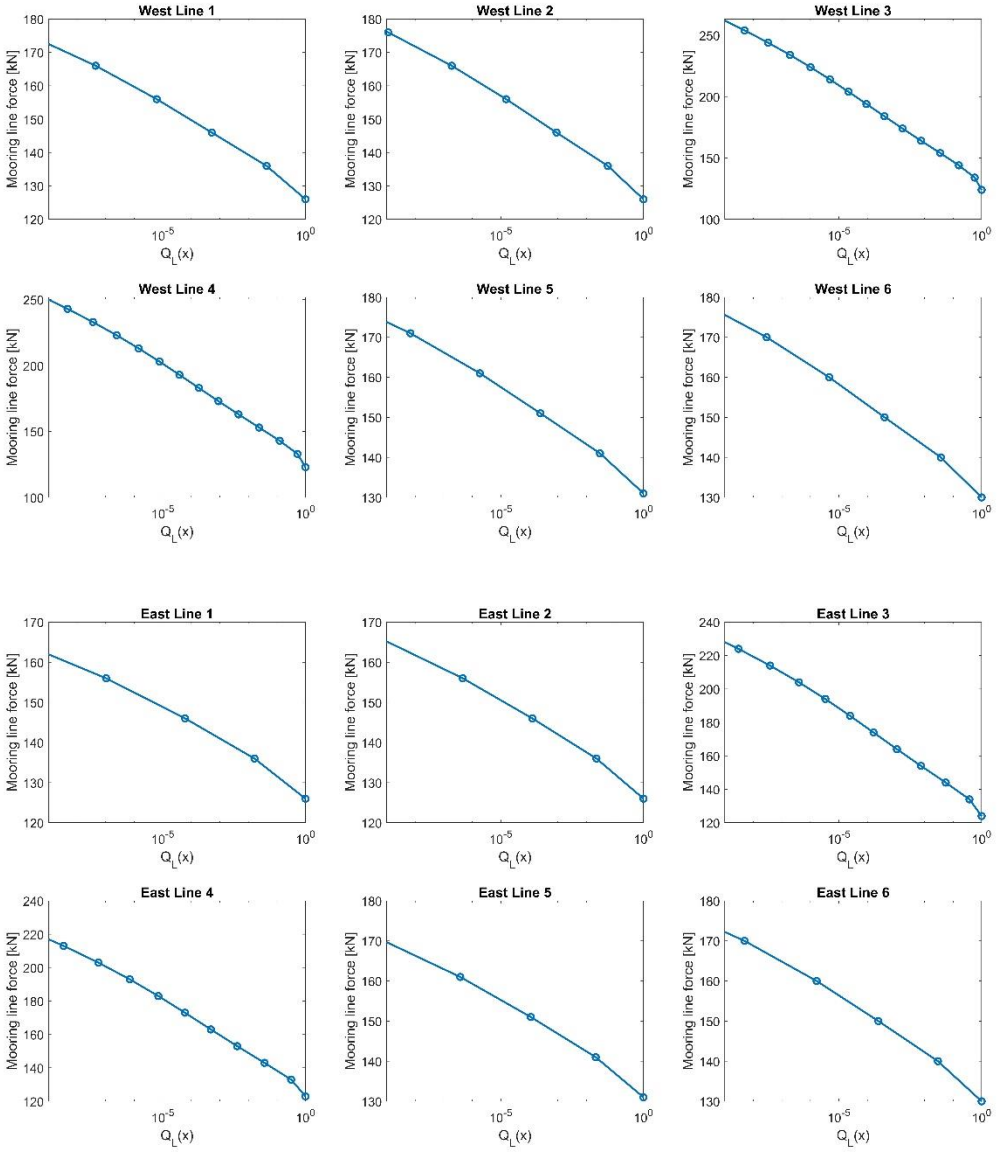

Figure 58 - Long term probability of exceedance of mooring line axial force

The intention was to verify the design of the installed mooring system, making use of the proposed numerical tool and method, by evaluating the choice of the anchors holding capacity. Therefore, a comparison between the holding capacity computed with the results of the above analysis and the holding capacity that listed in the data provided by the company would be made.

According to (DNV-GL 2015c) sea states with return periods of 100-year should be used and current conditions of 10-years. The data provided by the company did not had information regarding the currents. It was also not possible to find reliable and available information of currents around the interested area in the various environmental research bodies. Therefore, the best available option was the 10 years' worth of historical data provided by the *Centro Interdisciplinar de Investigação Marinha e Ambiental da Madeira* (CIIMAR). Although this data was not site specific, it provided a good

understanding of the current behaviours in the south part of the island. It was concluded that, on average, the current velocities did not exceed 0.5 m/s. Thus, a current velocity of 0.5 m/s will be used in this analysis. Regarding the wave data, using the scatter data provided a 100-year contour plot was made. From the contour plot, 4 points were chosen to analyse. The four chosen points and current can be summarised in Table 16.

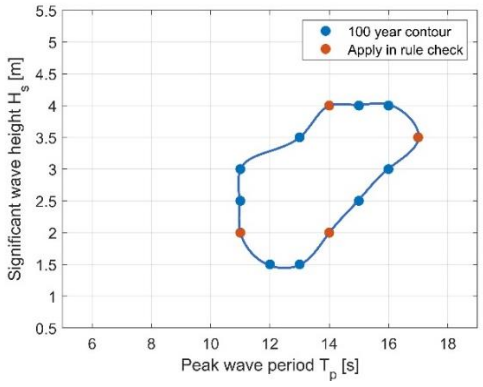

Figure 59 - Sea states along a 100-year contour line for the farm site

Table 16 - Environmental conditions analysed

Waves and Current	Uc [m/s]	Hwav [m]	Tp [s]
WC1	0.5	2	11
WC2	0.5	2	14
WC3	0.5	3.5	17
WC4	0.5	4	14

The four conditions stated above were run for the three major directions: 0º, 90º and 180º. From the calculation of the RAO, it is believed that these directions would give a broad coverage of the harsher scenarios. Only one current direction was used, 0º, for the calculations shown here. This decision was taken because, as mentioned, there is a lack on current data and therefore the most probable directions were not known and also due to the large computational time required to run these analyses. A more correct approach would have been to run the 100 year conditons for a varied set of current directions. Thus, a recommendation is made here to further develop this analysis into a more precise and complete one.

Following the approach established in this work, here only the values for the mooring lines 2,4 and 6 are shown , on Table 17.

Table 17 - Mooring lines maxima axial force for selected lines

	WC1	WC2	WC3	WC4
	Max. Axial Force [kN]			
W. Line 2	185	181	200	210
W. Line 4	218	215	279	287
W. Line 6	183	179	205	221
E. Line 2	113	114	128	127
E. Line 4	110	116	157	157
E. Line 6	123	124	142	150

As previously mentioned, the type of anchors installed, and respective anchor capacities, are not known. Thus, it is not possible to compute an anchor holding capacity with the purpose of evaluating the design decision made in this installation by the contracted company. Nonetheless, with the analysis' results it is possible to provide a rough recommendation on the required anchor holding capacity, by recommending that it should be higher than the maximum computed loads. Iddealy a safety factor should be applied to this maximum, altough such a simple approach is not found in the standards therefore no such factors will be used. Instead the procedure for the Ultimate State Analysis (ULS) required by (DNV-GL 2015c) is used as a coarse check of the design. The design equation is introduced on eq.(74), where γ_{mean} and γ_{dyn} are the mean and dynamic tension partial safety factors, 1.1 and 1.5 respectively. The design equation can also be redefined as the utilization factor, u.

$$S_C - T_{C-mean}\gamma_{mean} - T_{C-dyn}\gamma_{dyn} \geq 0 \tag{74}$$

$$u = \frac{T_{c-mean}\gamma_{mean} + T_{c-dyn}\gamma_{dyn}}{S_C}, u \leq 1 \tag{75}$$

For the selected lines the utilization factors are shown on Table 18 .For each 100 year environmental condition the highest utilization factor is shown.

Table 18 - Mooring lines utilization factors

	W. Line 2	W. Line 4	W. Line 6	E. Line 2	E. Line 4	E. Line 6
WC1	0.53	0.63	0.52	0.32	0.31	0.35
WC2	0.52	0.62	0.51	0.33	0.34	0.35
WC3	0.58	0.83	0.60	0.38	0.48	0.42
WC4	0.61	0.87	0.65	0.37	0.48	0.45

By examining the results, it is possible to verify that the current mooring system satisfies the class requirements regarding the ULS capacity of the lines. Although it is important to remark that this analysis was done for one single current velocity and direction. A full evaluation of this aquaculture

mooring system would require a much more thorough analysis. Thus, such analysis is thought to be out of the scope of this work, that intended, among other things, to demonstrate the feasibility of the numerical tool SIMA in the analysis of this kind of structures.

After the analysis of a real system, and together with the tools and knowledge already presented in this work, a proposal for a design to be used for offshore aquaculture production is presented. The following chapter will go through the preliminary design process of a aquaculture system, going in detail into the design considerations and decisions.

7. Proposal of a fish cage concept

In this chapter a concept is roughly designed and analysed. To serve as an example for the use of the specified design constraints and requirements associated with offshore aquaculture systems. The methodology pursued was to first establish the desired biomass capacity and then work from it. This capacity was decided by evaluating the information gathered in chapter 4, which led to the decision of using a density of 20 [kg/m^3], slightly below the average found, to account for the uncertainties of the information used to performed it. The proposed system has a cage volume of around 765 m^3, translating in a potential to produce around 19 [t] of biomass.

7.1. Design Process

The initial idea was to apply the emerging field of generative design in the design process. Although it was quickly found that this tool is practically not used yet on marine applications. Thus, the effort necessary to employ it would gain dimensions out of the scope of this work. So, the idea was abandoned.

A crucial point to take in consideration, as stated before, is to design a structure with a simple geometry that could be produced in shipyards with lesser means. So, simple elements, like tubular and flat plate members should be the base of the design.

Weighting all the requirements and constraints, the proposed solution grew around a hexagon shape prism. The submersible ability is achieved with several bottom ballast tanks, enclosed inside a bottom circular ring-like beam, Figure 60 shows some iterations of the concept, where different structures were proposed, although simplicity here is key, since a simpler design will lead to a lower building cost.

The use of ballast tanks, alternately to a self-submerged design, incurs a larger input of energy onto the system. It is a trade-off that has to be made with the chosen mooring system. The choice to not use a self-submerged design was based on the fact that less information regarding this design is available to consult. Therefore, a safer approach, with the knowledge obtained in the courses of the study program, was followed and a more traditional spread mooring design with a ballast system was used.

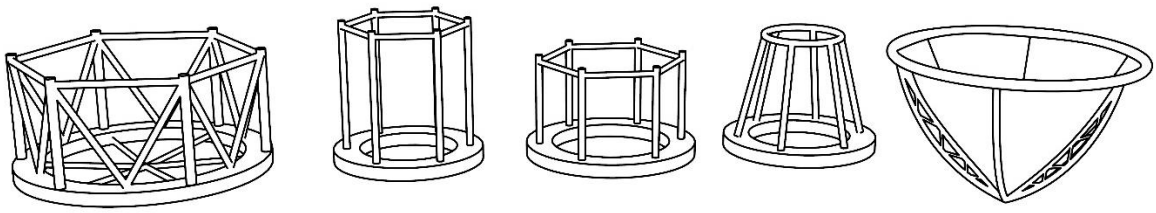

Figure 60 - Study of different concept geometries

7.2. Proposal

As said before the scope of this work is not to design a system in a detailed way, but rather, through this initial design analysis, show the feasibility of the numerical tool selected and the classification society rules that should be addressed. Therefore, neither a structural analysis of the cage nor a complete design process of the mooring will be carried out. Leaving this analysis for a possible future work.

7.2.1. Specifications

The specific dimensions of the structure were obtained with the help of a MATLAB code. The code script, using an inbuilt genetic algorithm, tried to find the combination of member dimensions and geometry in order to achieve the desired volume with the lowest amount of steel as possible. Some constraints regarding minimum dimensions were imposed. An overview of the script is shown in Figure 61.

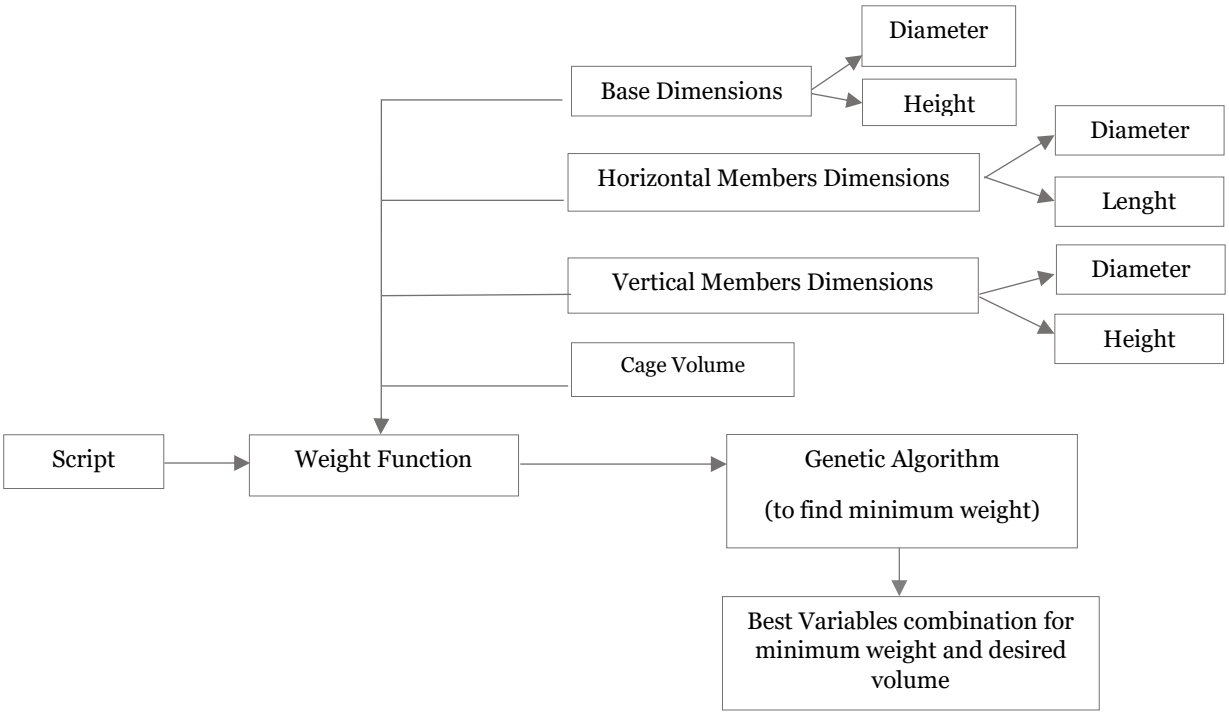

Figure 61 - Overview of the script used in the preliminary design

After several runs of the script, it was decided that a ratio of cage height/diameter should be equal or higher than one (with one being the used ratio). The differences of different ratios are related with fish biology and the wate temperature. A taller structure will have a bigger water temperature gradient, and therefore there is some risk that the fish growth is less uniform due to fish utilization of different depths, which economically is not desired. Since each harvested batch should be as uniform as possible.

In order to verify the feasibility of the chosen design, and proceed to a little tune of the dimensions, a preliminary check on the system buoyancy for different immersions was done. The results are shown on Figure 62.

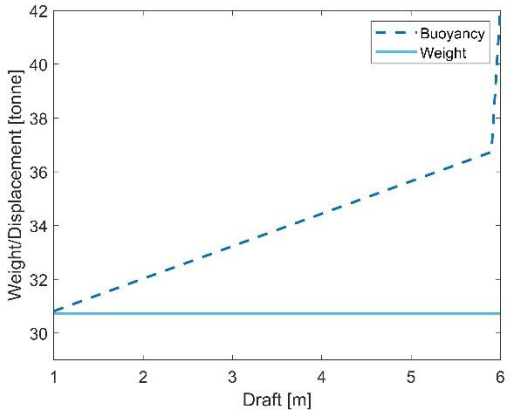

Figure 62 - Preliminary buoyancy and ballast capability of concept structure

From Figure 62 it can be seen that the proposed structure has enough buoyancy to be afloat if needed, for towing and maintenance operations for example, and has enough ballast capacity to be submerged, at different depths, for different operational conditions. The structure was design to be afloat with a draft of 1m, corresponding to the immersion of the bottom ring section, since this would be the ideal setup for towing the structure. Therefore, this design solution seems feasible to use. It is important to note that these computations were performed for a basic structure and were used in the preliminary design stage of the structure. The next section goes deeper into the design proposed by this work

7.2.2. Design

The concept proposal offer by this work is, as mentioned, a cage shaped in a hexagonal prism. With an outer rigid structure composed by two circular rings connected by rigid columns members. A visualization of the concept is presented on Figure 63 and its properties on Table 19.

(a) (b)

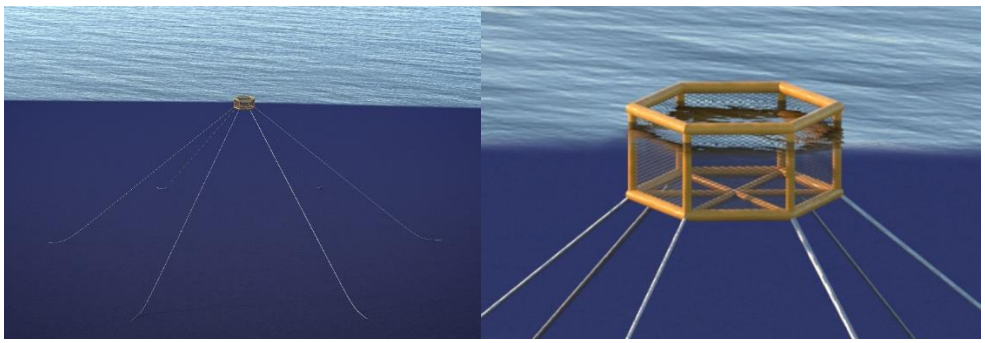

Figure 63 - Concept proposal of a 765 m3 cage. (a) Overview; (b) Detailed

Table 19 - Model properties

Cage		
Height	7	[m]
Diameter	8	[m]
Top and Bottom hexagons		
Diameter of tube	700	[mm]
Length (each member)	3.5	[m]
Density	7850	[kg/m3]
Weight	137	[kg/m]
Axial Stiffness	3.5e09	[N]
Cd	0.5	[-]

Nº elements	
Top hexagon	6
Bottom hexagon	6
Vertical columns	1
Connecting members	1
Mooring	60 (10+50)

Vertical Columns		
Diameter of tube	300	[mm]
Length (each member)	6	[m]
Density	7850	[kg/m3]
Weight	44	[kg/m]
Axial Stiffness	1.1e09	[N]
Cd	1.14	[-]
Connecting Members		
Diameter of tube	200	[mm]
Length (each member)	7	[m]
Density	7850	[kg/m3]
Weight	29	[kg/m]
Axial Stiffness	7.3e08	[N]
Cd	1.6	[-]

The proposed mooring system is based on the observations made during all the study process for the elaboration of this work, it fundaments itself in the tendencies of the industry as well as the knowledge gain during the course of *Floating Production Systems*, taught on this master program. Therefore, this mooring proposal is not the result of a full design process, but rather a realistic and possible proposal for the sake of showing the feasibility of the numerical tool to carry out the desired analysis.

The mooring system will be composed of catenary lines in a spread arrangement, with six anchor points. The structure will not have the typical arrangement of the aquaculture industry, discussed on section 4.6, but the configuration seen in the oil and gas/wind industry, where the mooring lines connect the structure at a fairlead. This decision was taken based on what is being done by the design teams that are at the forefront of the offshore cages development, as presented on section 1.3 and 4.5. The mooring lines will consist of multicomponent segments of chain and synthetic cable. The properties of the mooring system are presented on Table 20, the pre-tension on the system was of *22* kN. The data for the chain segment was obtained from (Chakrabarti 2005) and cable properties from (Wang et al. 2018), the coefficients from (DNV-GL 2015c).

Table 20 - Mooring System Properties.

Chain Segment			Synthetic Cable Segment		
Length	24	[m]	Length	142	[m]
Diameter(chain)	0.101	[m]	Diameter	0.3	[m]
Weight	200	[kg/m]	Weight	5	[kg/m]
Axial Stiffness	375	[kN/m]	Axial Stiffness	8.3	[kN/m]
Cd	2.6	[-]	Cd	1.6	[-]

The following sections will analyse the hydrodynamic behaviour of the structure. The mooring system will also be analysed, through the assessment of the behaviour of the cage under different environmental loads.

7.3. Analysis

In this section a hydrodynamic analysis of the concept will be performed. Firstly, the RAO of the cage itself (structure plus net) are computed. Thenceforth, the RAO are recomputed, but with the mooring system installed. In this way a brief comparison is made between the two conditions. Since the software SIMA doesn't allow for the simulation of irregular waves with the net element, something they are looking to improve as expressed in (Aksnes 2106), the procedure to compute the RAO was somewhat lengthy. For a specific and constant wave height, several time-domain simulations were done for a chosen range of frequencies. Then the ratio of the desired motion with the wave height was plotted against the frequency range.

This procedure is far from being time efficient and is prone to some errors along the way. Albeit, at the moment is the only way to compute RAO for structures with net elements, since the normal hydrodynamic tool of the SESAM package, HydroD, does not allow the modelling of nets. An interesting study will be to compute the RAO for the cage only (without nets) with HydroD and then compare the results with the approach followed in this work. Due to limited space available in this work, as well as some issues with the license of the software, this study was not performed. Therefore, here stays the suggestion for it.

In addition to the RAO, an analysis of the effect of currents on the axial force of the mooring lines is carried out.

7.3.1. Structure Analysis

The first step of the analysis was to access the hydrodynamic behaviour of the system, through the elaboration of the respective RAO. Due to the geometry symmetry of the structure, the angles investigated were 0º, 20º, 45º and 70º,Figure 64. The surge and sway movements were not analysed, since they were thought to be of minor interest on this phase, later they will be access for the moored system. The yaw was also thought of being of minor importance and therefore was not access. The roll and pitch motion for this radially symmetric structure are somewhat defined by the incoming -angle of the waves and current. Since the same motion can be defined as roll or pitch depending on the angle between the structure axis and the incoming load. Therefore, the motions that were analysed were the heave and pitch. The respective RAO are shown on Figure 65.

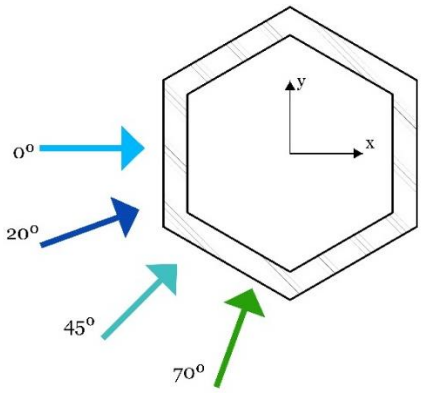

Figure 64 - Analysed angles.

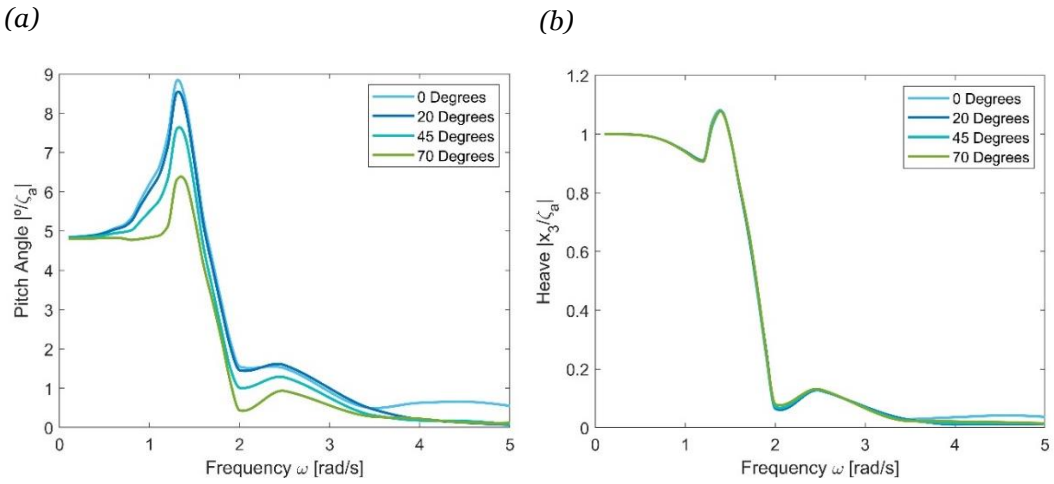

Figure 65 – (a) Cage structure RAO for pitch motion. (b) Cage structure RAO for heave motion

The next section will perform a similar hydrodynamic analysis for the full system, namely the cage plus the mooring set-up.

7.3.2. Moored Structure Analysis

As done in the previous section, a hydrodynamic analysis of the moored structure was performed. Following the same procedure, the RAO for heave and pitch were computed, as shown on Figure 66.

As expected, the overall reaction of the structure was reduced. Since the mooring restricts the heave and pitch motion.

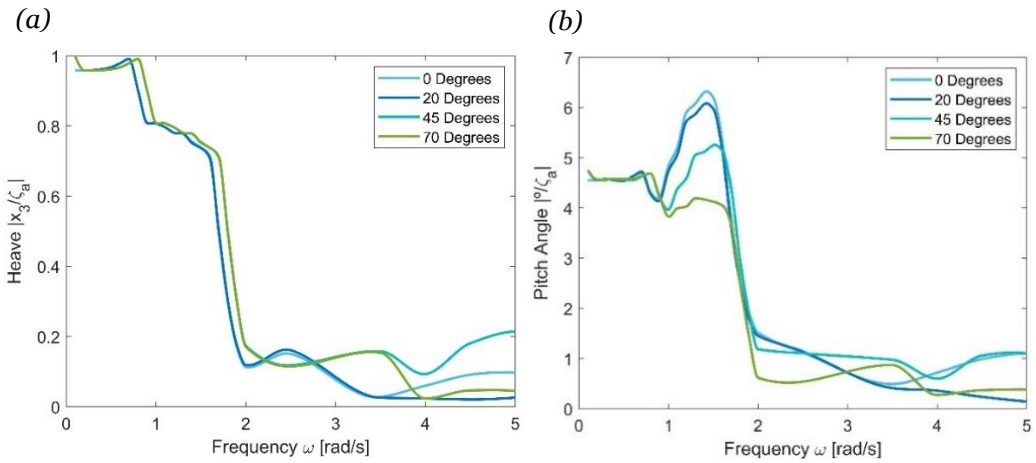

Figure 66 – (a) Moored structure RAO for heave motion. (b) Moored structure RAO for pitch motion

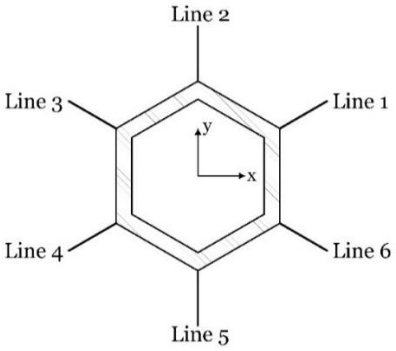

Figure 67 - Mooring arrangement

In addition, the RAO of the mooring line's axial force were also computed. The RAO of the moored system provides useful insight of the cage behaviour during the design process. The lines are numbered as shown in the mooring's arrangement of Figure 67.

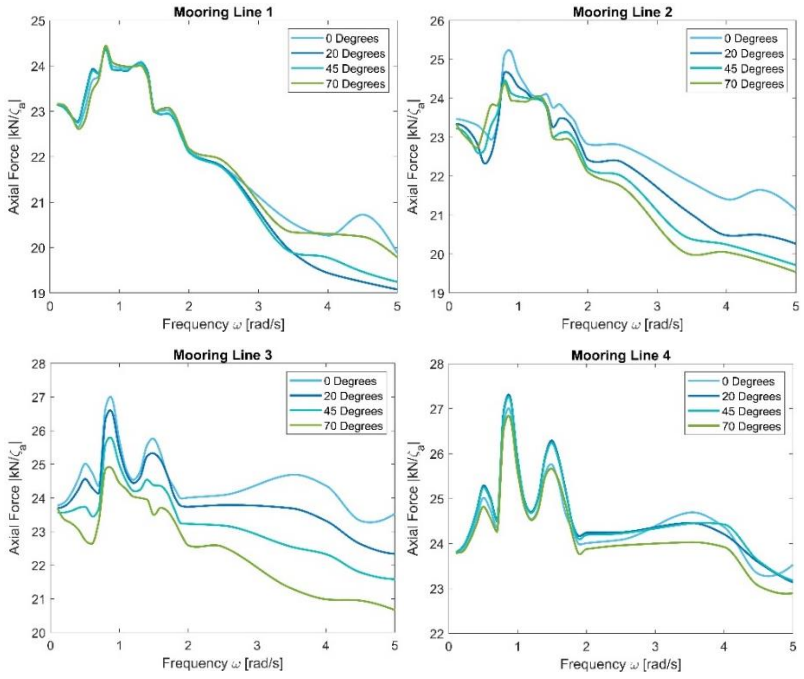

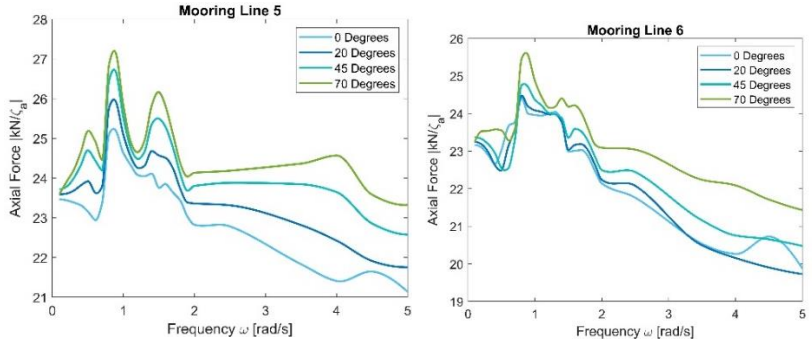

Figure 68 - Moored structure RAO of axial force of mooring lines

This structure does not have suspended nets, all net panels are attached to the structure at their boundaries. Consequently, the force caused by the current should be quite significantly since the net is not very deformed and the angle of attack of the net stays quite high, as talked about in section 2.1. To access this, a study of the axial force of the mooring lines was performed for different current velocities (without waves). Moreover, the computation of the overall current induced drag force on the cage is also computed.

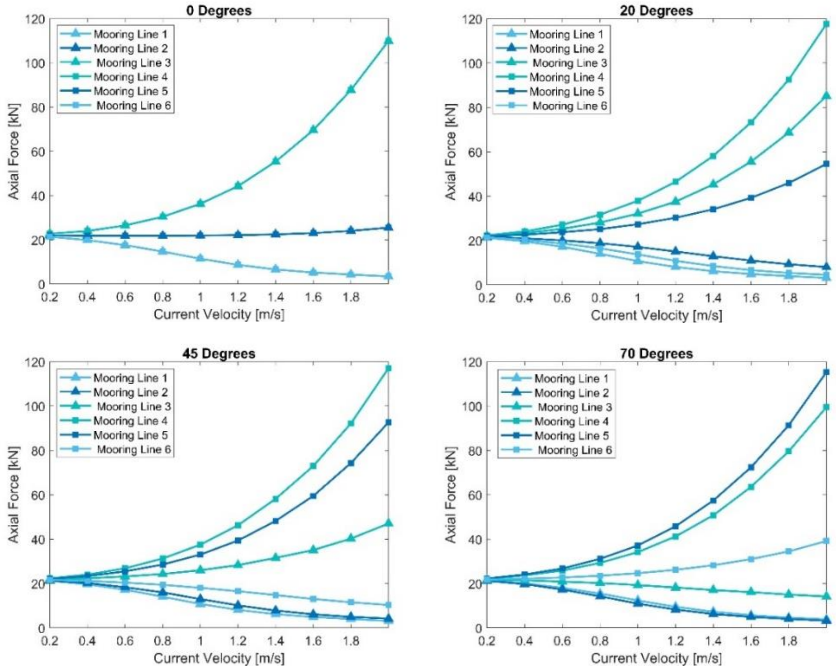

Figure 69 - Axial force of mooring lines under different current velocities

The drag force on the cage due to current exclusively was computed for the direction of 0 º. Due to the method employed in the computations and modelling it was not feasible to compute for the other directions. It would be possible, but the effort and time required to remodel was not worth the gain since the purpose of this chapter is to show the feasibility of this tool. The numerical tool does not offer the drag force on the cage as an output, it only outputs axial forces through the elements of the model, hence a method had to be conceived. A horizontal dummy spring was modelled and the force on it was computed, as a virtual dynamometer, in this way the drag force on the cage (without moorings) due to the current was computed.

Some information is being lost here, since the orientation of the net panels regarding the different directions is different, as Figure 64 shows, therefore the drag force on the cage will be different as well.

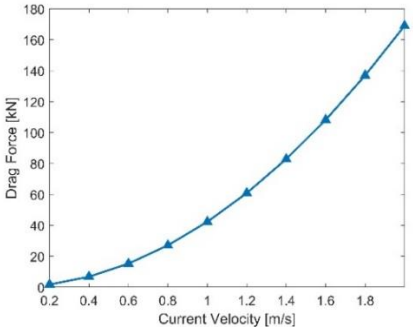

Figure 70 - Drag Force on the cage due to current, orientation of 0º

8. Conclusion

The purpose of the present work was to launch the interest for the aquaculture sector, more specifically the offshore, in our marine department and lay off the foundational work. This was done through the formulation of the design criteria, characteristic of this type of systems and environment. Plus the proposal of a numerical tool to assist in the study of the main components during the design process, and it ended with the analysis of an existing system and the design, plus analysis, of a new system concept.

The potential and importance of offshore aquaculture has already been acknowledged by the major countries and universities with connection and dependence of sea-going activities for some time. This has led to research initiatives all around the globe, and the first pilot projects being launched somewhere between the last years and the present time. Some of these players share more information about their activities, such as North America and Norway, others are more secluded, like China and Japan. This made it difficult to access precisely the present state of development of the sector, but the information available was enough to shed some light over it. The precocity of the industry is also reflected on the standards and regulations available, where there are still few dedicated standards, with ABS and DNV-GL leading the way. To remark that these standards borrowed a lot from the oil and gas industry. The offshore location in conjunction with the interests of the aquaculture industry shareholders prompt a series of design constraints and requirements, which were gathered and reviewed on this work. A commercially available software was chosen to perform the analysis in the initially design phase. This software was chosen due to its availability in our department and its integration in the SESAM environment, which is the package used in our classes and by some researchers as well. Prior to any analysis the tool had to be validated, since few works were available with this tool. The validation process also deepened the understanding of the strengths and weaknesses of the tool. The most important lesson from this process being the weaker performance of the tool, when compared with other codes, to access the net behaviour in a detailed way. Although it performed well in the assessment of the loads onto the nets. This two main observations can be summarised in a recommendation: this tool is not the best for a more academic study of the net behaviour, such as the sensitivity to different parameters or predicting the net shape, but it is a good choice for the study of more complete systems, where the focus is in the behaviour of the cages and its complementary elements (such as moorings). Ideally this tool should be used in association with experimental trials, in such a manner as to allow a good tuning of the model. It would be interesting to perform comparison analysis between the SIMA tool and other tools of the SESAM package, such as HydroD. In order to access if it is viable to use them for some parts of the analysis, the computations of the RAO for example, in a way to create a more efficient workflow in the analysis of these aquaculture systems.

Making use of the criteria and requirements discussed, a basic design concept was introduced. The main point was to illustrate the role that the different criteria and requirements had in each design decision and also how the SIMA tool could be used for an initially assess of the loads and mooring design. SIMA proved to be a very useful tool due to its in-built fish net element, that simplified the design and analysis. Although, there is a downside. It is a very time-consuming task, due to long computational times and required post treatment. Thus, why the recommendation for the integration

of this tool with the others of the package was made. The structural analysis was not performed as initially intended, because the familiarization with and validation of the SIMA tool took much more time than originally expected. Additionally, the analysis of marine structures was not a course I undertook during this master, thus it would imply a whole new study effort and time dedicated to it. Therefore, although it would be interesting and useful to gain this new knowledges and insights, the amount of work and time required for a structural analysis was considered to be out of the target of this work. Nonetheless, a recommendation is made to further develop this concept and investigate how the specific criteria and requirements of the offshore aquaculture systems influence the structural analysis. Lastly, using the knowledge gained throughout the elaboration of this work, a rough analysis was done to an existing system. The analysis was simple enough and the tool coped well with the size and complexity of the system, strengthening the point that this tool can be an aid in the design process. In addition, a recommendation for further work on the maximum loads on the mooring system was done.

After the completion of this work, the importance of this new subject in the marine sector is clear. Although not as strong and prominent as the offshore renewables, it will nonetheless have greater importance in the future of the global society and it will be a growing segment in the marine industry, as the big investments being done around it confirm. Therefore, our country, and more specifically our university, should not fall behind. We should instead take advantage of our knowledge and country conditions and spurred the research and developments in this sector.

9. References

Aarsnes, J.V., H. Rudi, and Geir Løland. 1990. “Current Forces on Cage , Net Deflection.” In *Engineering for Offshore Fish Farming*, Thomas Telford, 137–52.

Aksnes, Vegard. 2106. *Modelling of Aquaculture Net Cages in SIMA*. Trondheim.

Andresen, Jørgen. 2017. “Mooring Analysis of a Closed Fish Cage.” University of Stavanger.

Bagni, M. 2005. “Cultured Aquatic Species Information Programme - Dicentrarchus Labrax.” *FAO Fisheries and Aquaculture Department*.

Birkevold, Jens, Martin Føre, Arne Fredheim, and David Kristiansen. 2014. “Simulation and Validation of a Numerical Model of a Full Aquaculture Net-Cage System.” In *International Conference on Ocean, Offshore and Arctic Engineering*, , 1–11.

Bore, Pål Takle, and Pål Alexander Fossan. 2015. “Ultimate- and Fatigue Limit State Analysis of a Rigid Offshore Aquaculture Structure.” NTNU.

Le Bris, Fabien, and Dominique Marichal. 1999. “Numerical and Experimental Study of Submergde Supple Nets: Applications to Fish Farms.” *Journal of Marine Science and Technology* (1998): 161–70.

Bunnik, T H J et al. 2002. “Coupled Mooring Analysis in Large Scale Model Tests on a Deepwater Calm Buoy in Mild Wave Climates.” In *International Conference on Offshore Mechanics and Arctic Engineering*, , 1–12.

Cardia, Francesco, and Alessandro Lovatelli. 2015. FAO. Fisheries Technical Paper *Aquaculture Operations in Floating HDPE Cages: A Field Handbook*.

CEA, California Environmental Associates. 2018. *Offshore Finfish Aquaculture - Global Review and U.S. Prospects*.

Chakrabarti, Subrata K. 2005. I Offshore Structures Analysis *Handbook of Offshore Engineering*. Elsevier.

Chang, Shuenn Yih. 2009. “Numerical Characteristics of Constant Average Acceleration Method in Solution of Nonlinear Systems.” *Journal of the Chinese Institute of Engineers* 32(4): 519–29.

Chen, Hao, and Erik Damgaard Christensen. 2016. “Investigations on the Porous Resistance Coefficients for Fishing Net Structures.” *Journal of Fluids and Structures* 65: 76–107.

CNEXO, Centre National pour L’Exploitation des Océans. 1983. *Fiches Biotechniques D’Aquaculture - Le Dorade*.

Colloca, F., and S. Cerasi. 2005. “Cultured Aquatic Species Information Programme. Sparus Aurata.” *FAO Fisheries and Aquaculture Department*.

Dean, R.G., and R.A. Dalrymple. 1991. *Water Wave Mechanics For Engineers and Scientists*. World Scientific.

Decew, Judson et al. 2010. “Assessment of a Mooring System for Offshore Aquaculture.” *Ocean and Coastal Management* (2004): 32–36.

Decew, Judson, Steve Page, Chad A Turmelle, and Jim Irish. 2006. “Tow Test Result of an AquaPod

Fish Cage." In *OCEANS 2006,*.

Dee, D. P. et al. 2011. "The ERA-Interim Reanalysis: Configuration and Performance of the Data Assimilation System." *Quarterly Journal of the Royal Meteorological Society* 137(656): 553–97.

DGRM, Direcção-Geral de Recursos Naturais Segurança e Serviços Marítimos. 2014. *Plano Estratégico Para A Aquicultura Portuguesa, 2014-2020*.

———. 2018. *Ordenamento Do Espaço Marítimo Nacional-Plano de Situação:Volume III-A*.

DNV-GL. 2015a. *OS-A101: Safety Principles and Arrangements*.

———. 2015b. *OS-C201: Structural Design of Offshore Units - WSD Method*.

———. 2015c. *OS-E301: Position Mooring*.

———. 2016. *RP-C203: Fatigue Design of Offshore Steel Structures*.

———. 2017a. *RP-C205: Environmental Conditions and Environmental Loads*.

———. 2017b. *RU-OU-0503: Rules for Classification Offshore Fish Farming Units and Installations*.

Elliott, J. M., and J. A. Elliott. 2010. "Temperature Requirements of Atlantic Salmon Salmo Salar, Brown Trout Salmo Trutta and Arctic Charr Salvelinus Alpinus: Predicting the Effects of Climate Change." *Journal of Fish Biology* 77(8): 1793–1817.

Faltinsen, Odd M. 1990. *Sea Loads on Ships and Offshores Structures*. eds. I. Dyer, R. Eatock Taylor, J. N. Newman, and W. G. Price. Cambridge University Press.

FAO, Food and Agriculture Organization of the United Nations. 2018. *The State of the World Fisheries and Aquaculture*.

Flagstad, Ole Andreas, and Harald Tvedt. 2018. Ocean Space *Aquaculture Going Offshore*.

Frank, W. 1967. *Oscillation of Cylinders in or below the Free Surface of Deep Fluids*. Washington D.C.

Fredriksson, David et al. 2004. "The Design and Analysis of a Four-Cage Grid Mooring for Open Ocean Aquaculture." *Aquacultural Engineering* 32: 77–94.

———. 2007. "Development of Large Fish Farm Numerical Modeling Techniques with in Situ Mooring Tension Comparisons." *Aquacultural Engineering* 36(2): 137–48.

Froehlich, Halley E., Alexandra Smith, Rebecca R. Gentry, and Benjamin S. Halpern. 2017. "Offshore Aquaculture: I Know It When I See It." *Frontiers in Marine Science* 4: 154.

Gjøsund, Svein Helge, and Birger Enerhaug. 2010. "Flow through Nets and Trawls of Low Porosity." *Ocean Engineering* 37(4): 345–54.

Goda, Yoshimi. 2000. World Scientific *Random Seas and Design of Maritime Structures*. 3rd ed. ed. Philip Liu. World Scientific.

Grue, Ida Håøy. 2014. "Loads on the Gravity-Net-Cage from Waves and Currents." Institutt for marin teknikk.

Harkell, Louis. 2018. "China, De Maas Charge Ahead with Offshore Aquaculture | Undercurrent News." *Undercurrent News*. https://www.undercurrentnews.com/2018/10/01/china-de-maas-charge-ahead-with-offshore-aquaculture/ (March 15, 2019).

Høiland, Andreas Vangdal. 2017. "Dynamic Analysis of a Vessel-Shaped Fish Farm for Open Sea."

University of Stavanger.

Ibarz, A. et al. 2003. “Oxygen Consumption and Feeding Rates of Gilthead Sea Bream (Sparus Aurata) Reveal Lack of Acclimation to Cold.” *Fish Physiology and Biochemistry* 29(4): 313–21.

INE, Instituto Nacional de Estatísitca, and Direcção-Geral de Recursos Naturais Segurança e Serviços Marítimos DGRM. 2017. *Estatísticas Da Pesca 2017*.

Jo, Chul Hee, Do Youb Kim, and Yu Ho Rho. 2014. “A Comparison of Coupled and Uncoupled Dynamic Analysis for the Flexible Riser in Shallow Water.” In *International Conference on Offshore Mechanics and Arctic Engineering*, , 195–201.

Kiernan, Lynda. 2018. “Chinese Consortium Investing US$955M to Build Offshore Mega-Fish Farm.” *Global Ag Investing*. http://www.globalaginvesting.com/chinese-consortium-investing-us955m-build-offshore-mega-fish-farm/ (March 17, 2019).

Kristiansen, Trygve, and Odd M. Faltinsen. 2012. “Modelling of Current Loads on Aquaculture Net Cages.” *Journal of Fluids and Structures* 34: 218–35.

Lader, Pål Furset, and Birger Enerhaug. 2005. “Experimental Investigation of Forces and Geometry of a Net Cage in Uniform Flow.” *IEEE Journal of Oceanic Engineering* 30(1): 79–84.

Lader, Pål Furset, and Arne Fredheim. 2006. “Dynamic Properties of a Flexible Net Sheet in Waves and Current-A Numerical Approach.” *Aquacultural Engineering* 35(3): 228–38.

Lader, Pål Furset, Arne Fredheim, and Jorgen Krokstad. 2001. “Modelling of 3D Net Structures Exposed to Waves and Current.” In *Open Ocean Aquaculture Symposium*, , 1–27.

Li, Lin, Zhiyu Jiang, Jungao Wang, and Muk Chen Ong. 2018. “Predicting the Heading Misalignment of a Vessel-Shaped Offshore Fish Farm Under Waves and Currents.” In *International Conference on Ocean, Offshore and Arctic Engineering*, ASME.

Li, Lin, Muk Chen Ong, and Zhiyu Jiang. 2017. “A Preliminary Study of a Vessel-Shaped Offshore Fish Farm.” In *International Conference on Ocean, Offshore and Arctic Engineering*, , 1–11.

Li, Peng, and Odd M. Faltinsen. 2012. “Wave-Induced Vertical Response of an Elastic Circular Collar of a Floating Fish Farm.” In *10th International Conference on Hydrodynamics*,.

Li, Peng, Odd M. Faltinsen, and Marilena Greco. 2017. “Wave-Induced Accelerations of a Fish-Farm Elastic Floater: Experimental and Numerical Studies.” In *International Conference on Ocean, Offshore and Arctic Engineering*, , 1–10.

Li, Yu-Cheng et al. 2011. “Numerical Investigation of the Hydrodynamic Behaviors of Multiple Net Cages in Waves.” *Aquacultural Engineering* 48: 6–18.

Løland, Geir. 1991. “Current Forces on and Flow through Fish Farms.” *Aquaculture International* 1: 72–89.

Lorentzen, Torbjorn. 2008. “Modeling Climate Change and the Effect on the Norwegian Salmon Farming Industry.” *Natural Resource Modeling* 21(3): 416–35.

Lovatelli, Alessandro, Jose Aguilar-Manjarrez, and Doris Soto. 2013. FAO Technical Workshop *Expanding Mariculture Farther Offshore: Technical, Environmental, Spatial and Governance Challenges*.

Moe, Eirik. 2017. *The Norwegian Aquaculture Analysis 2017*.

Moe, Heidi et al. 2007. “Tensile Properties for Netting Materials Used in Aquaculture Net Cages.” *Aquacultural Engineering* 37(3): 252–65.

Moe, Heidi, Arne Fredheim, and Odd Sture Hopperstad. 2010. “Structural Analysis of Aquaculture Net Cages in Current.” *Journal of Fluids and Structures* 26(3): 503–16.

Pahl, G., W. Beitz, J. Feldhusen, and K.H. Grote. 2015. Real-World Engineering *Engineering Design - a Systematic Approach*. Third. eds. Ken Wallace and Lucienne Blessing. Springer.

Pérez, O. M., T. C. Telfer, and L. G. Ross. 2003. “On the Calculation of Wave Climate for Offshore Cage Culture Site Selection: A Case Study in Tenerife (Canary Islands).” *Aquacultural Engineering* 29(1–2): 1–21.

Person-Le Ruyet, J., K. Mahé, Nicolas Le Bayon, and H. Le Delliou. 2004. “Effects of Temperature on Growth and Metabolism in a Mediterranean Population of European Sea Bass, Dicentrarchus Labrax.” *Aquaculture* 237(1–4): 269–80.

Pillay, T.V.R. 1992. *Aquaculture and the Environment Second Edition*. Second. Blackwell Publishing.

Portugal, Goverment of. 2013. *Estratégia Nacional Para o MAR 2013-2020*.

Priour, Daniel. 1999. “Calculation of Net Shapes by the Finite Element Method With Triangular Elements.” *Communications in Numerical Methods in Engineering* 765(March): 757–65.

Reite, Karl-johan et al. 2014. “FHSIM-Time Domain Simulation of Marine Systems.” In *International Conference on Ocean, Offshore and Arctic Engineering*, , 1–10.

Remen, Mette et al. 2015. “Effect of Temperature on the Metabolism, Behaviour and Oxygen Requirements of Sparus Aurata.” *Aquaculture Environment Interactions* 7: 115–23. www.arvotec. (March 14, 2019).

Rudi, H., Geir Løland, and L. Furunes. 1988. *Model Tests with Net Enclosures. Forces on and Flow through Single Nets and Cage Systems*.

Seaculture. 2019. *Documento Suporte Ao Pedido [TUPEM] -Project Pilot Sea Culture*.

Shainee, Mohamed, Harald Ellingsen, Bernt J. Leira, and Arne Fredheim. 2013. “Design Theory in Offshore Fish Cage Designing.” *Aquaculture* 392–395(2013): 134–41.

Shainee, Mohamed, Bernt J. Leira, Harald Ellingsen, and Arne Fredheim. 2013. “An Optimum Design Concept for Offshore Cage Culture.” In *International Conference on Ocean, Offshore and Arctic Engineering*, , 85.

Shen, Yugao, Marilena Greco, Odd M. Faltinsen, and Ivar Nygaard. 2018. “Numerical and Experimental Investigations on Mooring Loads of a Marine Fish Farm in Waves and Current.” *Journal of Fluids and Structures* 79: 115–36.

SINTEF. 2019. *RIFLEX 4.16.0 Theory Manual*. Trondheim.

Strand, Ida Marlen. 2018. “Sea Loads on Closed Flexible Fish Cages.” NTNU.

Thyholdt, Sverre Braathen. 2014. “The Importance of Temperature in Farmed Salmon Growth: Regional Growth Functions for Norwegian Farmed Salmon.” *Aquaculture Economics & Management* 18(2): 189–204.

Tsukrov, Igor et al. 2002. “Finite Element Modeling of Net Panels Using a Consistent Net Element.” *Ocean Engineering* 30(2): 251–70.

Wang, Shan, Sheng Xu, Gong Xiang, and Carlos Guedes Soares. 2018. “An Overview of Synthetic Mooring Cables in Marine Application.” In *Advances in Renewable Energies Offshore: Proceedings of the 3rd International Conference on Renewable Energies Offshore (RENEW 2018)*, , 853–63.

Yılmaz, H. et al. 2011. “Thermal Tolerance of European Sea Bass (Dicentrarchus Labrax) Juveniles Acclimated to Three Temperature Levels.” *Journal of Thermal Biology* 37(1): 79–82.

Yu, Qing, Pao-lin Tan, Tzu-wei Lo, and Weng-yin Jan Chow. 2016. “New LRFD-Based Design Criteria for Mobile Offshore Units and Floating Overview of ABS LRFD-Based Structural Design Criteria.” In *Offshore Technology Conference*,.